Flow-Through Electroporation in Asymmetric Curving Microfluidic Channels

Hamid Hassanisaber

Thesis submitted to the faculty of the Virginia Polytechnic Institute and State University in partial fulfillment of the requirements for the degree of

Master of Science
in
Chemical Engineering

Chang Lu
Donald G. Baird
William A. Ducker

December 3rd, 2013
Blacksburg, Virginia

Keywords: Microfluidics, Electroporation, Particle focusing, CHO-K1 cells

Flow-Through Electroporation in Asymmetric Curving Microfluidic Channels

Hamid Hassanisaber

Abstract

Electroporation is an efficient, low-toxic physical method which is used to deliver impermeant macromolecules such as genes and drugs into cells. Genetic modification of the cell is critical for many cell and gene therapy techniques. Common electroporation protocols can only handle small volumes of cell samples. Also, most of the conventional electroporation methods require expensive and sophisticated electro-pulsation equipment. In our lab, we have developed new electroporation methods conducted in microfluidic devices. In microfluidic-base electroporation, exogenous macromolecules can be delivered into cells continuously. Flow-through electroporation systems can overcome the issue of low sample volume limitation. In addition, in our method, electro-pulsation can be done by using a simple dc power supply, without the need for any extra equipment. Furthermore, our microfluidic chips are completely disposable and cheap to produce.

We show that electroporation and electroporation-based gene delivery can be conducted employing tapered asymmetric curving channels. The size variation in the channel's cross-sectional area makes it possible to produce electric pulses of various parameters by using a dc power supply. We successfully delivered Enhanced Green Fluorescent Protein, EGFP, plasmid DNA into Chinese Hamster Ovary, CHO-K1, cells in our microfluidic chips.

We show that the particles/cells undergo Dean flow in our asymmetric curving channels. We demonstrate that there are three main regimes for particle motion in our channels. At low flow rates (from 0 to ~75µl/min) cells do not focus and they randomly follow stream lines. However, as flow rate increases (~75 to 500µl/min), cells begin to focus into one line and they follow a single path throughout the micro-channel. When flow rate exceeds ~500µl/min, cells do not follow a single line and demonstrate more complex pattern.

We show that the electric parameters affect the transfection efficiency and cell viability.

Higher electric field intensity results in higher transfection efficiency. This is also true in the cases with longer electroporation duration time. In our experimental work, we executed flow-through electroporation for various duration times (t = 2 ms, 5 ms, and 7 ms), and at various electric field intensities (from 300 to 2200 V/cm) while we utilized different flow rates as well, i. e. 150 μl/min (focused flow) and 600 μl/min (complex flow).

To explore the impact of individual electric pulse length and electric pulse number on electroporation results, we designed control channels with straight narrow sections. Cells experience different hydrodynamic forces in straight channels compared to curving channels. Flow pattern and cell focusing were also studied in control channels as well. Also, electroporation on CHO-K1 cells was successfully conducted in control channels. The hydrodynamic forces under the conditions we used do not appear to show substantial impact on transfection efficiency.

DEDICATION

This thesis is dedicated to my mother.

ACKNOWLEDGEMENT

It was a great opportunity to work under supervision of Dr. Chang Lu in microfluidic laboratory, chemical engineering department. I would like to express my sincere gratitude to my advisor whose kind support and warm encouragement has made this work possible.

I would also like to extend my gratefulness to all the members of my committee: Dr. Donald Baird and Dr. William Ducker, for their valuable time and helpful comments.

In addition, I would like to thank my kind and supportive labmates: Nelie Loufakis, Chen Sun, Zhenning Cao, and Sai Ma.

Table of content

List of figures

List of tables

OBJECTIVES

In this work we pursued multiple goals. Here, there is a list introducing our main objectives in this study.

- In this study, we wish to perform flow-through electroporation in an asymmetric curving microfluidic channel. In fact, we wish to conduct electroporation-based gene delivery to deliver EGFP plasmid DNA to CHO-K1 cells by using a DC power supply.

- We wish to examine the impact of various electrical parameters on transfection efficiency. Electroporation duration and the intensity of applied electric field could be changed to study their impact on the transfection efficiency and the cell viability.

- We wish to study cell focusing in our asymmetric curving microchannel under various flow rates. Cells would follow specific paths inside channel due to the effect of hydrodynamic forces present in curving channels.

- We are also interested to study the possible impact of hydrodynamic effects on transfection efficiency.

Chapter 1. Introduction

1.1. Cell membrane

The cell membrane or the plasma membrane is the interface between cell interior and extracellular fluid. The plasma membrane is comprised of phospholipid bilayer. Phosphatidylethanolamine is an example of materials which form cell membranes. Phospholipids are amphiphilic, i. e. they has both hydrophobic (hydrocarbon tail) and hydrophilic (polar head) properties [1]. Hydrophobic tails face each other while hydrophilic heads face aqueous solution inside and outside the cell, which results in the formation of phospholipid bilayer.

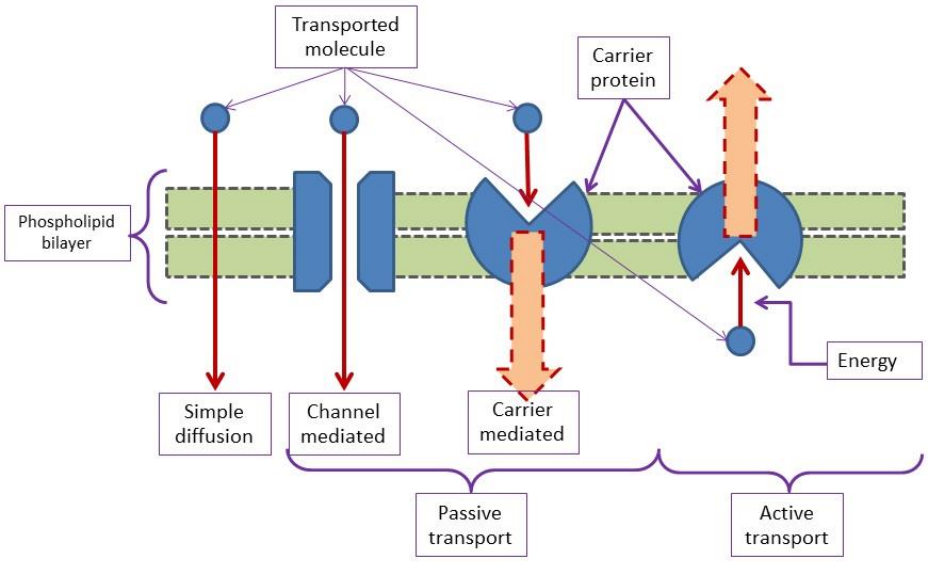

Figure 1.1. Schematic of different mechanisms of particle transport around phospholipid bilayer.

Under specific circumstances, materials need to enter and leave the cell. There are different mechanisms for transport around the cell membrane, i. e. diffusion, osmosis, passive transport, active transport, and vesicles. Figure 1.1 shows the schematic diagram of some transport mechanisms. Some lipid-soluble molecules such as steroid can diffuse directly to phospholipid bilayer. Also, for very small molecules such as H_2O, the cell membrane is

completely permeable. This kind of transportation cannot be adjusted by the cell [2]. Some molecules can diffuse across the membrane and enter inside the cell. Then they dissolve in an aqueous solution inside the cell. The essential factor for a molecule diffusion is simply a concentration gradient. In fact, no protein is involved in this simple mechanism. This happens for O_2, CO_2, and H_2O [3].

Osmosis refers to water diffusion from places with higher water concentration to areas with lower number of water molecules. Water enters inside cells with or without help of proteins of phospholipid bilayer. There are a group of proteins called Aquaporins which can form hydrophilic channels in membranes and allow water to go inside cells and pass the cell membranes [4]. Passive transport happens through certain proteins in the plasma membrane. These proteins would allow some molecules to go inside cells. This process does not require energy consumption and depends on concentration gradient. On the other hand, in active transport, proteins consume energy by splitting ATP to ADP and phosphate and act as a pump to transport certain materials into cells. Membrane vesicles also use energy to move larger molecules, such as proteins and polysaccharides, in and out of cells [2].

The cell membrane is impermeable to macromolecules such as DNA. Genetic modification of cells becomes possible via efficient and viable delivery of desired genes into cells. A diverse range of methods have been developed to fulfill this goal and deliver materials into cells and out of cells [5]. Electroporation is one of the common approaches for conducting transfection [6-8]. In reversible electroporation, temporary nano-scale pores are formed on the surface of the cell membrane by applying external electric field [9]. The cell membrane surface recovers itself after removal of an external electric field in reversible electroporation. In irreversible electroporation pores are not healed and the cell becomes inactivated [10].

1.2. Electroporation

The cell membrane can become transiently permeable to large molecules by being exposed to an external electric field and electro-pulsation [11-15]. This method is called electroporation and can be used for the purpose of gene delivery. By applying this method, cells can be genetically engineered and modified. Genetically modified cells can be examined to shed

more light on vital aspects of cell development stages. Also, by transferring specific genes to cells, cell and gene therapies can be conducted. For example, cells can be genetically modified after being isolated from the patient's body. These transfected cells would be introduced again to the body to cure a damaged tissue [16]. In fact, the application of an external electric field on the cell membrane has been studied by scientists as an effective technique [17-21]. Electroporation has been used to introduce genes and drugs to cells, both in vitro and in vivo [22-29].

Besides electroporation there are also other methods that have been used by scientists to introduce DNA into cells. Viruses can be used as gene transfer vectors. However, they can merge with target cells genome and cause mutagenesis [30, 31]. Even in cases without the risk of integration with genome, viruses can cause intense immune response in patient's body [32, 33]. There are also some non-viral (chemical) methods using cationic lipids and polymers which are highly dependent on the cell type [34, 35].

The main goal during electroporation process is to produce nano-scale pores on the surface of the cell membrane by changing the transmembrane potential. This can be done by employing external voltage. External electric field can increase transmembrane potential $\Delta\psi E$. When transmembrane potential reaches around 250 mV, nano-scale pores are formed which facilitates delivery of various molecules into cells [36].

Considering Equation 1.1, the transmembrane potential $\Delta\psi E$ is highest at the poles of a cell where the surface normal is aligned with the field direction (i. e. $\theta \rightarrow 0$). Permeabilization of the membrane and, therefore, gene delivery occur mostly around the poles. The fact that gene entry into cells is via a small fraction of the cell surface area is a considerable limiting factor in improvement of transfection efficiency [37-43]

$$\Delta\psi E = 0.75\, g(\lambda)\, a\, E \cos\theta \qquad 1.1$$

ψE: Transmembrane potential

$g(\lambda)$: a function of membrane and buffer conductivity

a: diameter of the cell

θ: angle between the normal to the membrane surface and field direction
E: electric field intensity

External electric field cannot be applied to cells for long periods of time. If cells be exposed to electric field for long time, the cell membrane would not have enough time to recover itself and cells would die. Thus, in conventional electroporation processes, the electric field is applied in short (millisecond) pulses to maintain the cell viability. Normally, these short pulses are generated with pulse generators which result in more expensive electroporation setups. In order to overcome the cost of pulse generators dc voltage can be used [44, 16]. In fact, by changing the cross-sectional area of microfluidic channel, it is possible to use dc voltage and completely eliminate the need for expensive and sophisticated electric pulse generators.

In mammalian cells, if transmembrane potential exceeds a certain threshold, these pores would appear and after the removal of external electric field, the cell membrane will be recovered and the pores will be sealed. This is known as reversible electroporation. However, if transmembrane potential exceeds a secondary threshold, electroporation will become irreversible and the pores would not be healed. Thus, cell viability decreases and cells would die. Molecules which cannot penetrate into the cell membrane under normal conditions, such as DNA, can be delivered into cells in reversible electroporation. For performing electroporation, the applied electric field intensity must reach a certain threshold. For example, for Chinese hamster ovary cells (CHO-K1, which we use in our study) the threshold is about 700 V/cm [16]. After applying electric field on the cell membrane, it would become charged due to change in ion movement inside and outside phospholipid bilayer. This ion flow causes localized rearrangement of membrane shape. At this phase, nano-scale pores would appear on the cell membrane surface. Water molecules would fill these pores and form hydrophilic channel.

Therefore, the cell's uptake of external molecules increases drastically. After removing external electric field, the cell membrane would be recovered while macromolecules are also confined inside the cell [45-51]. The intensity of electric field and electroporation duration time needs to be optimized in order to preserve cell viability during electroporation process. Figure 1.2 presents a schematic of discussed electroporation different steps.

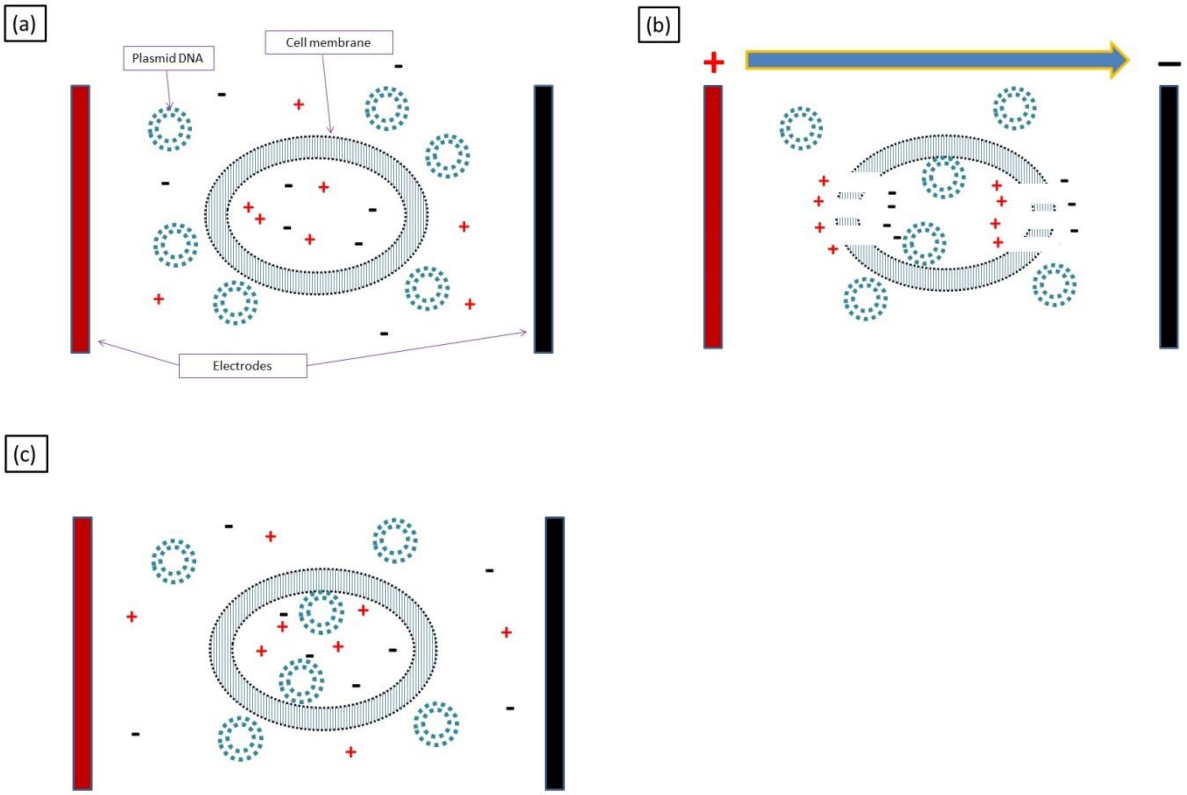

Figure 1.2. Schematic of electroporation different steps: (a) Before applying external electric field, ions have a balance. The cell membrane is undisturbed and plasmid DNA cannot be delivered into the cell. (b) After applying electric field, transmembrane potential increases and nano-scale pores are formed on the cell membrane surface. Plasmid DNA can enter the cell from these temporary pores. (c) After removing electric field, pores are healed while plasmid DNA is confined inside the cell.

Classical electroporation protocols are limited to small sample volumes and most of them need expensive, sophisticated equipment such as electro-pulse makers. Microfluidics can provide a basis for conducting electroporation for larger samples and continuously without the need for sophisticated equipment [16]. Furthermore, disposable microchannels can be produced with low cost and at short periods of time.

1.3. Microfluidics

Microfluidics is a science which deals with small volumes of fluids around 10^{-9} to 10^{-18} liters by using micro-scale channels. Microfluidics provides a basis for reliable, sensitive tests with considerably low amount of reagents. The cost of multiple tests can be reduced by employing microfluidics methods. Also, analysis time would become much shorter [52].

Surface area to volume ratio has a very important role in microfluidics. In fact, because of manipulating small amount of fluid volumes and micro-scale dimension of microfluidic channel surface area to volume ratio becomes considerably significant [53]. To have a better understanding about the effect of different physical properties in microfluidics, scaling with length (L) is beneficial. Table 1.1 shows scaling with L for various physical properties [54].

Table 1.1. Scaling with length for various physical properties. (Berthier & Silberzan, 2009) (Used under fair use guidelines, 2013.)

Quantity	**Scaling with L**
Distance	L
Area	L^2
Volume	L^3
Mass	L^3
Time	L^0
Velocity	L
Acceleration	L
Gravitational force	L^3
Hydrostatic	L^1
Pressure force	L^2
Capillary force	L
Centrifugal force	L^4
Volume flow rate	L^2
Inertial force	L^2
Viscous force	L^1

Dimensionless numbers shed more light on our knowledge about essential parameters in microfluidic systems. For example, Reynolds number represents the ratio of inertial and viscose

forces. Generally, microfluidic devices deal with laminar flow, i. e. low Reynolds numbers. However, in some cases, regarding channel geometry, flow can become more complex and inertial force must be considered [55].

In our work we use electroporation buffer which is a water based solution. Therefore, we have an incompressible flow. The continuity equation is:

$$\nabla . v = 0 \qquad 1.2$$

v: velocity vector

Also, Navier-stoks could be written as:

$$\rho \left(\frac{\partial v}{\partial t} + v \,. \nabla v\right) = \, -\nabla p + \, \mu \, \nabla^2 v + f \qquad 1.3$$

ρ: density,

v: velocity,

p: pressure,

μ: viscosity,

f: other body forces

In most cases Re number is low for microfluidic devices. That means inertial force is much smaller than viscose force. Thus, Navier-stokes equation can be simplified to Stokes equation:

$$\nabla p = \, \mu \, \nabla^2 v + f \qquad 1.4$$

However, in the presence of secondary flows, such as Dean flow, inertial forces must be considered in momentum balance equation [56].

At the absence of inertial forces and in low Reynolds numbers, floating particles follow stream lines in laminar flow. Particle focusing and lateral migration of particles first was observed in centimeter-scale cylindrical tubes [55, 56]. Inertial lift force can be employed in microfluidic channels. It is useful for different microfluidic manipulations and applications such

as particle separation [57]. Secondary flows in curved channels can introduce inertial force to system. In our experiments we use a special design with asymmetric curved turns. A similar design was previously used for the purpose of particle focusing and separation by Dino et al [58].

Particle focusing happens because of interaction of wall effect, centrifugal forces, Saffman forces, and Dean flows. Saffman forces happen in cases that particles lead or lag flow [57]. More details are discussed in the section of Focused and complex flow chapter. Figure 1.3 shows particle focusing in curving channel. Particles (cells) experience different hydrodynamic forces based on various geometries of fluidic channel.

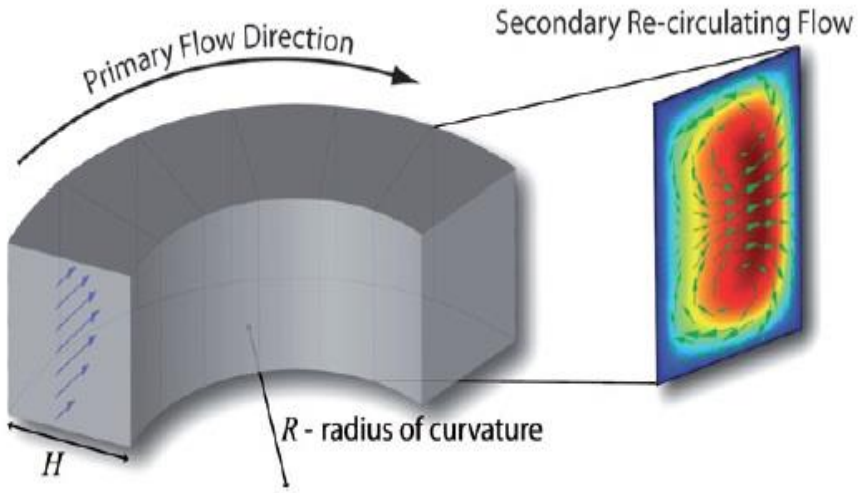

Figure1.3. This is a depiction of Dean flows vortices in curved channel. (Dino Di Carlo 2009) (Used under fair use guidelines, 2013.)

Dean flow is considered an important element affecting particle focusing in curved channel [55, 56]. This secondary flow can cause particle lateral migration and movement of particles to equilibrium position. Dean flow is the result of force imbalance between radial pressure and centrifugal force in curving channels. It is a combination of counter-rotating vortices at turns. The fluid with slower velocity near walls has inward vortex while fluid with higher velocity in the middle of channel experiences outward vortex [58]. This phenomenon can be employed for the purpose of separation and particle sorting in microfluidic chips [59].

Particles (cells) in straight channel are focused in multiple equilibrium positions because of inertial self-ordering. All the discussed effects are highly dependent on the size of particles which is desirable for particle separation based on size difference. There are two important Reynolds numbers which can describe particle flow in channels. The channel Reynolds number Rc and the particle Reynolds number Rp [60].

$$Rp = \frac{Um\, a^2}{\nu\, Dh} = \frac{Um\, Dh}{\nu} \cdot \frac{a^2}{Dh^2} = Rc \left(\frac{a}{Dh}\right)^2 \quad 1.5$$

U_m: maximum velocity in cross section

a: the diameter of particle

ν: kinematic viscosity

Dh: hydrodynamic diameter

$$Dh = \frac{2wh}{(w+h)} \quad 1.6$$

w: the width of channel

h: the depth of channel

The definition of Reynolds number regarding mean channel velocity can be related to channel Reynolds number Rc:

$$Re = \frac{2}{3}\, Rc \quad 1.7$$

Inertial lift forces dominate particle behavior when the particle Reynolds number is around 1 [55, 56]. Generally, the cell flow in microfluidic channels is dominated by viscous interactions. This is correct for systems where Rp << 1. In such systems, particle is under direct control of local fluid velocity. This happens due to viscous drag of the fluid over particle surface and in our case over the cell membrane. In fact, for dilute particle suspensions where the particles are naturally buoyant in fluid, they would follow stream lines and lateral migration over stream lines would not happen. However, as particle Reynolds increases (Rp) migration across

streamlines has been observed in micro-scale channels [58]. In cylindrical tube, particles form a focused annulus. This tubular pinch is the result of inertial lift forces. This phenomenon occurs where Rp is high. The dominate forces on rigid particles are the wall effect, where an asymmetric wake of a particle near the wall leads to a lift force away from the wall, and the shear-induced lift that is directed down the shear gradient and towards the wall. The balance between inertial lift and Dean drag forces dictates the equilibrium position for cells in a curving microfluidic channel [59].

1.4. Electroporation in microfluidic devices

Microfluidic devices offer a flexible basis for performing electroporation [61-67]. For example, electric field distribution can be efficiently adjusted in microfluidic devices. Electrodes can be installed in desired locations and different electrode types can be employed in microfluidic chips. In many experiments pulsatile electric field or ac voltage have been used for the purpose of electroporation [68-70]. In addition, the geometry of microfluidic channel can be changed to modify electric field distribution and pulse patterns without using extra equipment for pulse production [71-74].

Furthermore, microfluidic devices provide researchers with more opportunity in cell manipulating and cell handling. This becomes possible by benefitting from microchip design flexibility and hydrodynamic forces in channel [44, 75-78]. Also, microfluidic devices can be used in parallel for high-throughput applications [79, 80].

Hydrodynamic force can be considered as an effective tool in microfluidic channels for having more control on cells in electroporation process. Furthermore, microfluidics gives scientists the opportunity of real time monitoring of electroporation process. For example fluorescent labeling can be used for this purpose. Another considerable advantage of using microfluidic chips for performing electroporation is related to short surface to volume ratios in such devices. Small area to volume ratio which is noticeable in microfluidics makes heat decay faster. Heat will appear in electroporation due to Ohmic heating in the presence of an electric field. This important feature of microfluidic chips makes it possible to distinguish heat and

electric field effect on electroporation phenomena [71]. Also, in microfluidic devices, smaller volume of reagents such as electroporation buffer and DNA are needed for conducting experiments.

In order to perform reversible electroporation researchers use different strategies. There are eight main categories:

1. Cell trapping,

2. Membrane sandwich,

3. Polyelectrolite salt bridge,

4. Mechanical valves,

5. Microarray,

6. Droplet,

7. Optofluidic,

8. Continuous flow.

Our work is related to the last mechanism, i. e. continuous flow-based on chip electroporation. Wang et al. (2007) [16] present a microfluidic device for flow-through electroporation with dc electric field. They changed the cross sectional dimensions of channel to control the electric field intensity and to become able to produce desired electric pulses. They showed interesting results for cell transfection and cell viability for electric field intensity higher than 600 V/cm at electroporation duration times in millisecond range for CHO-K1 cells. Their work has many considerable advantages compared to other designs. For example, number of narrow sections (pulse number), electric field distribution, and electroporation duration time are perfectly tunable. They also benefited from the same approach in designing microfluidic chip to explore the changes in cell volume and size during electroporation. They conducted experiments to examine the effect of electroporation buffer properties, such as conductivity, and cell velocity on cell swelling phenomenon.

Bao et al. 2010 also employed continuous flow-based microfluidic chips to perform irreversible electroporation on circulating tumor cells (CTC), red blood cells (RBC), and white blood cells (WBC). Their results show a considerable dependency on cell size for electric field strength threshold in irreversible electroporation. In fact, cells with larger diameter need weaker external electric field for irreversible electroporation. This phenomenon allows scientist to develop more sensitive microfluidic techniques to inactivate circulating tumor cells in blood stream [81].

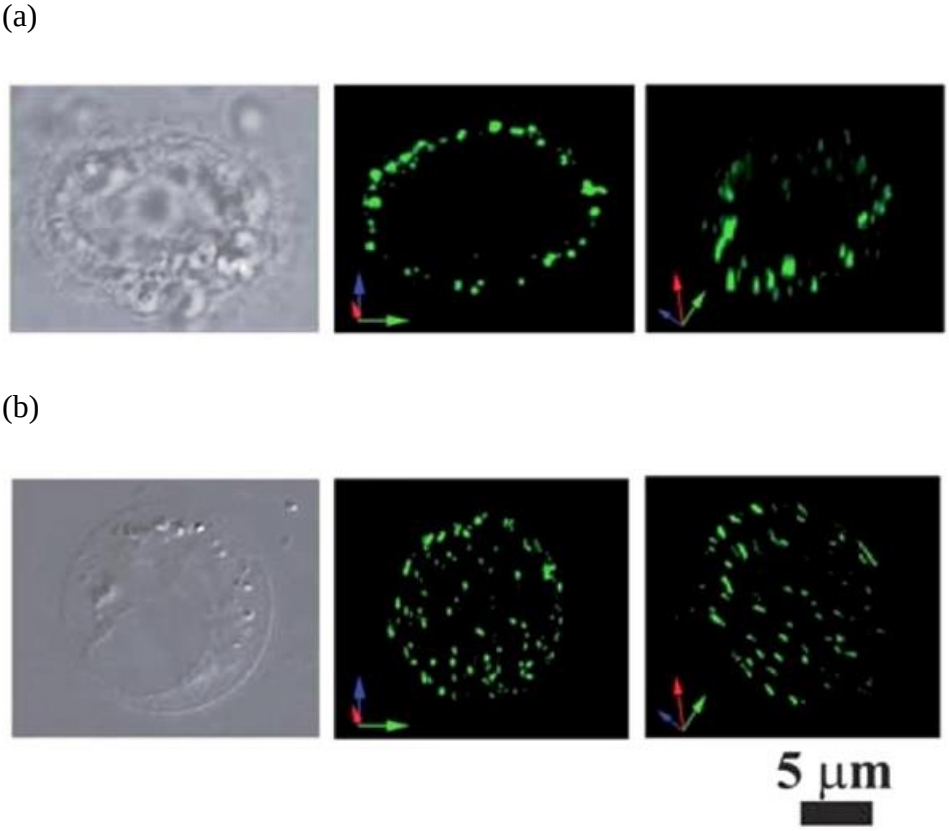

Figure 1.4. Phase contrast and confocal fluorescent images from different angles for (a) straight and (b) spiral channel. Green spots are YOYO-1 fluorescent dye which was used to label plasmid DNA during electroporation. From part (b), it is obvious that Dean flow vortices in curving path can improve transfection efficiency. The cell membrane is uniformly affected by electric field when Dean flow is present. (Wang et al. 2010) (Used under fair use guidelines, 2013.)

Also, Wang et al. (2010) [38] designed a microfluidic device with spiral geometry for the purpose of continuous flow electroporation. They showed the effect of Dean flows vortices on transfection efficiency. YOYO-1 fluorescent dye was used at their study to label plasmid DNA. Then confocal microscopy confirmed the increase of plasmid uptake on the cell membrane surface in this vortex-assisted continuous electroporation technique. In fact, Dean flows vortices would cause extra rotation of cells and would expose more spaces on the cell membrane in the directions parallel to electric field. Figure 1.4 is from their work (Used under fair use guidelines, 2013) which compares transfection efficiency for delivery of EGFP plasmid DNA into CHO-K1 cells. At straight channel without presence of Dean flow, only a limited section of the cell membrane becomes permeable while in spiral channel, nano-scale pores are formed uniformly on the cell membrane surface.

1.5. Plasmid DNA

In our experiments, we measure the efficiency of plasmid DNA delivery into CHO-K1 cells. Plasmid DNA is separated from chromosomal DNA and can separately be reproduced. We use plasmid extracted from E-coli. It is a double-stranded DNA molecule. The plasmid in our experiments (pEGFP-C1) encodes enhanced green fluorescent protein (EGFP). It can be extracted from E-coli by commercially available plasmid extraction kits. QIAfilter Plasmid Giga Kit (Qiagen, cat. no. 12291) is used in our work to obtain the plasmid molecule. At the end of extraction procedure, purified plasmid is solved in TE buffer with a pH of 8.00. UV absorbance at 260 and 280 nm are used to examine DNA purity after extraction process. The ratio of absorbance must be between 1.8 and 2.0. Ratios lower than 1.8 is an indication of protein contamination. And, a ratio higher than 2.0 confirms presence of unwanted chemicals [82].

Plasma DNA size is approximately 150 kb. One kb is 1000 base pairs. The base pair is the basic repeating nucleotide unit of the DNA chain. Each base pair has a length around 0.33 nm [83]. Fluorescent microscopy is used to determine the efficiency of pEGFP plasmid delivery into CHO-K1 cells. FITC UV filter is needed to acquire images. The experimental details are provided in Transfection Efficiency and Cell Viability Chapter.

Chapter 2. Fabrication of the Microfluidic Device

2.1 Soft lithography

Soft lithography is a widely used technique for fabricating microfluidic chips. It is very cost efficient. Also, it needs shorter time compared to other available methods and needs less sophisticated equipment [53].

Lithographic masters can be employed for molding soft materials. Polydimethylsiloxane known as PDMS is a polymer widely used in soft lithography. In fact, photoresist masters are used to produce a diverse range of microfluidic channels with PDMS which have different geometries. The multiple soft lithographic fabrication steps in our work are completely explained in the method section. PDMS is a silicon-based organic polymer. Its non-toxicity allows scientist to utilize it for biotechnological purposes. Non-toxicity is essential for working with living cells. PDMS is also non-flammable and inert. PDMS chemical formula is: $CH_3[Si(CH_3)_2O]_nSi(CH_3)_3$.

2.2. Method

We use Macromedia FreeHand software in order to design desired microfluidic channel. FreeHand is one of the most popular commercially available softwares for producing photomasks. The design is printed with high resolution (~5000 dpi). The print will be used for fabrication of master by the use of negative photoresist SU8-2025 (MicroChem). The channel design is transparent on the print so that UV light can pass the mask and cross-link the photoresist. These film transparencies are much cheaper than chrome masks however they are desired when features smaller than 20 micrometer is needed.

Three-inch Silicon wafer is placed on the center of spinner chuck and is fixed by vacuum. Then SU8 photoresist is added on top of the wafer. The spin rate and duration time depends on the thickness of microfluidic channel. The details are provided by MicroChem. Figure 2.1 shows the data regarding SU8-2000 series. The height of our channels is always 50 micrometer. For our

case, we use SU8-2025 and we spin the 3 inch wafer at 500 rpm for10 seconds and 30 second of 1650 rpm consecutively. At the end of fabrication process, by using a micro-scale transparent ruler and optical microscope, the exact height of microfluidic channel is measured. It is become possible by cutting the PDMS layer and placing it on top of the transparent ruler. Figure 2.2 provides more details about this procedure in an example.

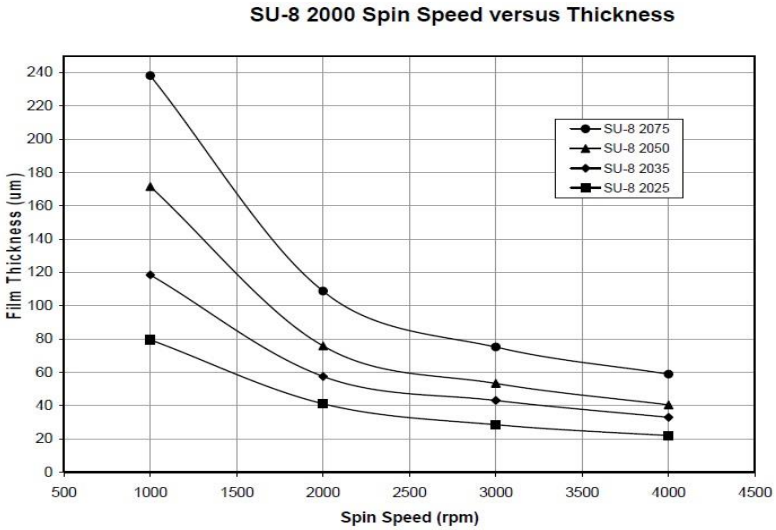

Figure 2.1. This graph shows the needed spin speed for desired SU8 thickness.
(MicroChem 2010) (Used under fair use guidelines, 2013.)

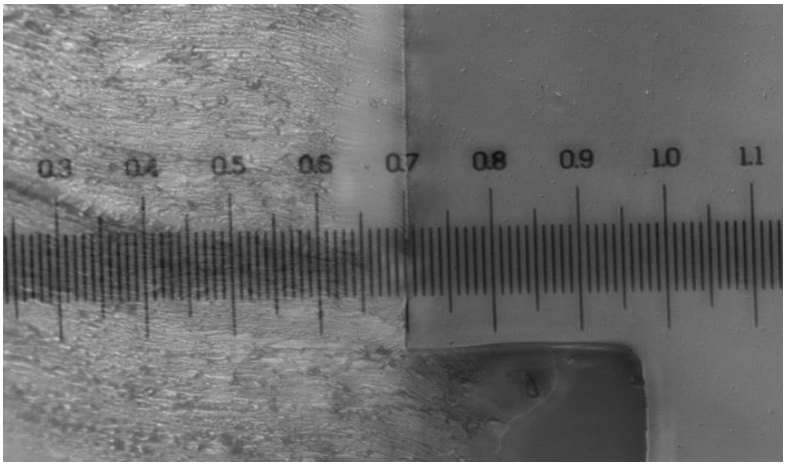

Figure 2.2. A simple, micro-scale transparent ruler can be used to measure dimensions of microfluidic channel by using optical microscope. This becomes possible by cutting PDMS layer and locating it on top of the transparent ruler. For this figure, 10X dry objective was used.

The whole process must be done under chemical fume hood since photoresist is considered a toxic material. After spin-coating step, wafer is placed on a heat plate. This step is called soft bake. The needed time and temperature depend on thickness of photoresist layer. More details are shown in table 2.1. After soft bake, wafer is placed under UV light with specific light intensity and duration time. The information needed regarding desired UV light intensity is provided by MicroChem and is presented in table 2.2. We found than 15 seconds of exposure is appropriate for 50 micrometer-thick SU8-2025 photoresist. And then wafer is again placed on heat plate for post bake. The desired heating time and temperature is mentioned in table 2.3.

Table 2.1. Time and temperature for soft bake in SU8-2000 series. (MicroChem 2010) (Used under fair use guidelines, 2013.)

Thickness Microns	**Soft bake time**	
	Minutes in 65 $_{o}$C	Minutes in 95 $_{o}$C
25-40	0-3	5-6
45-80	0-3	6-9
85-110	5	10-20

Table 2.2. UV light intensity needed for desired SU8-2000 series thicknesses. (MicroChem 2010) (Used under fair use guidelines, 2013.)

Thickness	**Exposure energy** mJ/cm^2
25-40	150-160
45-80	150-215
85-110	215-240

Table 2.3. Time and temperature for post bake in SU8-2000 series. (MicroChem 2010) (Used under fair use guidelines, 2013.)

Thickness Microns	**Post bake time**	
	Minutes in 65 $_{o}$C	Minutes in 95 $_{o}$C
25-40	1	5-6
45-80	1-2	6-7
85-110	2-5	8-10

After post bake step, wafer is washed with SU8 developer (MicroChem) solution for around 6 minutes and then is rinsed with isopropyl alcohol (IPA). Finally, the wafer is air dried with pressurized nitrogen. After this step, the master is ready to be used for PDMS molding.

PDMS pre-polymer and cross-linker are mixed in a ratio of 10 to 1. The mixture must be stirred vigorously until it obtains a milky color. The mixture is placed in vacuum chamber for around 2 hours to get rid of gas bubbles. The vacuum must not be extended because longer vacuum times would make the solution too viscose. The mixture is poured on top of wafer master placed in a petri dish. And, it is heated at 80 $_{o}$C oven for 1 hour.

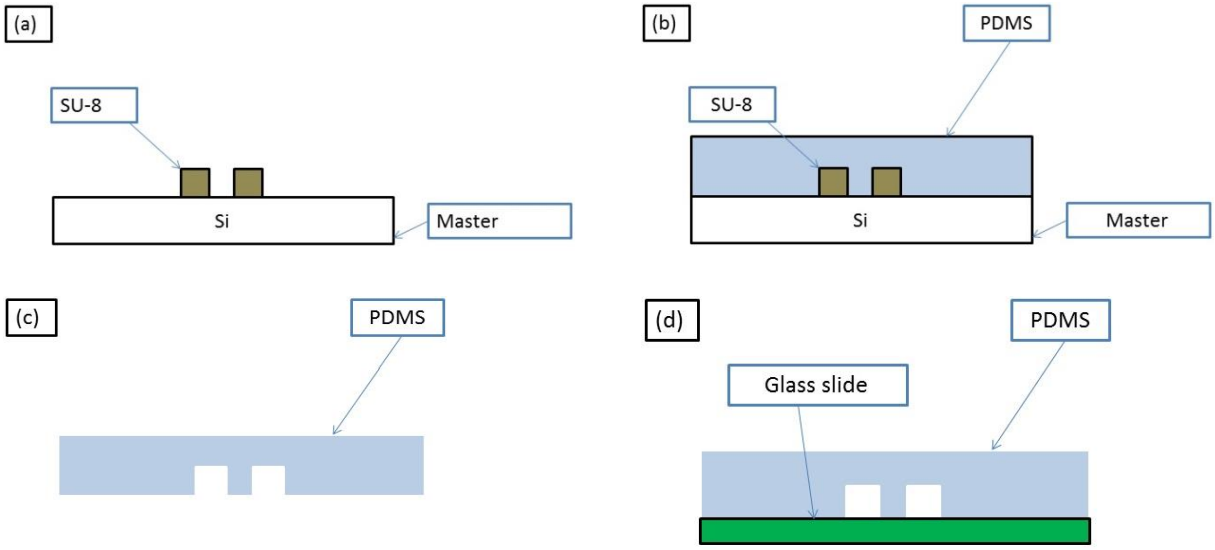

Figure 2.3. The schematic of PDMS device fabrication procedure: (a) Silicon wafer is used to fabricate master with cured SU-8 photoresist (b) PDMS polymer is poured on photoresist mold in a petri dish and cured in 80 $_{o}$C oven for 1 hour (c) PDMS layer is peeled off and channel outlet, inlet, and side chamber are punched (d) Plasma cleaner is used to irriversibly attach PDMS layer to glass slide and microfluidic chip is heated at 80 $_{o}$C oven for 1 hour.

After removing PDMS and master from oven, PDMS is peeled off from wafer by using a blade razor. The microfluidic channel inlet and outlet is punched with 1mm and 5mm diameter

punchers, respectively. Paper tape is used to remove dust from PDMS film. The punched PDMS layer and a pre-cleaned microscope glass slide (75×55×1 mm thick) are placed in plasma cleaner. The plasma cleaner is set on high radio frequency level. Inside plasma cleaner is under vacuum. We let a small volume of air into the chamber until observing bright violet color from inside. The PDMS and glass slide are kept in this condition for 1 minute. Then they are attached irreversibly together. Finally, the microfluidic device must be placed in 80 $_{o}$C oven for another hour. It would be ready for experiment after this part. Fiure 2.3 is a schematic about the steps of PDMS chip fabrication.

Microscope glass slide are cleaned by using hydrogen peroxide solution (30% vol/vol) and ammonium hydroxide solution (27% vol/vol). Five volumes of ultrapure water are added to one volume of each of the solutions in a glass beaker. The glass slide is placed in the solution and heated on hot plate at 75 $_{o}$C for around 2 hours. A magnet tablet is also used to make the solution uniform. After 2 hours, glass slides are rinsed with ultrapure water and are air dried.

Chapter 3. Focused and Complex Flow in Asymmetric Curving Channels

3.1. Particle (Cell) focusing in asymmetric curving channel

Inside our microfluidic channel, there are three main phases of cell focusing based on flow rate increase. Dino Di Carlo et al. 2008 also reported this behavior. Inside asymmetric curving microfluidic channel the focusing of particles happens at certain flow rates. In fact, at low particle Reynolds numbers (Rp) there is no focusing and particles (10 μm diameter fluorescent beads) follow stream lines. As flow rate increases, particles begin to focus. They become focused in two lines close to the walls. At Rp numbers around 1.82, particles become completely focused into only one single line However, after more increase in flow rate, cells would show a different pattern which is more complex.

(a) (b)

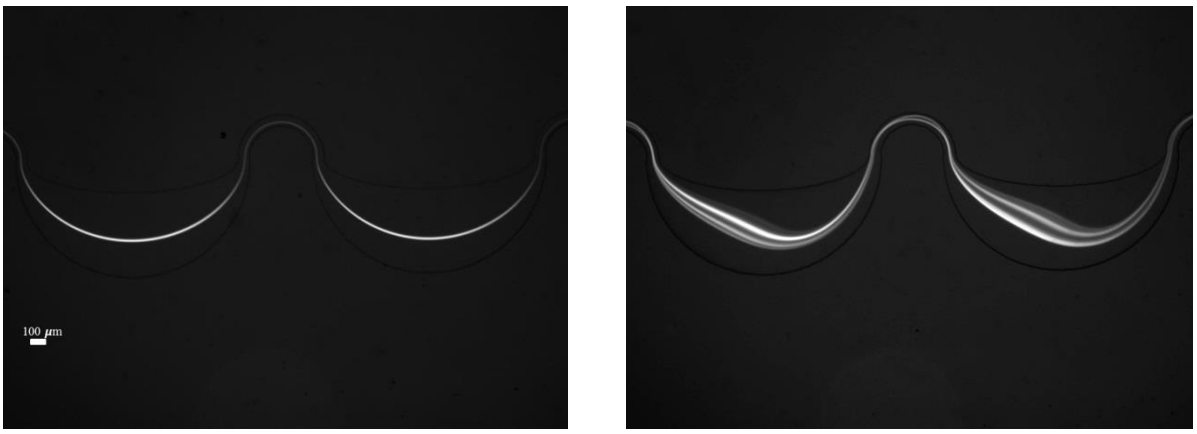

Figure 3.1. Cell pattern in (a) focused flow (150 μl/min) and (b) complex flow (600 μl/min) inside asymmetric curving microfluidic channel.

Our main channel is consisted of two main parts, i. e. wide and narrow section which is important for conducting electroporation with dc electro-pulsation. Electric field intensity is very low in wide section while it is strong enough for the purpose of electroporation in narrow section (above 400 V/cm for CHO-K1 cells). The width of wide section is 700μm at its maximum while

narrow section's width is equal to 100 μm. The height of channel is 50 μm throughout the channel (dimensions and details are provided in figure 3.3).

For our design, at low flow rates, i. e. from 0 to 50 μl/min, the cells are unfocused and mainly following streamlines. By increasing flow rate, we notice a different regime. Cells become focused into a single line. This happens approximately from 75 to 500 μl/min. In higher flow rates, cells enter another phase which includes more than one path. It happens in flow rates larger than 500 μl/min. We refer to this phase as complex flow. Figure 3.1 depicts cells equilibrium position inside the microfluidic channel under different flow rates, i. e. focused, and complex flow. Fluorescent trace is from labeled cells (CHO-K1) with Calcein AM green in different flow rates and the same asymmetric curving design. FITC UV filter is used to capture these images and ImageJ software is used for image analysis.

Normally cell focusing is not observed at the beginning of the channel. In fact, it takes some turns before cells reach the equilibrium positions. For lower flow rates this transient length is longer. It is very important to make sure electroporation is conducted in the part of channel with the desired flow. We are also interested to explore the possible effects of hydrodynamic forces associated with cells focusing on electroporation. In fact, we perform electroporation in these two cases, i. e. focused and complex flow, while we keep other electroporation parameters constant (field intensity and electroporation duration time).

When we wish to study electroporation while cells are in complex flow phase, we must make sure that electric field is applied on cells while they are in the fully developed sections of the microfluidic channel. This can be done by installing the electrodes at right location, i. e. in the locations which confine electric field only in the fully developed section of the channel. Since we are interested to keep electroporation duration time constant while changing the flow rate, we need to extend the effective length of channel in higher flow rate. Effective length refers to the section of channel which experiences electric field, i. e. the part confined between two electrodes.

In fact, two factors dictate the appropriate location of the electrodes in our channel. First, duration time, and second length needed for reaching uniform pattern, i. e. fully developed flow. For the first step, we calculated the exact velocity of cells in the microfluidic channel. The

procedure is explained with details in the chapter four. Cells are labeled by Calcein AM green for fluorescent microscopy. The appropriate numbers of turns for each desired electroporation condition is provided and discussed in chapter 4 as well.

To address the second issue, we install electrodes at the downstream of the channel to make sure cells have reached their equilibrium position. In fact, platinum wire connected to positive terminal of power supply is always in the outlet (to prevent cell accumulation in channel) of the microfluidic channel. Figure 3.2 provides some examples of different locations of electrodes for different desired electroporation duration times under different flow conditions. For example, when we apply 150 µl/min in the asymmetric curving channel, only one single turn (narrow section) is enough to reach duration time of 2 ms while for the case of 600 µl/min we need 6 turns for the same flow rate.

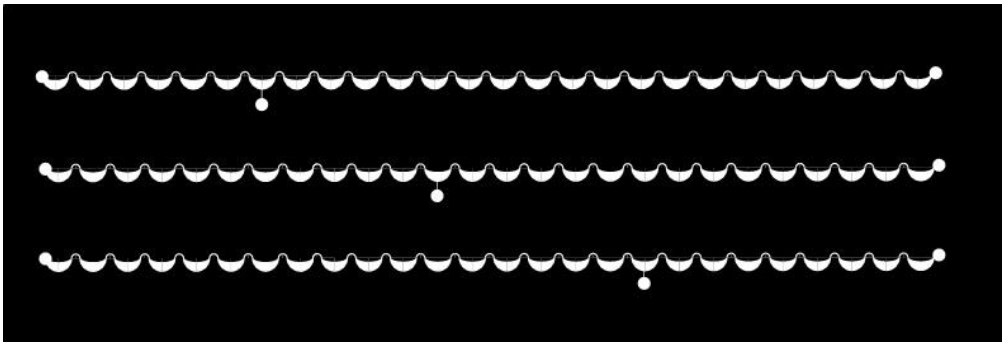

Figure 3.2. Electrode location can be adjusted by adding a side chamber connected to main channel. This is also helpful for solving of gas bubble issue during electroporation. (asymmetric curving channel)

3.2. Asymmetric curving channel versus symmetric curving channel

In addition to conducting flow-through electroporation in asymmetric curving channel, we wish to study the possible effects of hydrodynamic forces too. The change in hydrodynamic forces is associated with increase in applied flow rate. In fact, we are interested to explore the influence of cell focusing in microfluidic channel on transfection efficiency. However, in order to keep electroporation duration time constant, larger length of channel must be used which

means larger number of pulses (narrow sections) is present with shorter individual pulse length. Therefore, in order to independently study pulse number, we designed a control experiment.

We designed symmetric curving channel as control. In such channel the length of electric pulse and the number of pulses are similar to the main channel. However, instead of curving narrow sections, which cause specific flows like Dean flow vortices in main channel, control channel has straight narrow sections with no single line focusing and symmetric curving wide sections.

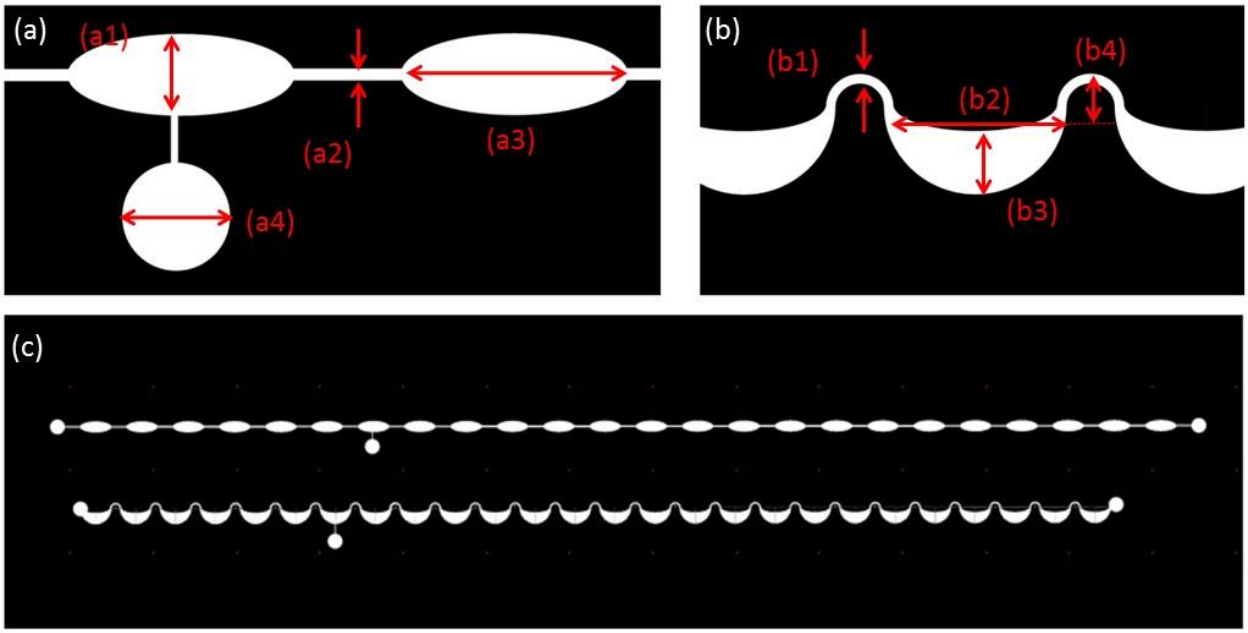

(a) Control channel: (a1): 700 μm (a2): 100 μm (a3): 1900 μm (a4): 1000 μm

(b) Main channel: (b1): 100 μm (b2): 1800 μm (b3): 700 μm (b4): 300 μm

(c) On top there is a sample of control channel design and at bottom there is a sample of main channel with asymmetric curving design.

Figure 3.3. The dimensions in both main and control channel. Channel height is 50 μm everywhere. The dimension for side chamber is the same in both symmetric and asymmetric designs (a4).

The length of wide and narrow section in symmetric channel are adjusted so that cells experience the same traveling time as what they experience in the asymmetric channel. Also, electrodes location is adjusted to reach the desired residence time for electroporation. The width of wide section is 700 μm at its maximum while straight narrow section has a width of 100 μm which is similar to main channel and would yield to the same electric field intensity. The height of control channel is 50 μm throughout the channel which is similar to main channel (dimensions with complete details are provided in figure 3.3).

Figure 3.4 shows the path that cells travel in the control channel under different flow rates, i. e. 150 μl/min and 600 μl/min. CHO-K1 cells are labeled with Calsein AM green. The images are chosen from videos captured by fluorescent microscopy and CCD camera. FITC UV filter is used to capture the images. Cell focusing in straight narrow section is totally different with curved turns. At 150 μl/min flow rate, cells begin to focus at two lines inside narrow section while the distribution of cells in these two paths is not the same. This is noticeable from the difference in fluorescent light intensity comparison. However, by having 600 μl/min flow rate, cells become focused in two similar straight lines near the walls in narrow section.

(a) (b)

Figure 3.4. The path that cells travel in the control channel at (a) 150 μl/min and (b) 600 μl/min

For having the same electric field distribution as in the main channel, COMSOL Multiphysics is used to simulate electric field intensity in control channel as well. The results are reported in Electroporation and electric field distribution chapter. Figure 3.5 shows different

electrode locations for obtaining different electroporation duration times in symmetric curving channel. As it was discussed earlier, longer effective length of channel is needed at high flow rates to fix electroporation duration time.

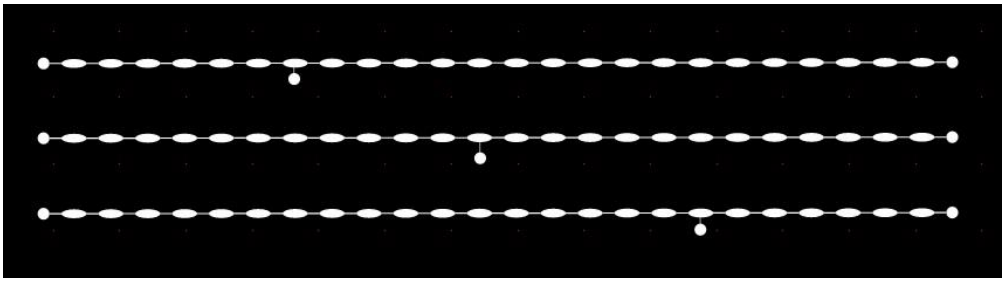

Figure 3.5. Electrode location can be adjusted by adding a side chamber connected to fluidic channel. This is also helpful for solving of gas bubble issue during electroporation. (symmetric curving channel)

Chapter 4. Flow Velocity versus Particle Velocity

4.1. Cell velocity and duration time

Since we need higher flow rates (600 µl/min) to obtain complex pattern inside our design, it is necessary to find a method to keep electroporation duration time fixed. In fact, we want to maintain the same duration time as what cells experience in focused flow condition. So, in order to examine the reliability of duration time calculations, we designed experiments to measure real cell velocity in our system. We also compared the result with theoretical velocity of flow which is calculated by knowing the flow rate and channel dimensions.

Two important factors must be explored to properly calculate electroporation duration time. First, we measured the cells' velocity inside microfluidic channel. Second, we evaluated the change in cell's traveled path inside the channel. In fact, by increasing flow rate, cells would travel a different distance. Knowing this difference is vital for calculating the desired number of turns (effective length) to maintain the needed electroporation duration time.

In order to collect the data for real (observed) cell velocity and the change in cell's travelling path, we use inverted microscope (Inverted phase-contrast and epifluorescence microscope system with 100 W mercury lamp (IX-71; Olympus)) which is connected to CCD camera (Hamamatsu, ORCA-285). We captured real time videos from cells inside the microfluidic channel under different flow rates. Flow rate can be digitally adjusted for desired flow rate on the control panel of syringe pump.

4.2. Method

CHO-K1 cells are collected from culture flask by using Trypsin-EDTA. We put cells in 15 ml centrifuged tubes and centrifuge them at 300 g for 5 minutes at room temperature. The cells then are washed with PBS and are centrifuged at the same condition. The supernatant is discarded. Again, PBS is added to cells until obtaining desired concentration. The cell

concentration is evaluated by using a hemocytometer. Then cells are ready to be labeled by fluorescent dye.

Calcein green AM is a cell-permanent dye for living cells. The non-fluorescent Calcein green AM is converted to green fluorescent after acetoxymethyl ester hydrolysis by intracellular esterases[84]. For proper labeling, a concentration of 10 μM of Calcein green AM is needed. It is added to cells when they are floated in PBS. The solution is incubated for 20 minutes at room temperature. Cells and dye can be mixed by gentle pipetting. After incubation, the solution is centrifuged at 300 g for 5 minutes at room temperature. Cells then will be washed with PBS at the same centrifugation condition. Washed cells are diluted with PB (electroporation buffer) and are counted by hemocytometer to reach the needed concentration before capturing real time images. We used around 300×10^3 cell/ml to be able to capture images from single cells in flow.

Then labeled cells are transferred to 1 ml plastic syringe connected to tubing. Before priming the channel with cell solution, the microchannel must be washed with electroporation buffer for at least 5 minutes to get rid of air bubbles and contaminations. After adjusting flow rate on syringe pump control panel, cells are introduced to channel. For Calcein green AM, FITC filter is needed for fluorescent microscopy.

(a) (b)

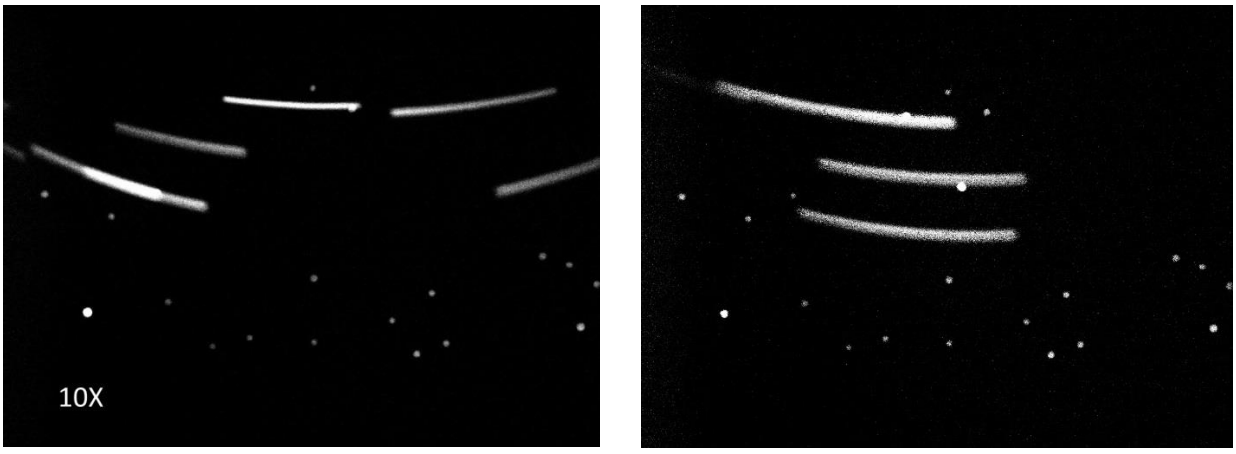

Figure 4.1. These fluorescent images are from CHO-K1 cells labeled with Calcein green AM inside microfluidic channel. (a) Flow rate is 50 μl/min and UV light exposure time is 7 ms. (b) Flow rate is 100 μl/min and UV light exposure time is 7 ms.

In order to calculate the real velocity we set exposure time for UV light. It is adjusted to be able to record the fluorescent trajectory of a single cell movement inside channel. By capturing the fluorescent trace of cell movement in microfluidic channel, we can quantify the length traveled by a single cell for the known exposure time. UV light exposure time is completely adjustable by using the discussed microscope's commercial software (Q-capture Pro).

Exposure time must be optimized. In fact at short exposure time, image resolution can drastically fall while in long exposure time, the complete length of trajectory cannot be recorded inside one fixed frame of microscope objective. Figure 4.1 shows two different examples of fluorescent images which are captured in order to measure cell real velocity (observed velocity) by using the discussed method. ImageJ is used to quantify the length of fluorescent trajectory.

In order to calculate real velocity, after capturing needed images, we also capture phase contrast image from the microfluidic channel. Mixed images are produced by the help of ImageJ. These images are used to determine the location of a single cell inside channel. By knowing the location and velocity of the cell in the channel, we are able to compare these data with theoretical velocity of flow in the middle of the microfluidic channel at different flow rates. Figure 4.2 shows different images which are needed in obtaining data for real velocity of cells and location of cells inside the microfluidic channel.

(a) (b) (c)

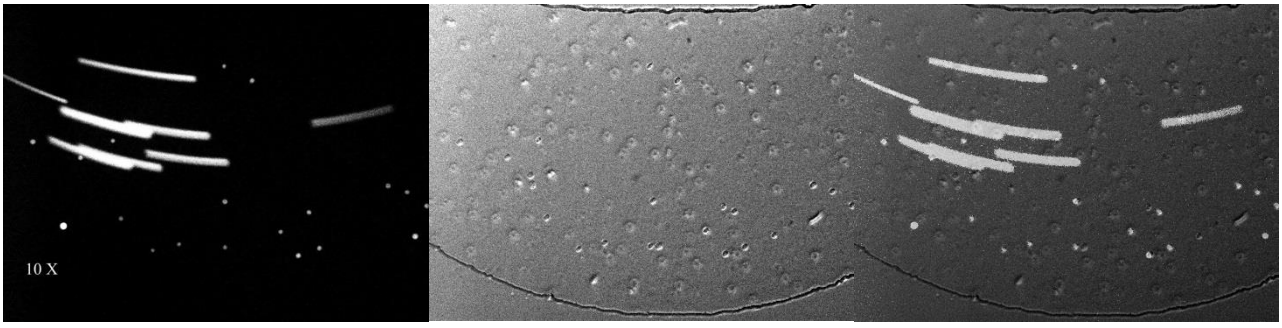

Figure 4.2. (a) This is a fluorescent image taken from labeled CHO-K1 cells with Calcein green AM. Flow rate of 50 μl/min and exposure time of 7 ms. (b) The phase contrast image. (c) The overlap image which is used to determine cells' location in the channel.

4.3. Result

The data are collected for different flow rates. Figure 4.3 is an example for measured cell velocities in the microfluidic channel. Red point represents theoretical velocity of flow calculated at the middle of the microfluidic channel (wide section). Horizontal axis shows location of a certain cell in micrometer inside channel, x = 700 µm is at the center of wide section. For the presented example flow rate is equal to 200 µl/min.

The data for cell velocity at different flow rates is collected and is reported in figure 4.4. The two last data points are obtained from extrapolation. As it is shown in figure 4.4, the increase in flow rate can result in larger difference between observed velocity of a cell and theoretical velocity of flow. With our equipment it is almost impossible to measure cells velocity in narrow section. We can evaluate the change in traveled distance under application of various flow rates in both narrow and wide section. We use the same ratio of change in cell velocity at wide section for narrow section as well however traveled distance is measured separately by means of fluorescent microscopy.

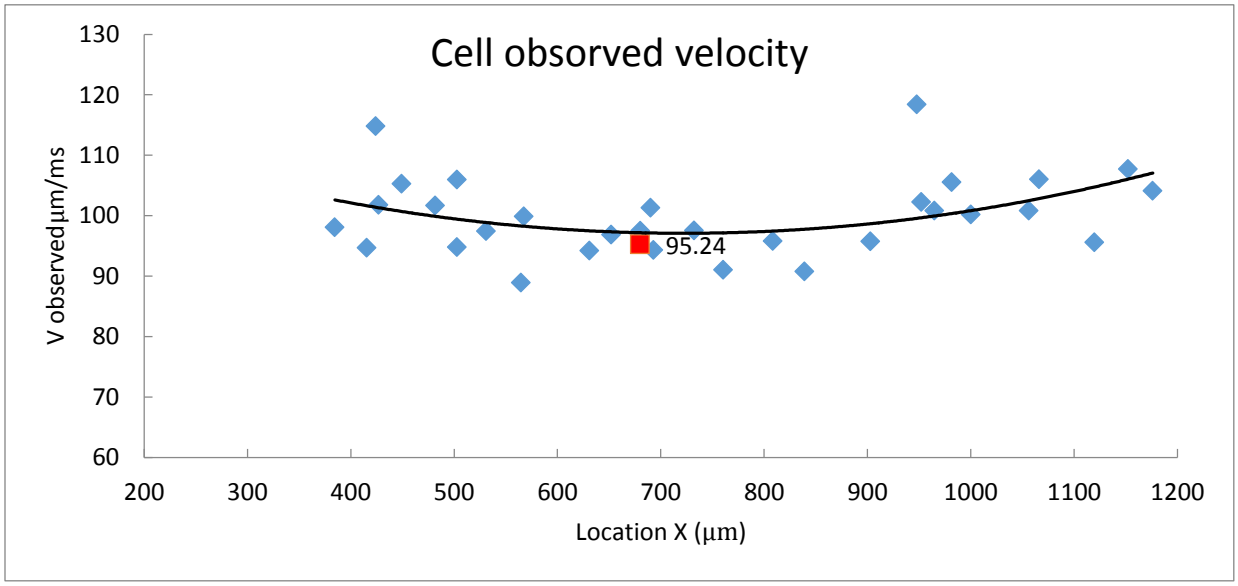

Figure 4.3. Blue points are measured cell velocities in wide section. Red point represents theoretical velocity of flow calculated at the middle of wide section. x = 700 µm is the centerline of wide section. Flow rate = 200 µl/min.

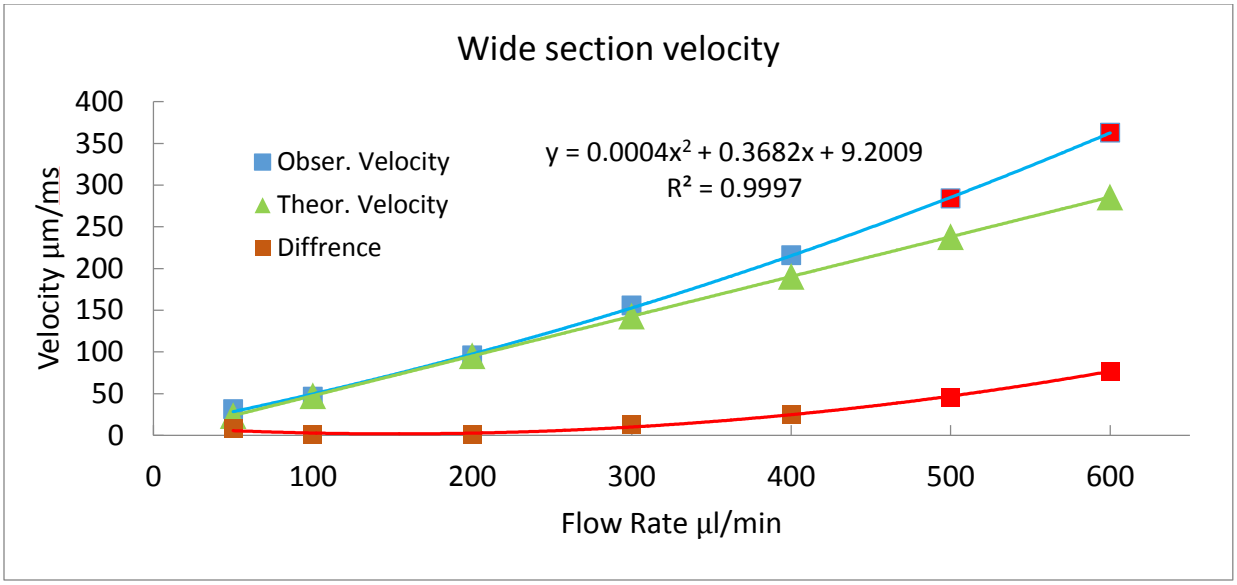

Figure 4.4. The observed velocity of cells in the center of wide section at different flow rates (blue squares) and flow velocity at the center of wide section (green triangles). The two last data points are obtained from extrapolation.

As we discussed earlier in this chapter, at higher flow rates cells follow a different path and travel a longer distance. So, in order to calculate real electroporation duration time, this change must be evaluated. Fluorescent images are taken by using Calcein green AM at different flow rates. Figure 4.5 is a sample that shows the usage of ImageJ for quantifying the traveled distance by cells in both narrow and wide sections in different flow rates. In each captured image, the mean traveled distance of cells is labeled by connected straight lines and is recorded in µm for both narrow and wide section.

In addition, we performed flow velocity simulations by COMSOL Multiphysics as well. The simulation shows flow velocity profile in two different flow rates for asymmetric curving channel. One sample of the set of simulations is presented in figure 4.6. This specific velocity profile simulation is performed for 750 µl/min (complex) and 160 µl/min (focused) flow rates. COMSOL simulation result also indicates signs of changes in flow pattern with rise in flow rate.

(a) (b)

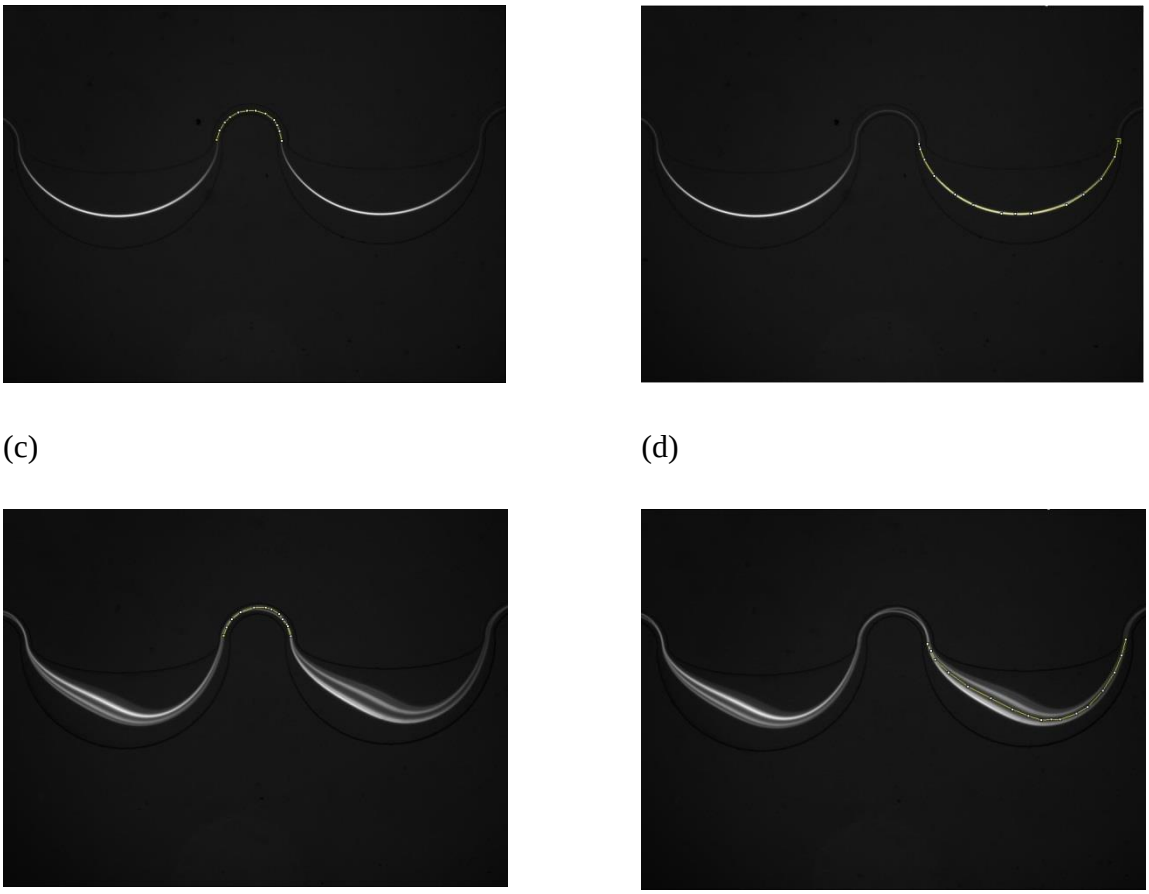

(c) (d)

Figure 4.5. Fluorescent microscopy is used to determine real traveled distance of cells in both narrow and wide section. Part (a) and (b) are images taken when flow rate is 150 µl/min for both narrow and wide section, respectively while part (c) and (d) are for 600 µl/min. The connected yellow lines show cells mean traveled distance in each part.

After gathering data for observed velocity and traveled distance, the number of needed turns for each desired electroporation duration time (2 ms, 5 ms, and 7 ms) is calculated. Table 4.1 shows the result of calculation for all desired conditions. It includes the result for both 150 µl/min (focused) and 600 µl/min (complex) flow rates.

Table 4.1. The number of needed turns (narrow sections) to obtain the desired electroporation duration time at 150 and 600 µl/min flow rates, in the asymmetric curving channel.

Cells pattern inside channel	Applied flow rate µl/min	Duration time for a single turn (narrow section) ms	Number of needed turns for 2 ms	Number of needed turns for 5 ms	Number of needed turns for 7 ms
Focused	150	2.34	1	2	3
Complex	600	0.36	6	14	20

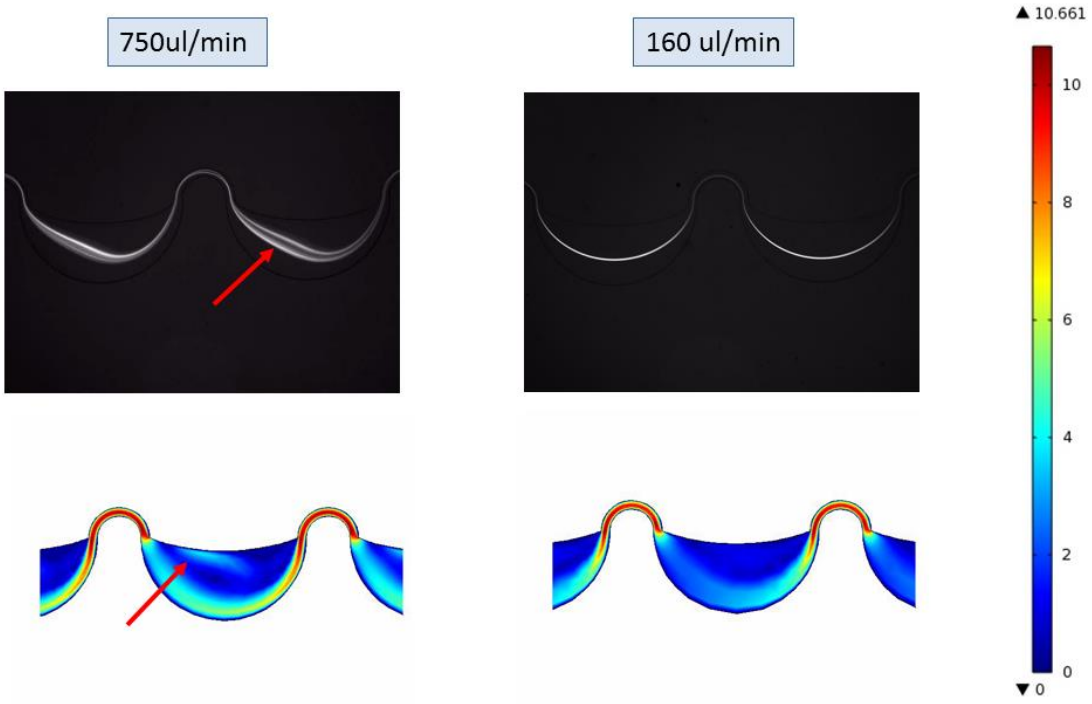

Figure 4.6. A sample of COMSOL simulation for flow velocity profile in microfluidic channel with asymmetric curving design at 160 and 750 µl/min flow rates. Red arrows point at the location where change in velocity results in change of cell focusing pattern in wide section.

Chapter 5. Electroporation and Electric Field distribution

5.1. Ohms' law

In our experiments we use a simple dc (direct current) power supply which produces up to 5000 volts (PS350, Stanford Research System). As it has been discussed earlier, by changing the location of electrodes in microfluidic channel, the electric field distribution can be adjusted. Based on Ohms' law, the intensity of electric field is proportional to cross-sectional area of the channel. Since the height of the channel is the same everywhere, the electric field intensity is proportional to the width of different sections (narrow and wide) in microchannel.

$$E_i/E_j = A_j/A_i = W_j/W_i \quad (5.1)$$

E: field intensity
A: cross-sectional area
W: width

The intensity of the applied electric field is measured with the unit of V/cm. The intensity of electric field is higher in the sections with shorter widths. In our microfluidic device, the channel is made from two different sections, i. e. narrow and wide. In narrow sections the intensity is higher and electroporation happens in areas with shorter widths. For current device, the width of narrow section is 100 μm. In wide parts of the microfluidic channel the electric field intensity is very low (less than 90 V/cm) which does not affect the cell membrane. In our experiments, wide section has a curving geometry with gradual change in width. It covers a range between 100 μm and 700 μm. The dimensions are explained with details in fabrication chapter.

5.2. Electric field intensity and COMSOL simulation

We performed COMSOL Multiphysics (version 4.2) simulations to determine electric field distribution in our curving channels. For making the calculation simpler, we assumed that

there is no ion concentration gradient in the flowing buffer which carries the electric current. Also, heating is considered negligible.

The continuity equation $\nabla . J = Q$ yields Poisson's equation. And Poisson's equation with absence of current source would yield to Laplace equation which is used for simulations:

$$\nabla . (-\sigma \nabla V) = 0 \qquad 5.2$$

J: current density ($J = \sigma E$)
E: Electric field ($E = \nabla V$)
V: voltage
Q: current source
σ : conductivity (S/m)

The conductivity of electroporation buffer (PB) could be considered isotropic and it is equal to 0.127 S/m [16]. In the microfluidic channel, all the boundaries except the parts which include electrodes are considered insulated for boundary conditions, i. e. $n . J = 0$.

Table 5.1 is a sample of the data for desired electric field intensities which is obtained from COMSOL simulation. In the first column one can see the voltage provided from dc power supply and the second column shows the electric field intensity in narrow sections. Longer effective lengths of the microfluidic channel need higher electric field intensity the same value of electric field intensity. Effective length of channel is the section confined in between two platinum wires (electrodes).

For very long effective lengths we need to apply high voltage from power supply in order to get the right field distribution in channel. This may result in gas bubbles formation in microchannel. We solve this problem by designing side chambers for installation of electrodes. More details are discussed in next section regarding gas bubble formation.

Table 5.1. Voltages needed to obtain different desired electric field intensity in the asymmetric curving channel from COMSOL Multiphysics simulation, 5 ms electroporation duration time, flow rate of 600 µl/min (14 pulses)

Voltage from dc power supply V	**electric field intensity in narrow section** V/cm
1160	600
1560	800
1960	1000
2360	1200
2760	1400
3160	1600
3560	1800
3960	2000

In figure 5.1 a sample of performed COMSOL simulation is provided for asymmetric channel with one turn. This sample shows that 150 V is needed to obtain 700 V/cm in narrow section. This is for the case of 2 ms electroporation duration time and 150 µl/min. Figure 5.2 shows the result of electric field intensity simulation for the case of 2 ms and 600 µl/min. In this case 6 narrow sections are needed and 750 V is needed from power supply to reach 700 V/cm in narrow sections. The side chamber location is changed to obtain desired number of pulses.

Also figure 5.3 shows the result of COMSOL simulation for applied electric field in control channel and 2 ms electroporation duration time is desired. This is a sample of conducted simulation when field intensity in narrow section is 700 V/cm. Simulation shows that for this specific condition 90 V is sufficient.

When flow rate is 150 µl/min only one narrow section is enough for 2 ms duration time. However, at 600 µl/min, 6 narrow sections are needed to obtain 2 ms. Figure 5.4 shows the simulation for field intensity of 700 V/cm in control channel when we apply 600 µl/min flow rate. Based on simulation result 580 V is needed to reach 700 V/cm in each narrow sections.

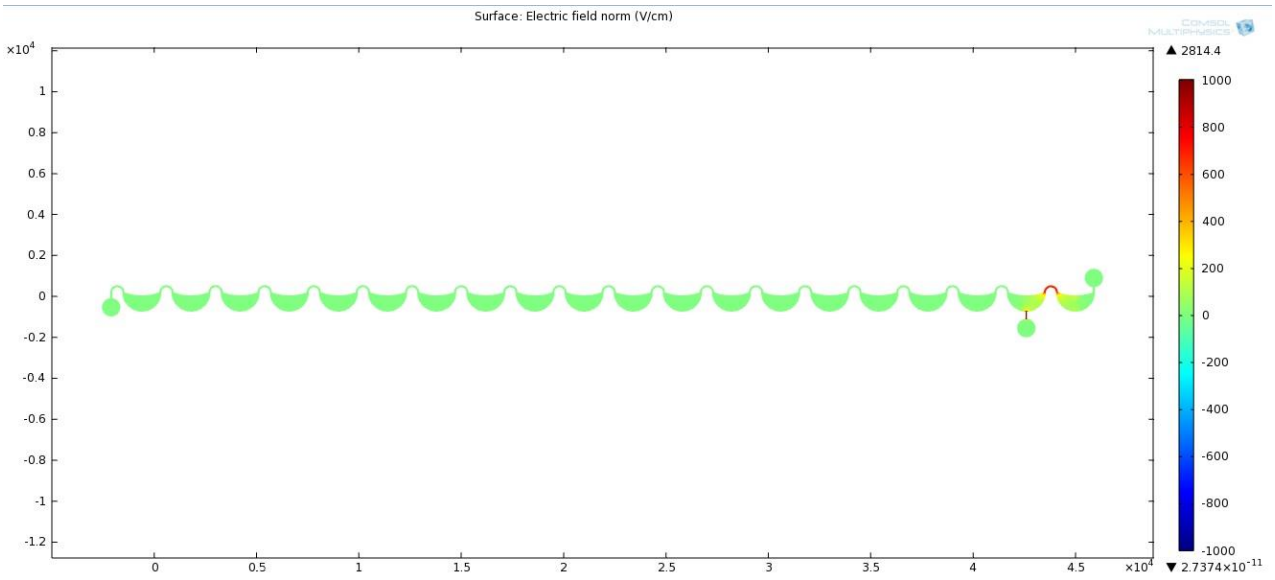

Figure 5.1. 150 V is needed to obtain electric field intensity of 700 V/cm in the asymmetric curving microfluidic channel based on COMSOL simulation, for the case of 2 ms electroporation duration time at flow rate equal to 150 µl/min

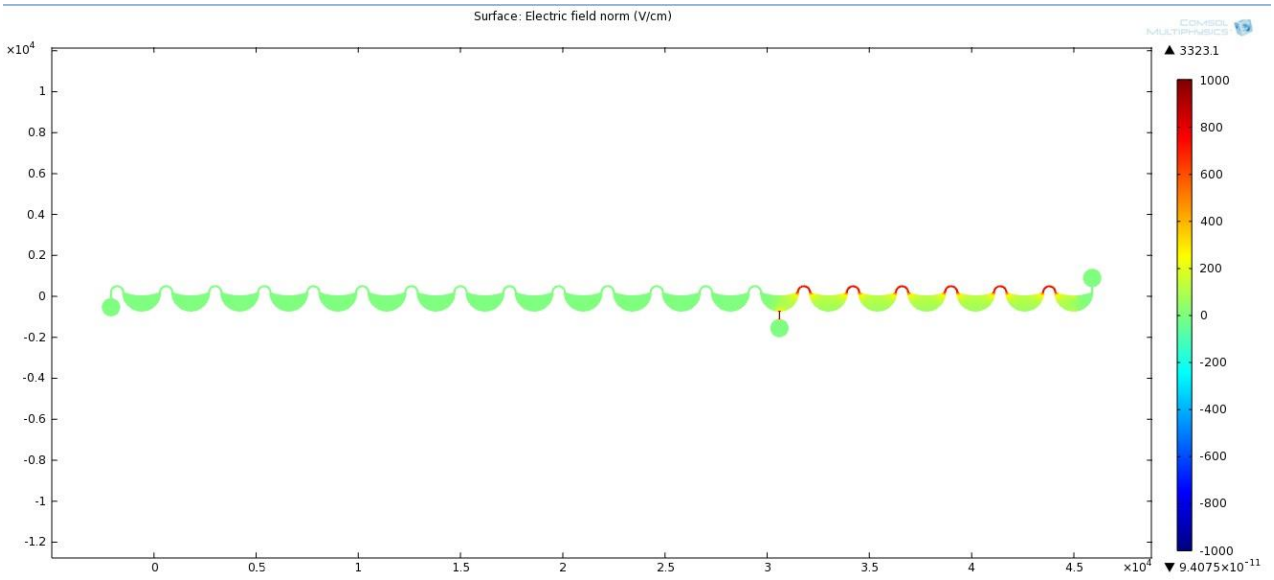

Figure 5.2. 750 V is needed to obtain electric field intensity of 700 V/cm in the asymmetric curving microfluidic channel based on COMSOL simulation, for the case of 2 ms electroporation duration time at flow rate equal to 600 µl/min

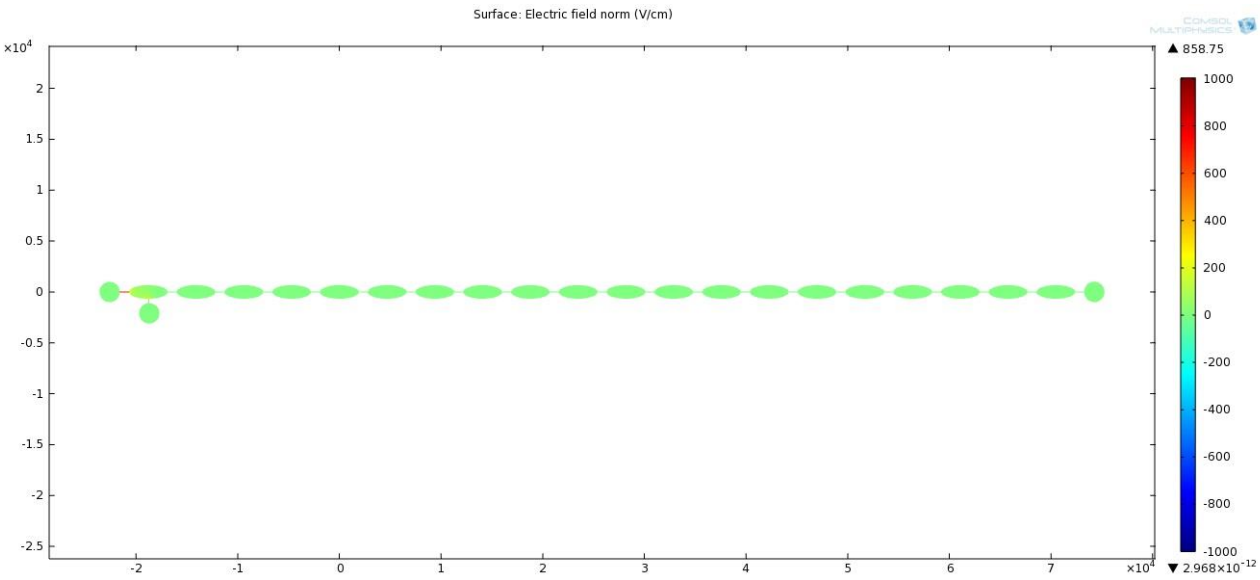

Figure 5.3. 90 V is needed to obtain electric field intensity of 700 V/cm in control channel based on COMSOL simulation, for the case of 2 ms electroporation duration time at flow rate equal to 150 µl/min

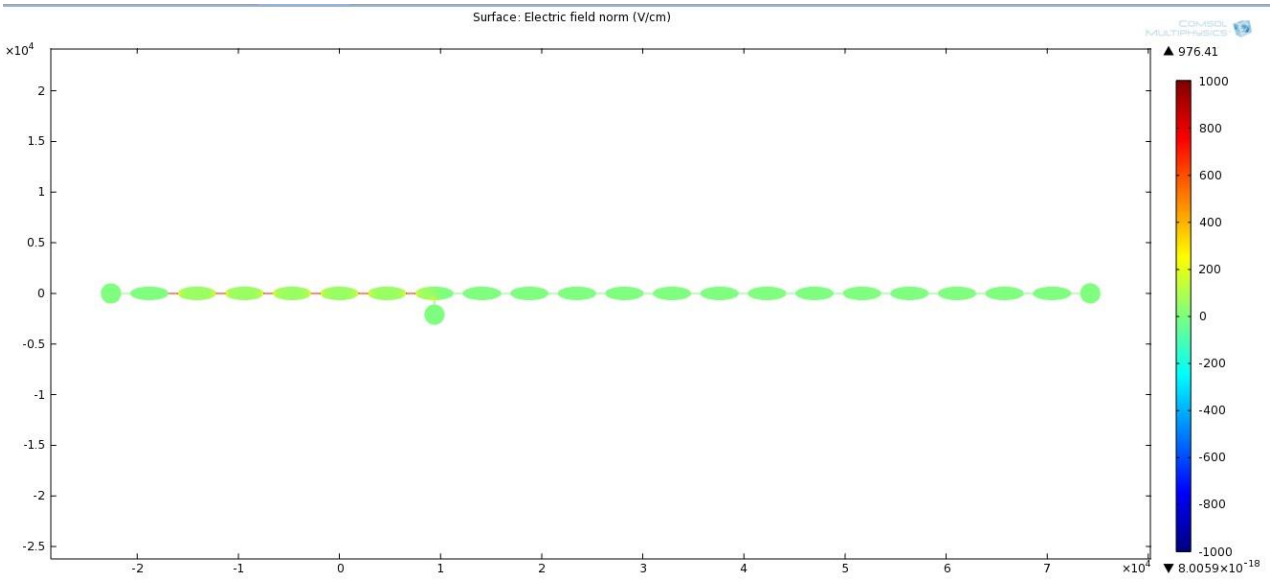

Figure 5.4. 580 V is needed to obtain electric field intensity of 700 V/cm in control channel based on COMSOL simulation, for the case of 2 ms electroporation duration time at flow rate equal to 600 µl/min

5.3. Gas bubble formation in microfluidic channel

External electric field can result in gas bubble formation around electrodes in microfluidic channel. This is more common in dc field due to Joule heating and electrolysis of water [64, 65]. In fact, if electric field intensity reaches a certain threshold (normally around 1100 V/cm for our design) gas bubbles are formed.

Gas bubbles are undesired and problematic in electroporation. The presence of gas bubble can completely change electric field distribution since it has different conductivity and is considered an electrical insulator. In addition, bubbles can dramatically reduce cell viability and damage cells.

The bubble formation can be prevented by reducing the conductivity of buffer by decreasing salts concentration. However, the conductivity of electroporation buffer cannot be lower than a certain value (~0.14 S/m) if we want to have effective electroporation. In order to solve this problem, we include a side chamber in our design, connected to main channel.

We install the platinum wire (electrode) in the chamber to collect the bubbles and prevent them from entering the microfluidic channel. Electrode should not touch the glass bottom of the channel. This extra side chamber is also helpful for adjusting the effective length of channel need for electroporation at different duration times and flow rates.

First, the electrode is placed inside a tubing connection in order to prevent leakage of buffer. Side chamber is prepared by punching the PDMS layer with a puncher that has the same diameter as tubing (1/16 inch). The size is similar to inlet of the channel. Figure 5.5 provides more details about electrode structure. Platinum wire is placed inside tubing and then is connected to copper wire. The copper wire later on would be connected to high voltage alligator clip. Some water-resistant paste is also used to fully seal around the tubing in order to prevent possible leakage from microfluidic channel.

(a) (b)

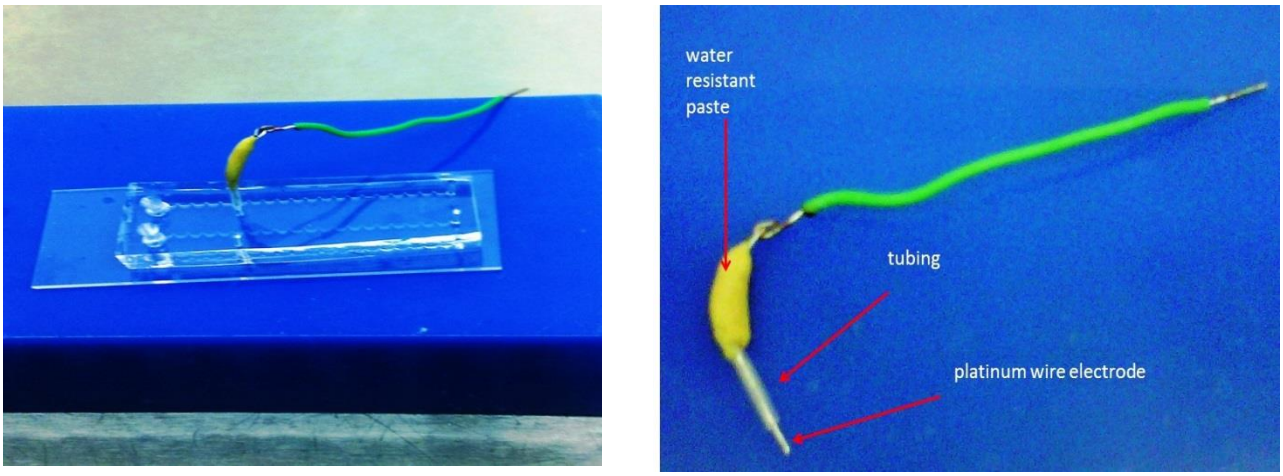

Figure 5.5. (a) An installed sealed electrode before performing electroporation. (b) The structure of modified electrode with water resistant paste and tubing.

Chapter 6. Transfection Efficiency and Cell Viability

6.1. Experiment design

Electroporation was successfully conducted in asymmetric curving channels under various conditions. Electroporation duration times equal to 2 ms, 5 ms, and 7 ms were examined. The electroporation was conducted under two different flow rates, i. e. 150 µl/ min (focused flow) and 600 µl/ min (complex flow). Electric field intensities were applied covering a range between 300 V/cm and 2200 V/cm. We show that higher field intensity in general would result in higher transfection efficiency. The same outcome is correct for longer electroporation duration times and fixed electric field intensity. Also, we successfully performed electroporation in control channel as well. Here, in chapter 6, the experimental procedure and the results are presented and are discussed.

6.1.1. Equipment list

-laminar flow hood equipped with UV irradiation system
-Syringe pump (Fusion 400, Chemyx)
-DC power supply (PS350, Stanford Research System)
-High voltage alligator clips
-Inverted phase-contrast and epifluorescence microscope system with 100 W mercury lamp (IX-71, Olympus) equipped with 20X, 10X, and 2X objectives
-High-resolution CCD camera (Hamamatsu, ORCA-285)
-Fluorescence filter cubes (for EGFP: exciter HQ480/40x, emitter HQ535/50m, and beam splitter Q505LP; for PI: exciter HQ535/50x, emitter HQ645/75m and beam splitter Q565LP, Chroma Technology)

6.1.2. Reagent and cell sample

Chinese hamster ovary cells (CHO-K1) are cultured at 37 $_{o}$C with 5% CO_2. DMEM culture medium is used (Mediatech, Inc., Herndon, VA). 10% (v/v) fetal bovine serum (FBS, Sigma, St. Louis, MO) and 1% (v/v) of streptomycin (100 mg/mL, Sigma) are also added to culture medium.

Electroporation buffer is comprised of 8 mM Na_2HPO_4, 2 mM KH_2PO_4, and 250 mM sucrose. The pH of the solution is equal to 7.4. Electroporation buffer is always filtered with 0.2μm filter to prevent channel clogging

6.1.3. Experiment procedure

CHO-K1 cells are harvested in exponential phase. Trypsin-EDTA solution is used to detach cells from the surface of flask. CHO-K1 cells are adherent to surface. Cells are cultured to reach around 80% confluency.

The cell concentration is measured by using a hemocytometer to make sure that cells are healthy and are naturally proliferating. Cells which are used for electroporation must be healthy and be able to actively reproduce. CHO-K1 cells are passaged for every two days. And, in each time the ratio for passage is one to ten. Normally one can get around $2 \times 10^{\wedge 6}$ cell/ml from each 25 ml flask. There is always a limitation for the number of cell passages. In fact, multiple passages may change cell properties and therefore results in poor transfection efficiency.

After detaching CHO-K1 cells from flask by employing Trypsin-EDTA, we put them in a 15 ml centrifuge tube while they are suspended in 2.5 ml of culture medium. Then they would be centrifuged at 300 g and room temperature for 5 minutes. Supernatant is aspirated and is thrown away. A small amount of culture medium must be remained in the tube to prevent cell damage, around 50 μl is enough.

Around 5 ml of electroporation buffer is added to the tube and cells are gently dispersed by pipetting. Vigorous pipetting must be avoided to prevent cell damage. It can also affect both

cell viability and transfection efficiency. Cells become resuspended. At this point cells are ready to be washed and be centrifuged at 300 g for 5 minutes at room temperature.

After this part, supernatant will be removed and cells be resuspended in electroporation buffer again. The amount of buffer volume added at this point depends on optimum cell concentration for the experiment which for our case is $2 \times 10^{\wedge 6}$ cells/ml. The buffer volume can be determined by using a hemocytometer to find out cell concentration at the beginning. Then appropriate amount of buffer can be used to produce the right cell concentration for electroporation buffer.

At this point, EGFP plasmid DNA is added to the solution. Plasmid DNA must have a desired concentration around 40 μg per ml of solution. The electroporation solution contains both cells and plasmid DNA. The solution must be mixed by multiple, gentle pipetting. This will result in a single cell suspension that provides a good mixing of plasmid DNA and cells with a uniform distribution. Also, this will prevent possible channel clogs.

Plasmid DNA concentration is important not only for transfection efficiency but also for cell viability too. As mentioned above, the desired concentration for plasmid DNA (EGFP-C1 Plasmid) is 40 μg per ml while the desired concentration for CHO-K1 cells is $2 \times 10^{\wedge 6}$ cells per ml for electroporation. Higher concentrations of plasmid can damage cell health and is toxic.

At this point cells are left in ice exactly before starting electroporation. This ice incubation stage increases cell viability. The ice incubation cannot last more than one hour because long incubation time makes cells unhealthy and would also affect transfection efficiency and cell viability too. After ice incubation, cells are ready for flow-through electroporation. Electroporation buffer which also includes cells is loaded to a 1 ml sterile plastic syringe. Then it will be introduced to microfluidic channel by using a syringe pump and tubings (connected to 1/16-inch male flangeless nut and a 1/16-inch flangeless ferrule and a female adaptor connected to the syringe). Figure 6.1 shows the experimental setup which includes dc power supply, syringe pump and the microfluidic chip.

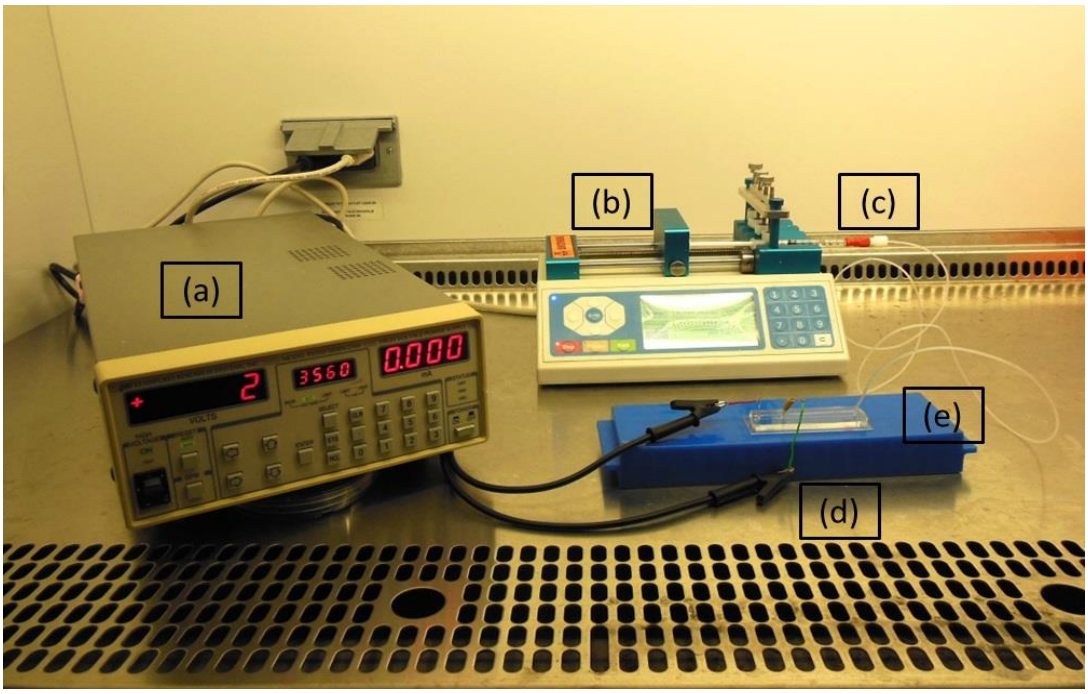

Figure 6.1. Experimental setup for flow-through electroporation in laminar flow safety cabinet equipped with UV for disinfection, (a) dc high voltage power supply, (b) Syringe pump, (c) 1 ml plastic syringe, (d) High voltage alligator clips connected to copper and platinum wires, (e) Microfluidic chip located on top of a plastic base.

In order to prevent contamination, electroporation is conducted in a laminar flow safety cabinet. The tubing and connections can be reused. They just need to be sterilized before experiment by UV exposure for at least one hour. The microfluidic chip must also be sterilized by UV exposure prior to electroporation.

Before priming channel with electroporation solution, the channel must be washed with PB buffer. This should be continued for around five minutes to get rid of air inside the channel and remove all possible non-microbial impurities such as PDMS residues. At this point, the tubing must be removed from the channel's inlet very gently. If one removes the tubing without enough care, there is a high risk of introducing air bubbles to microfluidic channel. Microscope can be used to make sure that there is no air bubble present in the channel before performing electroporation.

After washing step, the negative platinum electrode is carefully placed in the side chamber connected to main fluidic channel. Before starting the electroporation one can also check the sealing of the connection between side electrode's tubing and side chamber demonstrated in figure 5.5. The platinum wire in side chamber is connected to the negative terminal of power supply by clipping the wire to a copper wire.

By using a side chamber and connecting platinum electrode to PDMS via tubing, the risk of leakage becomes very little in compare to inserting platinum wire directly in PDMS elastic layer. The positive electrode is placed in outlet reservoir which is punched at the end of microfluidic channel as explained in fabrication section. The platinum wire in outlet is connected to positive terminal of power supply by using high voltage alligator clips. The alligator connector must be ranked for high voltage currents above 5000 V.

Before turning on the syringe pump, one must make sure that electrodes are completely connected to electroporation solution. Pump parameters must be set. It includes syringe type and diameter, syringe volume, and flow rate. Also, electric parameters must be set for dc power supply as well. The details about power supply parameters and electric field distribution in the channels have been comprehensively discussed in Electroporation and electric field distribution chapter.

On the power supply equipment there are separate digital displays which show voltage in V and current in mA. The maximum power of the supplier is 25 watts. And maximum voltage is 5000 V. Also, the maximum current is 5 mA. Throughout the electroporation process, the current must be fixed. If current changes or fluctuates during the experiment, it is mostly a sign of having gas bubbles in channel and therefore the conductivity of solution would change as well which is not favorable.

After setting all the parameters on syringe pump and power supply, it is time to start electroporation process. One should turn on the syringe pump and power supply at the same time and turn them off at the same time too to preserve the desired electroporation duration time.

After pumping electroporation buffer into microchannel, in which cells and plasmid DNA are floated, through the microfluidic channel, cells will be collected in outlet reservoir by using pipet. The collected cells then are transferred to two separate well plates. One well plate would

be used for viability test and the other one for transfection efficiency tests. 96 sterilized well plates are used. They are filled with culture medium incubated in 37 $_{o}$C water bath before the electroporation for pre-warming. A volume of 15 µl of collected cells (electroporation solution) at the end of electroporation will be transferred to a well filled with 200 µl of culture medium for each well plate (30 µl in total). Three separate samples are collected for each different electric field distribution for fixed duration time and flow rate. While working with high voltage current one must be very careful to not touch electric connections to avoid any possible risks of electric shock.

After transferring electroporated cells to well plates with pre-warmed culture medium, the well plates immediately are placed in incubator with 37 $_{o}$C temperature and 5% CO_2. The well plate for viability assay is incubated for one hour before starting viability assay. While the well plate for transfection efficiency test is kept in the same condition for 48 hours.

6.2. Parameters controlling cell viability

6.2.1. Electroporation duration time

Electric field intensity reaches the electroporation threshold just in narrow sections. Electroporation threshold is around 300 V/cm for the case of CHO-K1 cells (Chinese hamster ovary). This threshold can be reached as discussed in Electroporation and electric field distribution chapter. It is determined by dc constant voltage applied to effective part of channel and the geometry of channel (cross section width). The electric field distribution inside microfluidic channel can be simulated by COMSOL Multiphysics.

Electroporation duration time can be adjusted by controlling cell velocity, length of narrow sections, and pulse number. By increasing duration time of electroporation, cell residency time will also be increased and cell will be exposed to electric field for longer time. So in a fixed electric field intensity, by increasing electroporation duration time, we expect drop in cell viability rate and increase in transfection efficiency. Thus, transfection efficiency reaches its peak in shorter duration times. The same fact is correct for decrease in cell viability.

6.2.2. Electric field intensity

Stronger electric fields would cause larger pores on the surface of cell membrane which are harder to be recovered. This will increase cells inactivation rate. Therefore, by increasing electric field intensity in the same electroporation duration time, we expect reduction of cell viability. Electric field intensity in wide section is not strong enough to reach the threshold for electroporation in the case of CHO-K1 cells (~300 V/cm). So, narrow sections are the only part of the microfluidic channel that can be effective for delivering plasmid DNA.

6.3. Viability assay

Cell viability can be determined by PI staining. After one hour, the well plate for viability test is removed from incubator (37 $_{o}$C and 5% CO_2). The sample is centrifuged at 300 g for 5 minutes at room temperature. After this floating cells will precipitate at the bottom of the wells. Supernatant is removed gently by pipet. Cells are rinsed with pre-warmed PBS, 200 µl for each well.

Again, the sample must be centrifuged at the same conditions as before to settle the washed cells at the bottom of the wells. The PBS is aspirated and discarded. Again, pre-warmed PBS is added to wells. This time PBS contains PI dye. PI working concentration is 1 µg per ml of solution. Then after adding PBS and PI, the sample is incubated at room temperature in dark for around 10 minutes. By following this protocol dead cells will be stained.

When using PI special care is required since it is considered to be carcinogenic. And, it must be collected in special boxes prepared for biohazard waste. Two sets of gloves can be used to prevent possible contact of skin with PI.

After 10 minutes, the sample must be centrifuged again in the same condition to make sure all the cells are settled in the bottom of wells. Cells must be rinsed again with pre-warmed PBS (~200 µl for each well). Then after another centrifugation stage the sample is ready for fluorescent microscopy.

Phase contrast and fluorescent images are taken with inverted phase contrast epi-fluorescence microscope which is equipped with a 20X or 10X dry objectives and a CCD camera. For PI, appropriate filters must be chosen for excitation and emission in a range of 493 nm and 632 nm respectively (exciter HQ535/50x, emitter HQ645/75m and beam splitter Q565LP, Chroma Technology). The images are taken in different locations of each sample to cover more cells. Images are transferred to a computer by CCD camera and will be saved. ImageJ is used to perform image analysis on collected images. Around 2000 cells are enumerated by ImageJ for each sample.

In order to calculate viability for each sample, the number of dead cells is determined by counting the cells which express fluorescent. Then by counting all the cells in each sample in phase contrast image, one can calculate the value of viable cells. For obtaining reliable data, around 2000 cells are enumerated for each sample (well). For providing more details on image analysis figure 6.2 is presented here. The images are taken one hour after electroporation. Figure 6.2 (a) shows a phase contrast image taken by the microscope. Part (b) shows fluorescent image. Part (c) is an overlap image from previous images to make sure that the shiny spots match the shape of cells and are not from any other sources like possible contaminations.

(a) (b) (c)

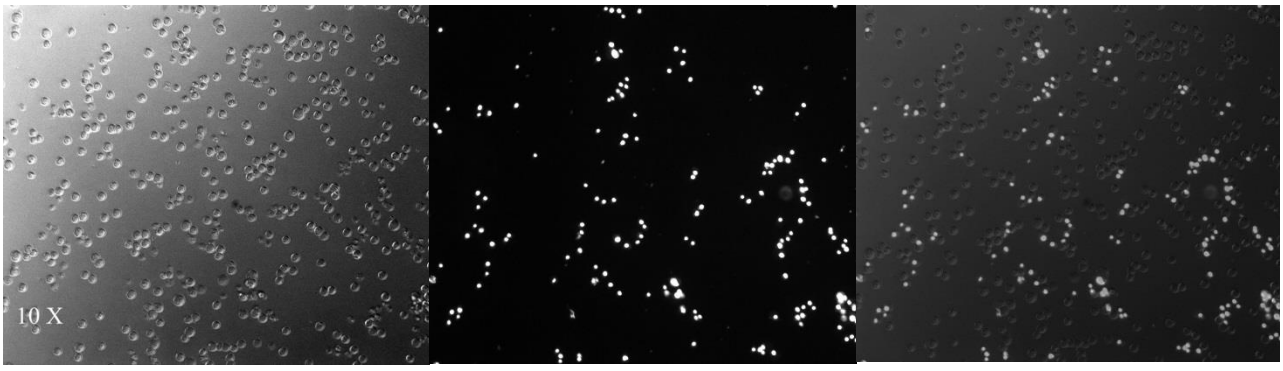

Figure 6.2. (a) Phase contrast image of cells from viability assay sample, after one hour post electroporation. (b) Fluorescent image after PI labeling. (c) The overlap of images.

Also, figure 6.3 depicts the change in cell population by the rise in applied external electric field intensity, at fixed electroporation duration time. These post electroporation images are taken after 1 and 48 hours, being cultures at 37 $_{o}$C and 5% CO_2.

6.4. Parameters controlling transfection efficiency

6.4.1. Electroporation duration time

Generally we expect higher delivery rates by increasing duration time for electroporation however there is a limit for extending duration time. In fact, if duration time exceeds the desired range, all cells could die because of overexposure to electric field.

Electroporation duration time can be adjusted by changing flow rate, geometry of microfluidic channel, and changing the location of electrodes which defines effective length of microfluidic channel. Electroporation duration time is associated with narrow sections. Resident time of cells in wide section can be ignored due to low electric field intensity.

6.4.2. Electric field intensity

Electric field distribution is also another key factor in determining transfection efficiency. It cannot be below electroporation threshold which is around 300 V/cm for CHO-K1 cells. It means in the areas below this value, electroporation would not happen and the cell membrane would not be affected by the presence of external electric field. Thus, narrow sections in our asymmetric curving microfluidic channel are the regions that electroporation happens.

Generally by increasing electric field intensity at fixed electroporation duration time we expect to see higher rates of transfection. However, after exceeding certain levels cells can be damaged and be killed. Also, our results confirm previous claims in literature about the fact that exceeding a certain limit of electric field intensity can sometimes decrease transfection efficiency [85].

(a) (d)

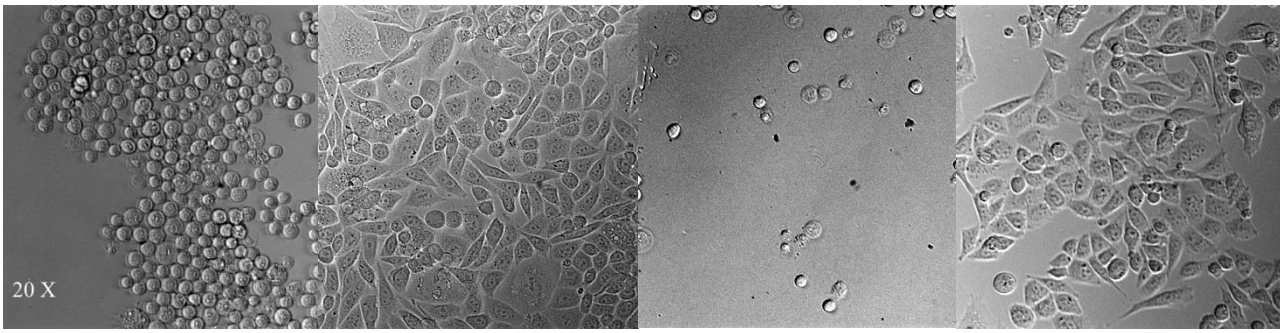

(b) (e)

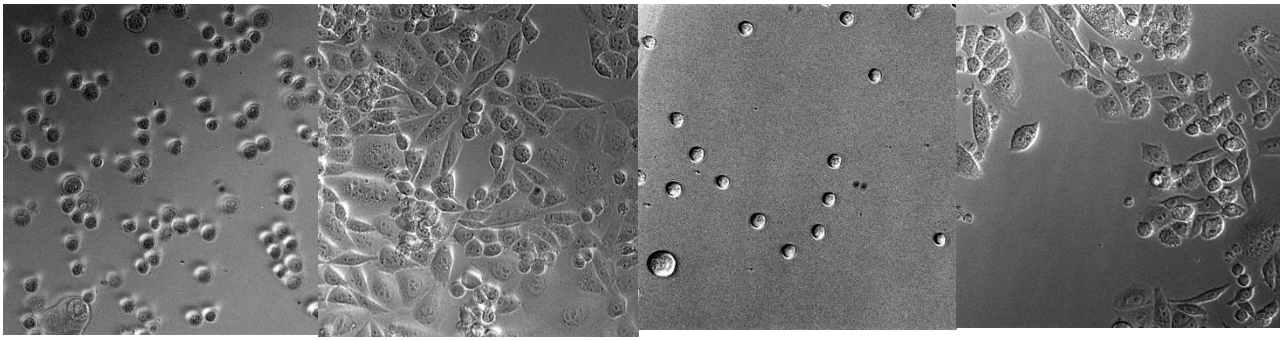

(c) (f)

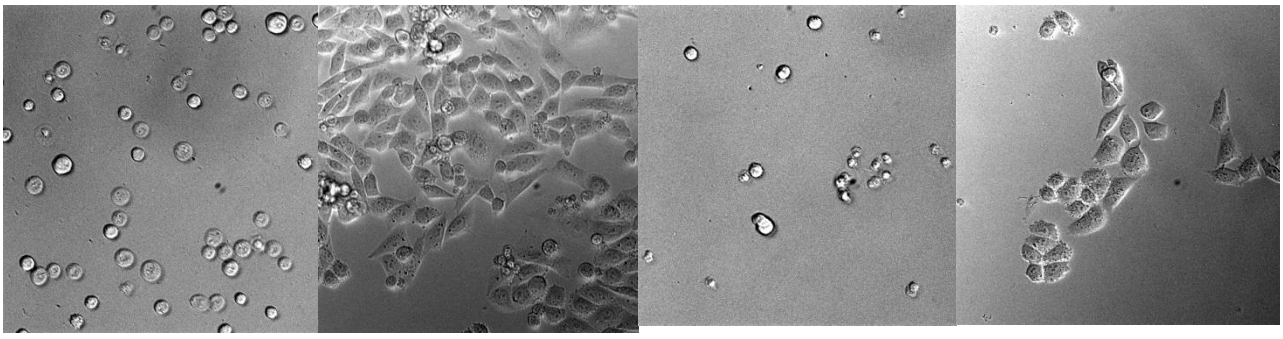

Figure 6.3. In each part,(a) to (f), left image is from viability well plate (taken one hour post electroporation) while left image is from transfection efficiency sample (taken 48 hours post electroporation). The electric field intensity is increased from (a) to (b) while the electroporation duration time is kept constant. Cell population decrease happens by rise in electric field intensity.

6.5. Transfection efficiency assay

Electroporated CHO-K1cells need around 48 hours to reach the pick of expressing EGFP. So, after incubating the sample for 48 hours at 37 $_{o}$C and 5% of CO_2, we centrifuge the well plate at 300 g for 5 minutes at room temperature. This is to make sure cells are settled at the bottom of wells. Then the supernatant which is culture medium is gently removed by pipet and be discarded. PBS is added to wells to wash cells, 200 µl for each well. Again the sample is centrifuged at the same condition. After this part cells are ready for imaging.

Both phase contrast and fluorescent images are taken with inverted phase contrast epi-fluorescence microscope which is equipped with 20X or 10X dry objective. The microscope is connected to a CCD camera (Hamamatsu, ORCA-285) that can collect the images and transfer them to a computer for further processing.

For EGFP one must use appropriate UV filters to be able to take fluorescent images. The excitation filter for EGFP is maximum = 488 nm and emission maximum = 507 nm exciter HQ480/40x, emitter HQ535/50m, and beam splitter Q505LP). Both phase contrast and fluorescent images are taken in deferent locations of the sample in order to cover more areas and collect unbiased data. ImageJ is used to analyze collected images. For obtaining reliable data, around 2000 cells are enumerated for each sample (well).

In order to quantitatively calculate transfection efficiency for each experiment, first the number of all viable cells after 48 hours is obtained from phase contrast images. Then, the number of cells which express EGFP are found from fluorescent images. An overlap image by adding phase contrast and fluorescent images together is obtained. This can confirm that the source of fluorescent light is a cell and not any possible contamination. Figure 6.4. shows a phase contrast, fluorescent, and overlap image. In part (b) and (c) of figure 6.4 the shiny spots are healthy CHO-K1 cells expressing EGFP after 48 hours post electroporation.

(a) (b) (c)

Figure 6.4. (a) Phase contrast, (b) fluorescent, and (c) overlap images of electroporated CHO-K1cells after 48 hours, being cultured in 37 $_{o}$C and 5% of CO_2.

6.6. Cell viability and transfection efficiency in asymmetric curving microfluidic channels

In figure 6.5 the result for viability assays are shown for different electroporation duration times, under focused regime which happens at 150 µl/min flow rate. These data are from asymmetric design, i. e. the main channel. Blue data points represent 2 ms duration time. In the main channel, when the flow rate is equal to 150 µl/min, only one narrow section is enough to get this duration time. As we expect, in fixed electroporation duration time, the increase in electric field intensity decreases cell viability. For example, when field intensity is 600 V/cm and the duration time is 2m, cell viability is 99.5%, while when field intensity is 1800 V/cm, cell viability is 89.7%. The drop in cell viability is not very intense at 2 ms duration time because it is a very short period and cells do not stay long in narrow section. Thus, they are less affected by external electric field. For 5 ms duration time, red squares, the drop in cell viability with field intensity increase is more drastic. The cell viability decreases from 99.0% at 600 V/cm to 24.5% at 1800 V/cm. The viability difference between 2 ms and 5 ms is more noticeable in higher electric fields. At 1800 V/cm electric field intensity, the difference in cell viability between 2 ms and 5 ms is around 60%. This difference is smaller in lower field intensities and is almost zero at 600 V/cm. Green data points (triangles) are for longest electroporation time in our experiments, i. e. 7 ms. As we expect, for 7 ms duration time, the drop in cell viability is even more intense

compared to 5 ms, and 2ms. It decreases from 99.0% to 37.3% at 400 V/cm and 1400 V/cm respectively. The difference between viability rates for various duration times increases at higher field intensities. On the other hand, in low field intensities, viability percentage is almost the same. For example, at 600 V/cm the viability result is above 99% for all duration times.

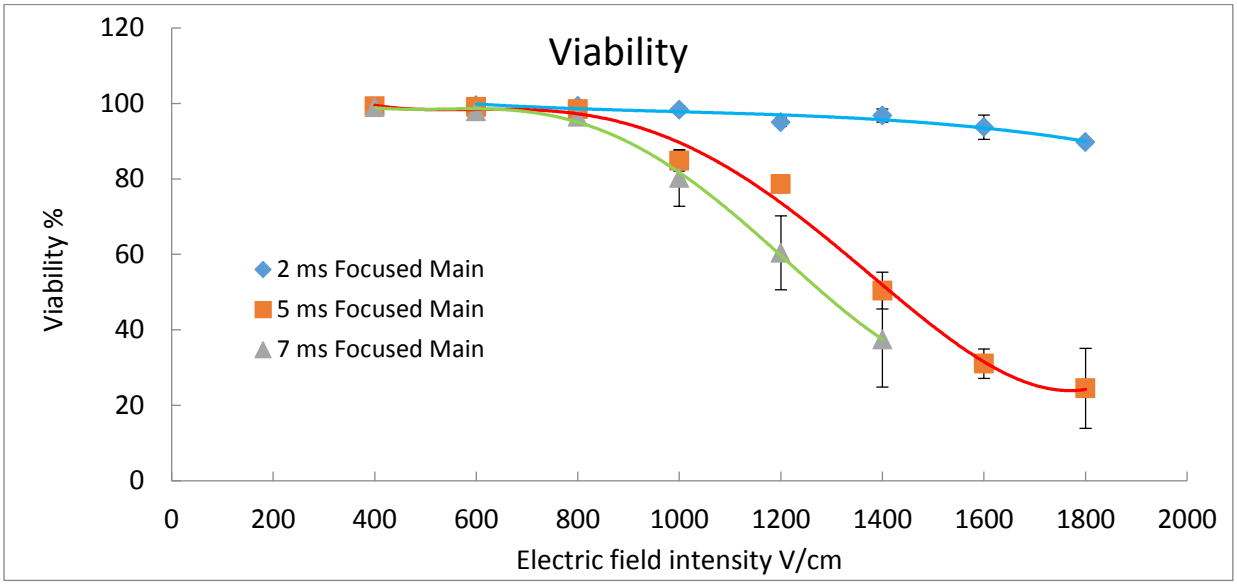

Figure 6.5. Viability result for focused flow (150 µl/min) in asymmetric curving channel (main channel)

As it is discussed earlier, electroporated cells are examined for transfection efficiency after being cultured for 48 hours at 37 $_{o}$C and 5% CO_2. The result for transfection efficiency for asymmetric design is presented in figure 6.6. This data is for flow rate equal to150 µl/min which results in a focused flow for cells. Better delivery of plasmid DNA (higher transfection rate) is reached by optimizing electroporation duration time and electric field intensity. Normally, the effect of longer duration time is similar to higher field intensity. Therefore, transfection efficiency would reach its peak in larger field intensities at shorter duration times. Blue dots represent data points for transfection efficiency for 2 ms electroporation duration time. The highest delivery rate happens at 1800 V/cm. For 2 ms, transfection efficiency rate is under 5% from 600 to 1000 V/cm field intensities. It increases up to12.9% at field intensity equal to 1800 V/cm.

As we expect, the peak for transfection happens at lower field intensities for 5 ms duration time in comparison with 2 ms. As it is shown on figure 6.6 (red squares), delivery reaches its peak at 1200 V/cm (18.6%) for 5 ms duration time, while, according to our data, for 2 ms, the highest delivery happens at 1800 V/cm. The increase in field intensity does not always favor transfection rate. At 5 ms duration time, transfection efficiency drops when field intensity is higher than 1200 V/cm. The efficiency rate at 1800 V/cm is comparable to the rate at 400 V/cm in 5 ms duration time, i. e. 0.76% and 0.63% respectively.

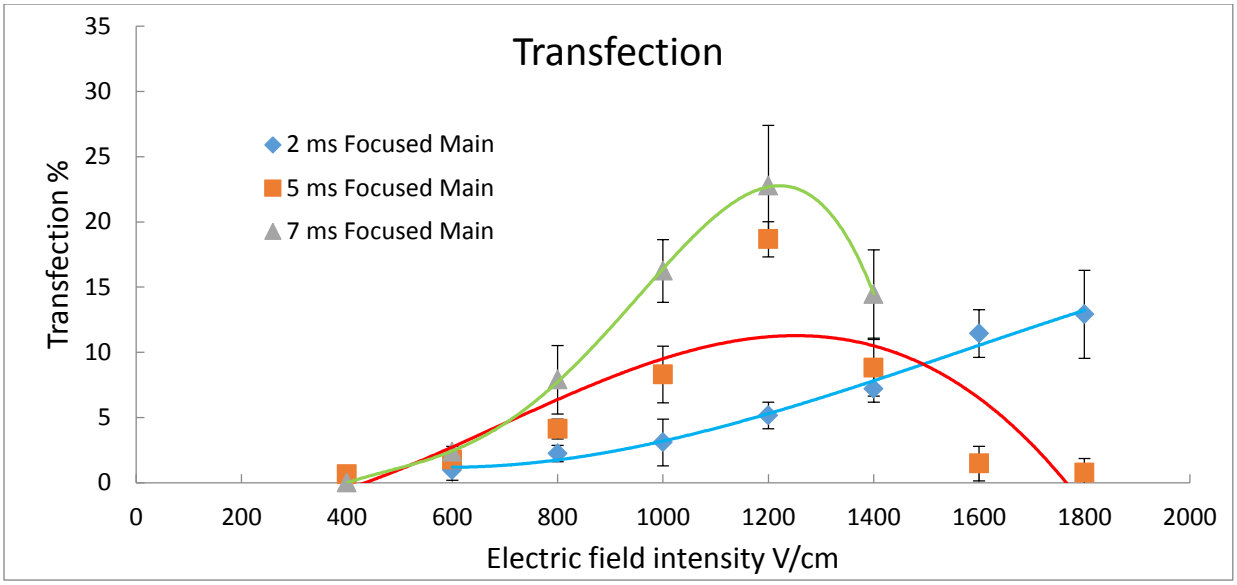

Figure 6.6. Transfection efficiency result for focused flow (150 µl/min) in asymmetric curving channel (main channel)

For 7 ms electroporation duration time, the delivery rate reaches its peak at 1200 V/cm. The transfection rate is bigger at lower intensity fields compared to 5 ms and 2 ms duration times. For example, at 1000 V/cm, the transfection efficiency at 7 ms is equal to 22.7% while it is 18.6% for 5 ms, and 5.15% for 2 ms which is considerably lower than the result for 7 ms. By exceeding 1200 V/cm, field intensity acts unfavorable. In fact, transfection rate drops from 22.7% at 1200 V/cm to 14.4% at 1600 V/cm. At very low field intensity (around 400 V/cm) all three duration times result in low transfection rate. Even at 7ms, electric field intensity is not high enough to increase transmembrane potential for nano-scale pore formation.

For the case of higher flow rate (600 µl/min) which results in a complex pattern for particles (cells) inside asymmetric curving microfluidic channel, cell viability data is collected for various electroporation duration times, i. e. 2 ms, 5 ms, and 7 ms. Larger number of turns (pulses) are present for electroporation at the flow rate of 600 µl/min compared to 150 µl/min. This is inevitable because we want to maintain the same duration times. Therefore, we need to use longer length of the channel (effective length). For example, in order to obtain 2 ms duration time at focused flow (flow rate = 150 µl/min) just one turn (narrow section) is enough, however, based on cell velocity in asymmetric channel in complex flow (flow rate = 600 µl/min) 6 turns are needed to maintain 2 ms duration time.

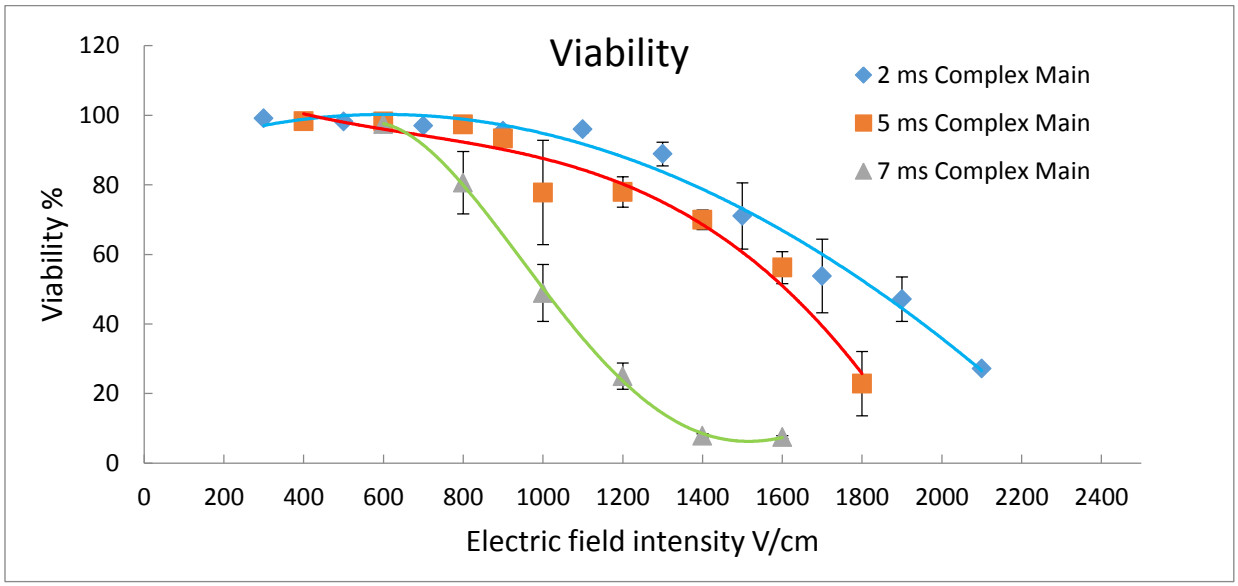

Figure 6.7. Viability result for complex flow (600 µl/min) in asymmetric curving channel (main channel)

Cell viability rate is higher at lower duration times at fixed electric field intensity. For complex flow, the increase in field intensity would also result in lower cell viability percentages. The drop in viability is smaller at 2 ms. In figure 6.7, blue dots show the viability rates for 2 ms at various field intensities. The change is very little at lower field intensities, from 300 V/cm to 1300 V/cm. In this range, cell viability changes only around 4%, i. e. from 99.0% at 300 V/cm to

95.9% at 1100 V/cm. The drop in viability begins from field intensity equal to 1300 V/cm. The decrease in viability is gradual at lower field intensities; however it becomes more drastic after 1500 V/cm. The lowest viability rate for complex flow and 2 ms duration time happens at 2100 V/cm which is only 27.1%.

For 5 ms electroporation duration time under complex flow condition (flow rate = 600 µl/min), the decrease is more intense than 2 ms, as it is expected. Cell viability reaches its minimum value (22.9%) at 1800 V/cm for 5 ms duration time which is 400 V/cm lower than the case for 2 ms. At lower field intensities, i. e. from 300 V/cm to 900 V/cm the drop in viability is not considerable and it is similar to 2 ms case. Viability is equal to 93.3% at 900 V/cm for 5 ms while it is 95.5% at 2 ms.

When the duration time is equal to 7 ms in complex flow (600 µl/min) inside asymmetric curving channel, cell viability decreases more drastically. The drop begins at filed intensities as low as 800 V/cm where the viability rate is around 97% for both 2 ms, and 5 ms, it is only 80.6% for 7 ms. Cell viability reaches 25% at a field intensity of 1200 V/cm while this happen at much higher field intensity for 2 ms (higher than 2200 V/cm), and it happens at 5 ms in 1800 V/cm. For 7 ms, the viability is around 7.8% at 1400 V/cm while it is 70% for 5 ms which shows a considerable drop. The minimum value recorded for cell viability at 7 ms is 7.5% at 1600 V/cm electric field intensity. For 7 ms at 600 V/cm (97.5%) the result is almost similar to viability rate at 5 ms which is 98.2%.

The data for transfection efficiency at flow rate of 600 µl/min are shown at figure 6.8. This is from asymmetric curving channel. As it is discussed earlier, cells would experience complex flow at this flow rate. Figure 6.8 shows all data for 2 ms, 5ms, and 7 ms electroporation duration times for the discussed condition. When duration time is 7 ms, transfection efficiency has a peak at 800 V/cm. At higher field intensities (larger than 800 V/cm) the transfection rate drops, until it approaches 0.95% at 1600 V/cm. The delivery rate is 2.47% at 600 V/cm.

For 5 ms duration time, transfection efficiency reaches its maximum value at 1000 V/cm which is 200 V/cm higher than the field intensity associated with the peak for 7 ms. The maximum transfection percentage is 7.56% for 5 ms at 1000 V/cm. At 600 V/cm, the delivery rate (1.41%) is close to delivery rate for 7 ms (2.47%). The transfection efficiency drops when

field intensity exceeds 1200 V/cm. This drop happens in lower field intensities for 7 ms, i. e. around 800 V/cm. At 800 V/cm the transfection rate is 8.08% for 7 ms while it is 3.57% for 5 ms which is around 4.5% lower. Transfection rate is very low at 400 V/cm (0.5%) as expected. Also, delivery rate is as low as 0.53% at 1800 V/cm.

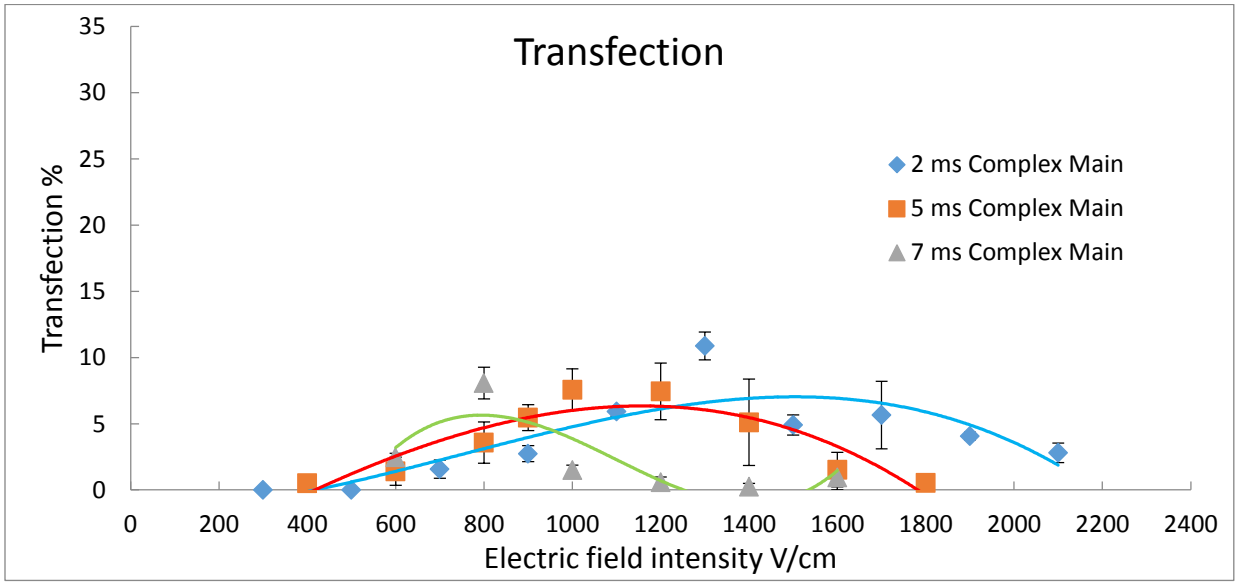

Figure 6.8. Transfection efficiency result for complex flow (600 µl/min) in asymmetric curving channel (main channel)

In the case of 2 ms (blue dots in figure 6.8) transfection efficiency has a peak at 1300 V/cm. The peak for 2 ms is reached at higher field intensity in comparison with 5 ms, and 7ms. It is expected because cells are exposed to electric field for a shorter period of time. The transfection efficiency rises from 0.0% at 300 V/cm and 500 V/cm to its maximum value, i. e. 10.8% at 1300 V/cm. The transfection rate drops after exceeding 1300 V/cm. This drop happen at lower electric field intensities for 5 ms, and 7 ms duration times, i. e. 1200 V/cm and 800 V/cm respectively. The value for transfection efficiency is 2.8% for the highest field intensity which is 2100 V/cm for 2 ms duration time.

6.6.1. Comparison between focused and complex flow (main channel)

Figure 6.9 presents viability data for 2 ms electroporation duration time. The presented curves are both for asymmetric curving channel. The blue dots represent focused flow results (flow rate = 150 µl/min) while red squares show the outcome for complex flow (flow rate = 600 µl/min). In order to maintain the same duration time (2 ms) in higher flow rate, the channel effective length (section between two electrodes) is extended. Therefore, in the case of complex flow we used 6 turns (narrow sections) to obtain 2 ms electroporation duration time while only one turn is enough when applied flow rate is 150 µl/min.

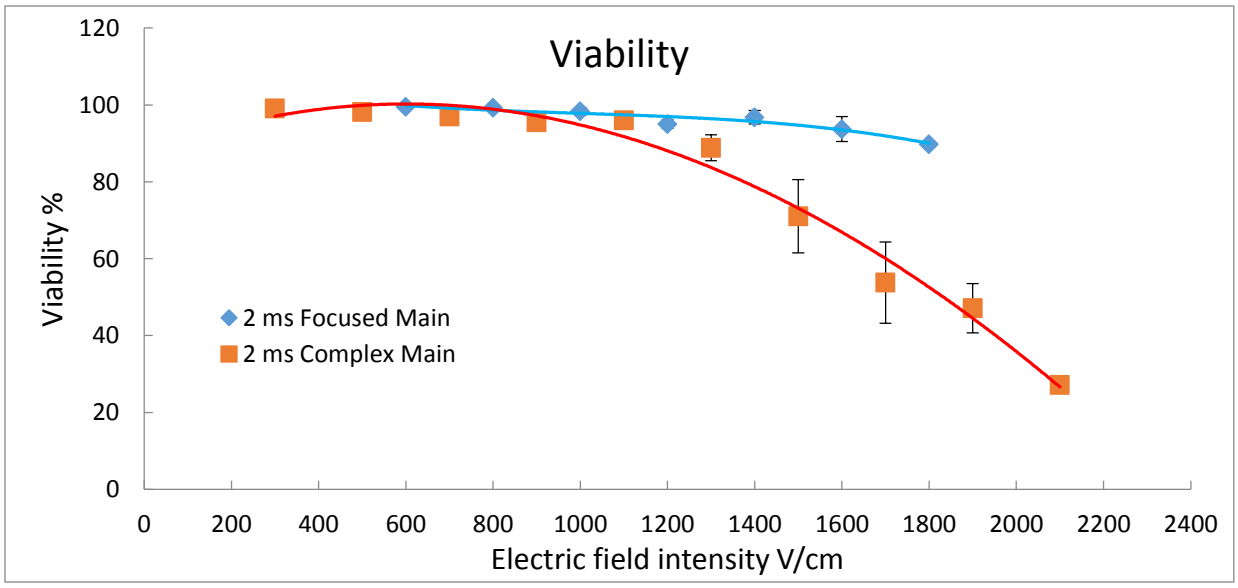

Figure 6.9. Viability result for 2 ms electroporation duration time, comparison between focused and complex flows (main channel)

Viability percentages are very close for both cases at lower field intensities, i. e. from 400 V/cm to 1100 V/cm. After exceeding 1200 V/cm cells in both channels experience higher rates of inactivation; however the drop is more noticeable in complex flow condition. The difference between viability rates in two channels becomes larger at higher electric field intensities.

Transfection efficiency result is presented in figure 6.10 for 2 ms duration time in both focused and complex flow conditions, in asymmetric curving channel. The delivery rate has a maximum value at lower field intensity for complex flow case. It reaches the maximum percentage at 1300 V/cm, which is 10.8%, while the transfection rate is around 6.2% for focused flow at the same field intensity.

The peak for focused flow shows up at 1800 V/cm and is a higher value from the maximum delivery rate in complex flow. The highest transfection rate for 2 ms in focused flow is 12.9% which is 2.1% higher than the highest value in complex flow.

The data for viability rates at 5 ms electroporation duration time in asymmetric curving channel is reported in figure 6.11. This figure includes the result for both focused and complex flow. The number of pulses (i. e. narrow sections) for complex flow condition (flow rate = 600 µl/min) is higher compared to focused flow (flow rate = 150 µl/min). We need a longer length for the channel in order to maintain 5 ms duration time at the higher flow rate. Based on calculations for cell velocity and the traveled distance for cells in narrow section (where electric field intensity is high enough for the purpose of electroporation) concluded in Table 4.1, 14 turns are needed for the case of complex flow while 2 turns are enough for focused flow to obtain 5 ms duration time.

The difference in viability rates at lower field intensities is very short. In fact, from 400 V/cm to 1000 V/cm field intensities, the results for viability are almost the same under both regimes, i. e. focused and complex flow. The changes begin from 1000 V/cm while the difference is not considerable at first; however it increases at higher field intensities.

The highest divergence happen at 1600 V/cm where the viability rate for complex flow (red squares) is 56.2 % while it is 31.0% for focused flow (blue dots) condition. At very high field intensity, 1800 V/cm, the inactivation rates of cells are almost the same in both conditions, i. e, around 23%.

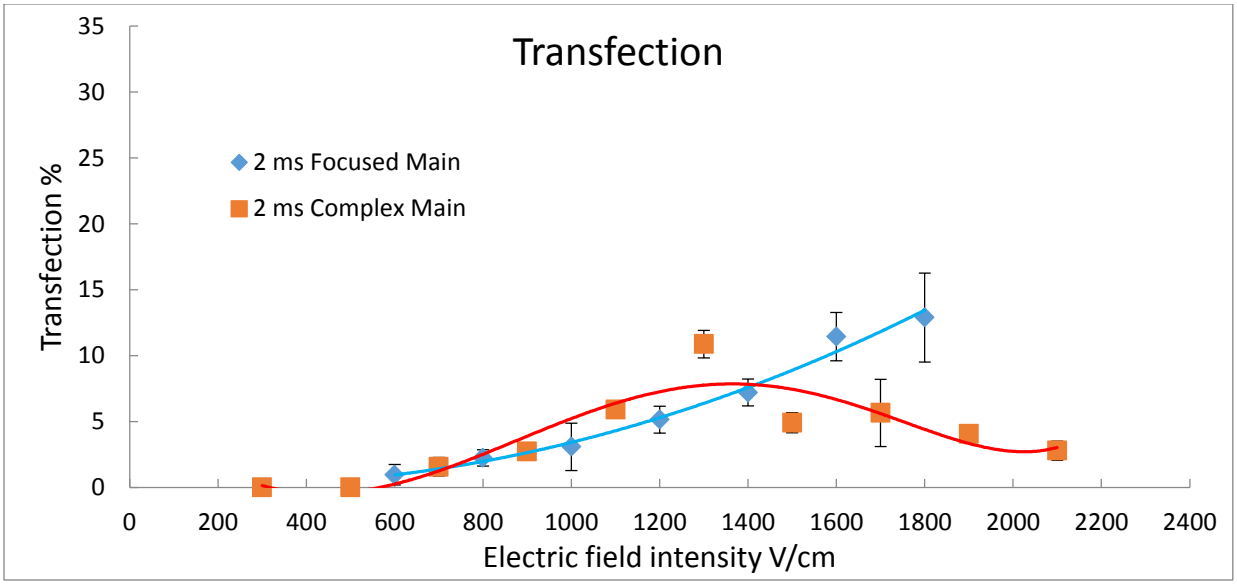

Figure 6.10. Transfection efficiency result for 2 ms electroporation duration time, comparison between focused and complex flows (main channel)

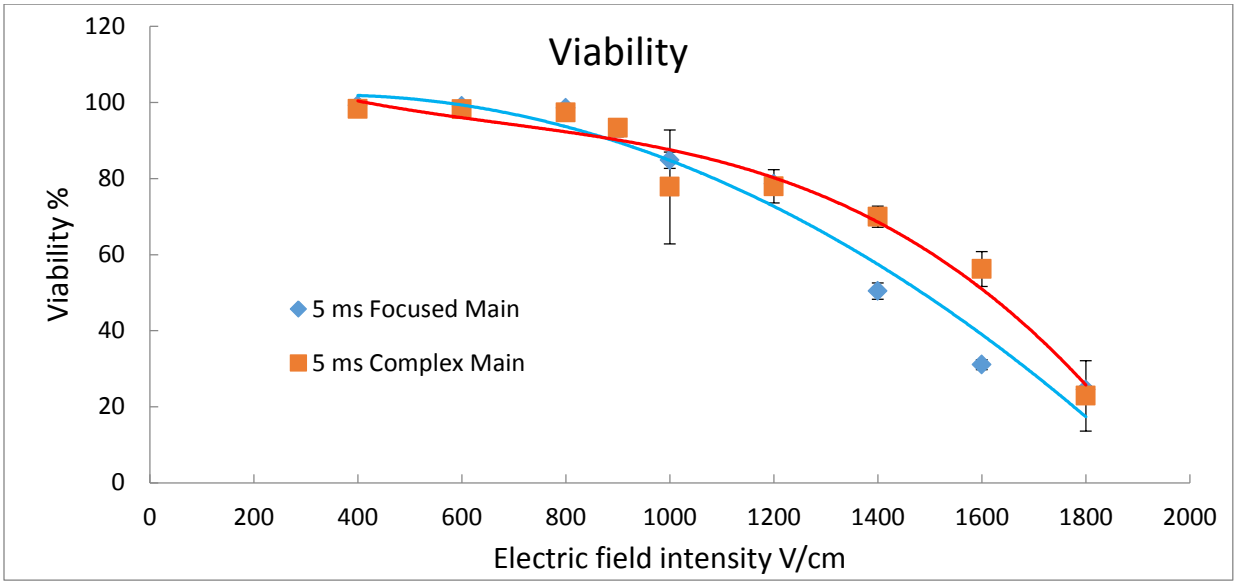

Figure 6.11. Viability result for 5 ms electroporation duration time, comparison between focused and complex flows (main channel)

The transfection efficiency result for both flow conditions (focused and complex) are shown in figure 6.12 for 5 ms duration time. Generally, the delivery rate is higher at the lower flow rate (150 µl/min) compared to higher flow rate (600 µl/min). The highest difference is at 1200 V/cm where the transfection efficiency is 18.6% for focused flow while it is 7.44% for

complex flow condition. The delivery rate at both conditions reaches its maximum value at the electric field intensity of 1200 V/cm.

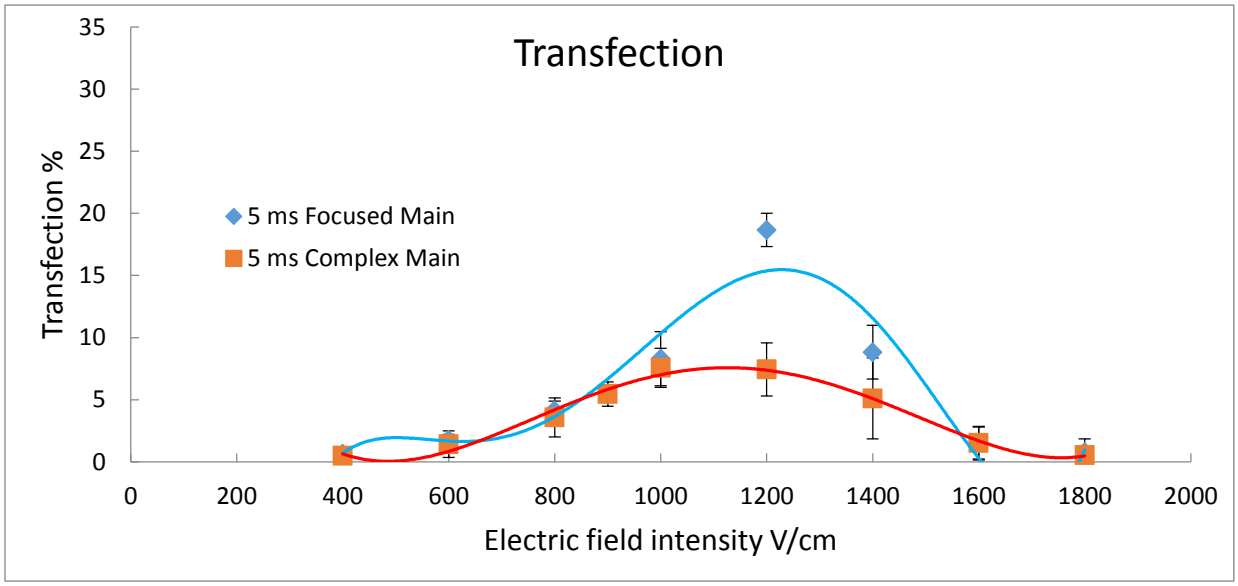

Figure 6.12. Transfection efficiency result for 5 ms electroporation duration time, comparison between focused and complex flows (main channel)

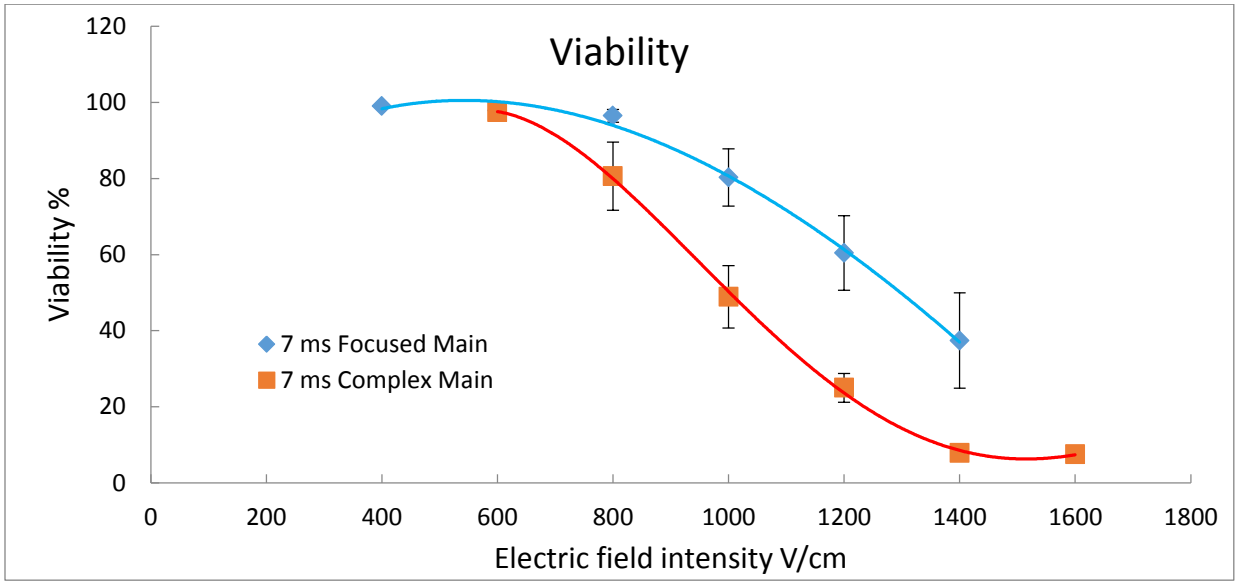

Figure 6.13. Viability result for 7 ms electroporation duration time, comparison between focused and complex flows (main channel)

Figure 6.13 shows the result for cell viability rates at 7 ms electroporation duration time at both focused (150 µl/min) and complex (600 µl/min) flow conditions. To maintain 7 ms duration time in higher flow rate a longer channel is needed. Therefore, the number of pulses (narrow sections) for complex flow is higher and cells experience more pulses. Based on calculations for cell velocity and its traveled distance at different flow rates in asymmetric curving channel (table 4.1) 20 turns are needed when flow rate is 600 µl/min to maintain 7 ms duration time. However, only 3 turns are enough for the lower flow rate. The viability rate is generally lower in complex flow at 7 ms. The difference becomes more drastic at higher field intensities. For example, when the electric field intensity is at 1200 V/cm, the viability percentage at focused flow is 60.4% while it is 25%.

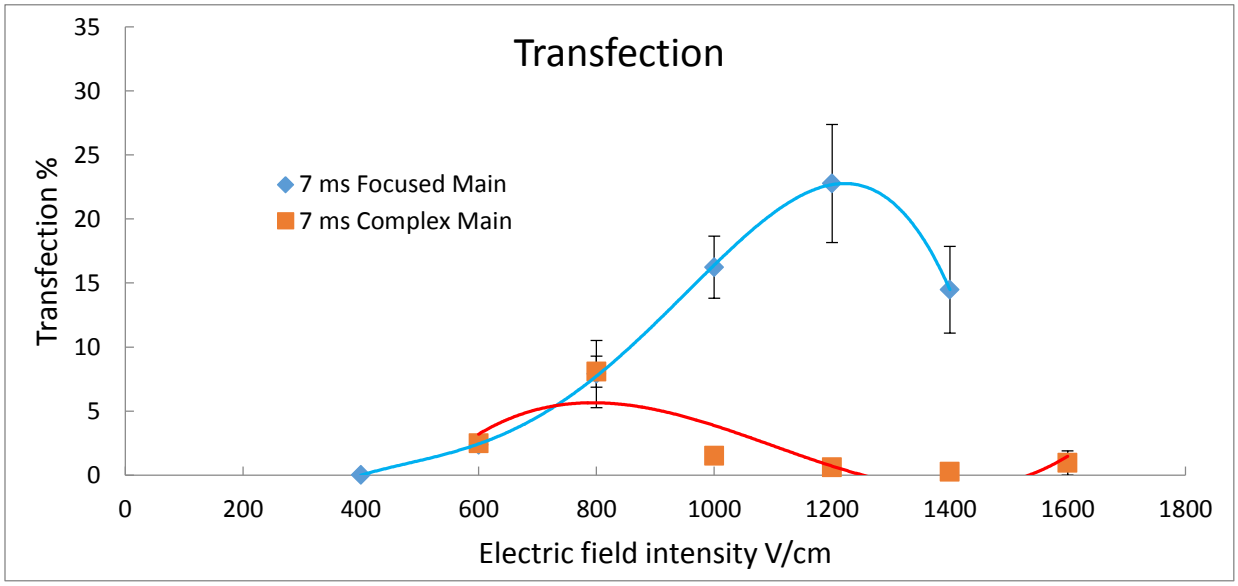

Figure 6.14. Transfection efficiency result for 7 ms electroporation duration time, comparison between focused and complex flows (main channel)

Transfection efficiency result is for both 150 and 600 µl/min flow rates are shown in figure 6.14 at electroporation duration time of 7 ms. The delivery rate is higher in focused flow condition. The peak for transfection is reached at 1200 V/cm for focused flow while the maximum value happens at 800 V/cm for the case of complex flow. This is a confirmation for cell velocity and real duration time calculation. In fact, if the cell velocity were higher than our calculated value at the flow rate of 600 µl/min, then the peak for complex flow would happen at higher field intensities in comparison with the peak for 150 µl/min flow rate. At electric field

intensity of 1200 V/cm the difference is considerable. It is 22.7% for focused flow while it is only 0.6% at complex flow. At 600 µl/min, the transfection efficiency does not exceed 8.08% which happens at 800 V/cm.

After collecting transfection efficiency data from asymmetric curving channel, we notice that the transfection rate is normally higher in focused flow condition compared to complex flow. This is generally true for all examined duration times. The change in hydrodynamic forces that cells experience under the effect of different flow rates can be the reason behind this shift in transfection efficiency (regarding Dean flow in curving channels). However, hydrodynamic forces and fluid mechanic of the system is not the only varied parameter between focused and complex flow. In fact, if we want to have an unbiased study we need to also consider the effect of number of pulses at different conditions. Thus, we also conducted flow-through electroporation under the same condition in the control channels with symmetric wide sections and straight narrow sections. The details are discussed in the next section.

6.7. Cell viability and transfection efficiency in control microchannel (straight narrow section)

The number of pulses (narrow sections or turns) is larger when we use higher flow rate (600 µl/min). This is inevitable when we want to maintain the same electroporation duration time as what cells experience under lower flow rate or focused flow (150 µl/min). For example, if we want to have 7 ms of duration time in narrow sections, 3 turns (pulses) are enough for focused flow while 20 turns are needed when the flow rate is 600 µl/min (table 4.1 for more details). Therefore, the change in the number of turns which results in shorter individual electric pulses needs to be explored separately. To properly address this issue, we designed a set of control experiments.

In the control, cells experience the same number of pulses with the same duration times while the focusing is different from that in asymmetric curving channel. The control channel consists of straight narrow sections with the same length as curved turns. Wide section in control channel is symmetrically curved. The height of both channels is the same. Also, the width of

narrow section in control channel is the same as main channel. More details about the dimensions are discussed in chapter three.

Figure 6.15 shows the result of cell viability assays in control channel for 150 µl/min flow rates. At 2 ms electroporation duration time the change in viability rate is gradual when applied electric field is increased. This is correct specifically for lower electric field intensities. The viability percentage is above 98.5% for field intensities from 600 to 1000 V/cm. After exceeding 1000 V/cm, cell viability begins to drop at 2 ms duration time. The minimum value for cell survival range is 89.3% at 1800 V/cm. The result is consistent with our expectation because at short duration times cells are not exposed to electric field for a long period of time.

When the duration time is 5 ms in control channel (straight narrow sections) the drop in cell viability is very little at low electric field intensities (from 400 to 1000 V/cm). However, cell viability rate is decreased more intensely after field intensity exceeds 1200 V/cm. The viability rate at 1200 V/cm is 93.8% while it decreases to 82.6% at 1800 V/cm. As it is predictable, the viability rate is lower at 5 ms duration time compared to 2 ms especially at higher field intensities. For example, the value for viability rate is 7.3% higher in 2 ms at 1800 V/cm compared to 5 ms duration time.

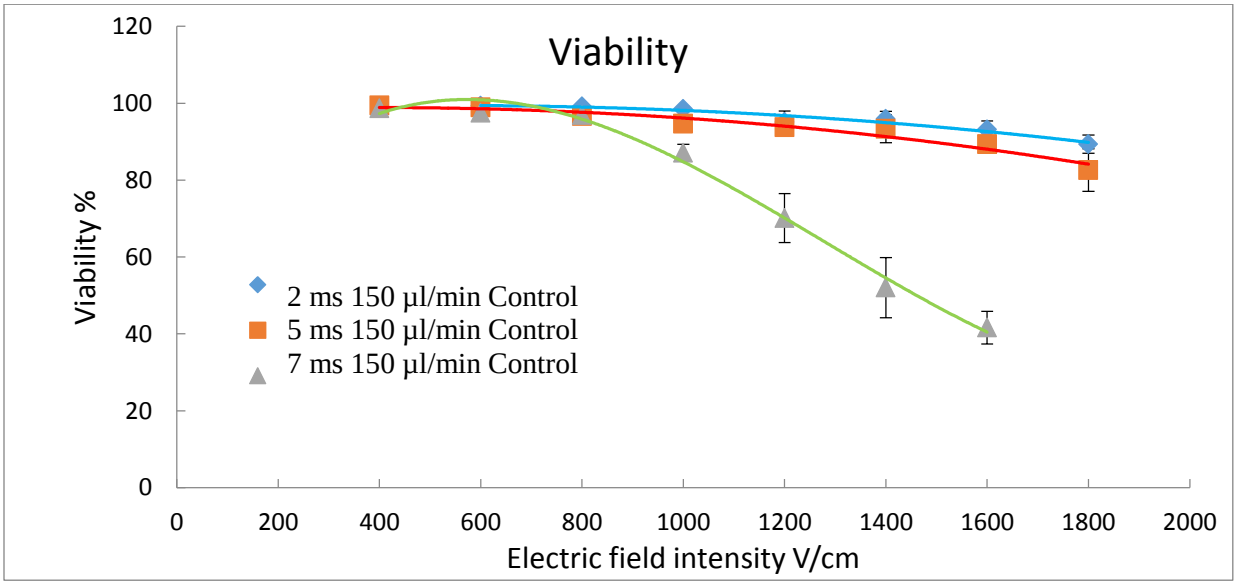

Figure 6.15. Viability result for flow rate of 150 µl/min in symmetric curving channel (control channel)

For 7 ms duration time in control channel with a flow rate of 150 µl/min, the drop in cell viability, with rise in field intensity, is considerable. At low field intensities the decrease in viability is not noticeable and is almost similar to the result for 5 ms. In fact, low electric field cannot affect cells even in longer duration times. For example, at 400, 600 V/cm the viability rates are 99.4% and 98.9% respectively for 5 ms while they are 98.7% and 97.5% for 7 ms. However, in higher field intensities, the difference between viability at 7 ms and shorter duration times (2 ms, and 5 ms) is drastic. At 1600 V/cm, the viability rate for 7 ms is equal to 52.02% while it is 93.1% for 2 ms and 89.3% for 5 ms. This happens because cells are exposed to the electric field for longer period of time which would decrease cell membrane recovery and cause higher cell inactivation rate.

Transfection efficiency for control channel at 150 µl/min flow rate is also collected for all desired duration times. Figure 6.16 presents the data for delivery rate in control channel. The delivery rate at 2 ms duration time (blue dots) is very low. At its peak, it reaches 8.83% when the applied external electric field is 1800 V/cm. The increase in cell transfection rate has a gradual rising slop by increasing field intensity. At lower field intensities, the delivery rates are even lower. For example, at 600 V/cm, the transfection rate is only 0.46% at 2 ms duration time.

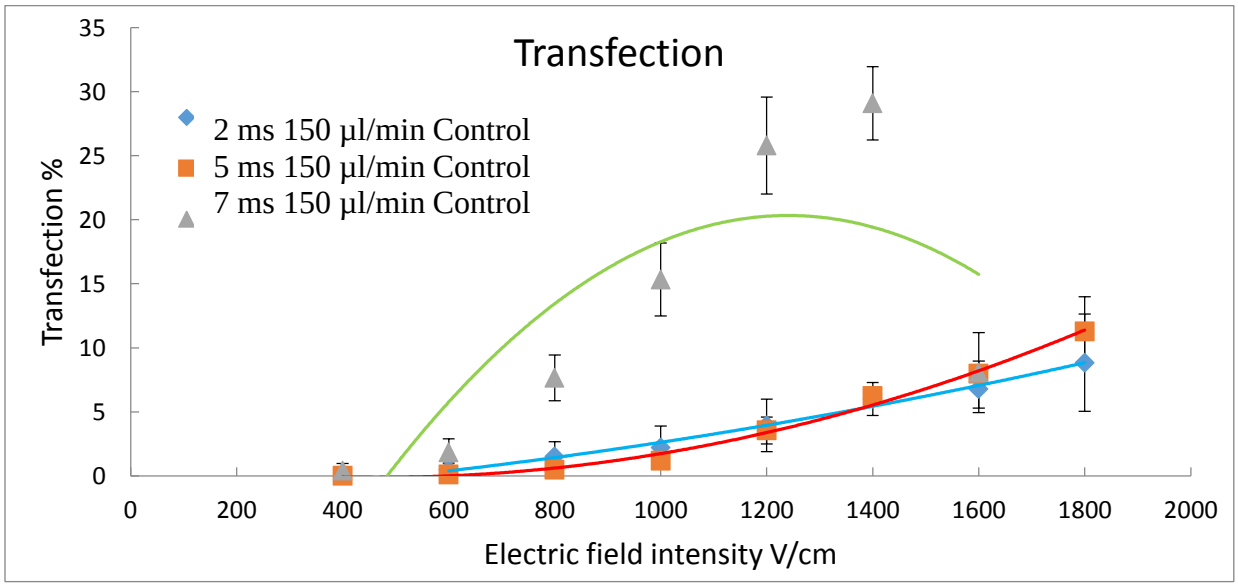

Figure 6.16. Transfection efficiency result for flow rate of 150 µl/min in symmetric curving channel (control channel)

When the duration time is 5 ms at control channel and flow rate is 150 µl/min (red squares) the increase in transfection efficiency is gradual by rise in electric field intensity. The result generally is close to 2 ms duration time. However, specifically at higher field intensities (1400, 1600, and 1800 V/cm) the value for delivery rate is larger for 5 ms compared to 2 ms. The efficiency rate at 1800 V/cm is 11.2% for 5 ms while it is 8.83% at 2 ms duration time and the same field intensity .

Green triangles represent transfection efficiency rate for 7 ms electroporation duration time in control channel for 150 µl/min flow rate (figure 6.16). The delivery rate is considerably higher than the results for 2 ms, and 5 ms. The maximum value for delivery rate happen at 1400 V/cm where the transfection percentage is 29.1% for 7 ms while it is only 6 % for 2 ms and 6.23 for 5 ms. The transfection rate drops when electric field intensity exceeds 1400 V/cm. The value of transfection rate becomes equal to 8.06% at 1600 V/cm and 7 ms. Furthermore, by increasing field intensity , delivery rate rises much faster than 5 ms, and 2 ms. This is consistent with our knowledge, since generally longer duration time yields higher transfection at fixed field intensity .

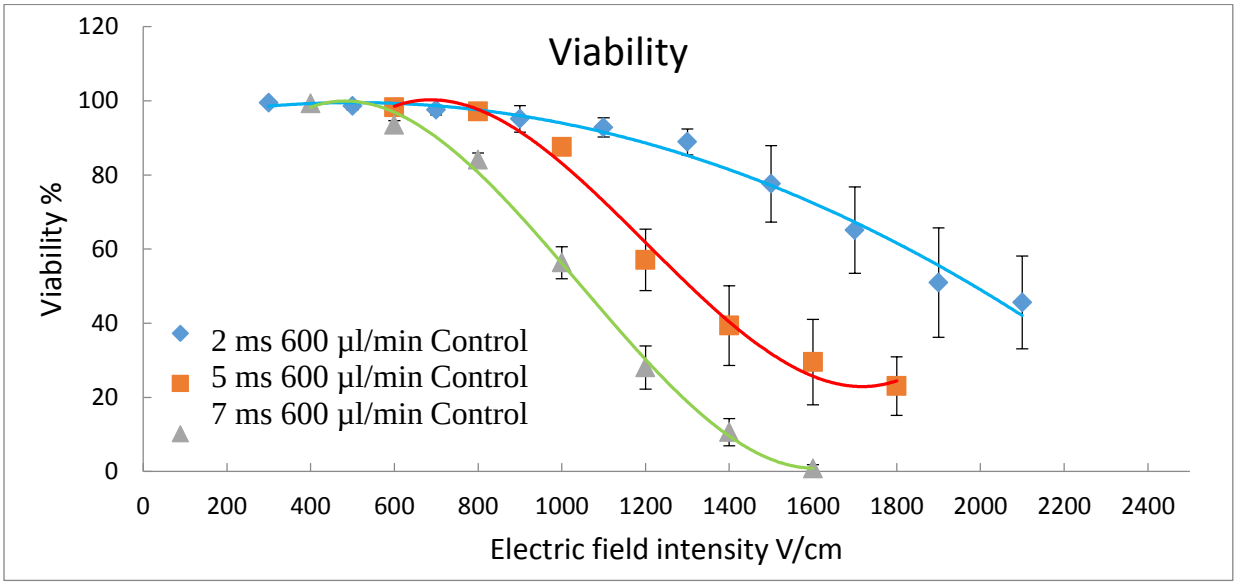

Figure 6.17. Viability result for flow rate of 600 µl/min in symmetric curving channel (control channel)

The control channel with straight narrow sections is also used for electroporation under higher flow rate (600 μl/min). Figure 6.17 shows cell viability results for all desired duration times similar to ones in the main asymmetric curving channel, i. e. 2 ms, 5 ms, and 7 ms. The number of narrow sections is larger when the flow rate is higher. This allow cells to experience the same electroporation duration time. Blue dots represent data for 2 ms which is obtained with 6 narrow sections in the control channel. Cell viability rate slightly changes in lower field intensities while the drop is noticeable at higher values for electric field intensity. Viability rate is higher than 97.2% when field intensity is below 900 V/cm. By increasing field intensity cells inactivation rate increases until it reaches its lowest value at 2100 V/cm which is equal to 45.6%.

When the duration time is 5 ms decrease in cell viability rate with rise in field intensity is much higher than the drop at 2 ms duration time. At 1400 V/cm and 5 ms duration time, viability becomes as low as 39.9% while for 2 ms it is not lower than 45.6% at much higher field intensity, i. e. 2100 V/cm. However, at lower field intensities such as 600, and 800 V/cm the viability rate is close to 2 ms duration time result. The lowest value for cell viability at 5 ms happens at 1800 V/cm and is equal to 23%.

As it is expected, the drop in cell viability rate is even more intense in the case of 7 ms duration time. Green triangles show the result for cell viability rate at different electric field intensities in control channel. More cells become inactivated at lower field intensities compared to 2 ms, and 5 ms duration times. This happens because cells are exposed to the applied electric field for longer period of time. The viability percentage becomes almost zero (0.8%) at 1600 V/cm while the rate is 71.4% for 2 ms and 29.4 % for 5 ms duration times. The drop slop for viability percentage becomes even larger at higher field intensities for 7 ms.

The data for transfection result is collected for control channel with high flow rate (600 μl/min). The delivery rate is reported for all desired electroporation duration times in figure 6.18. Blue dots present the transfection efficiency for 2 ms duration time. The maximum value for delivery rate happens at 1500 V/cm which is 8.26%. After exceeding 1500 V/cm the efficiency drops, until it becomes equal to 1.83% at 2100 V/cm. The transfection rate at 300 and 500 V/cm is very close to zero (0.0% and 0.5% respectively).

For 5 ms duration time (red squares) transfection efficiency experiences a peak at 1200 V/cm equal to 7.96%. The maximum value for delivery rate at 5 ms duration time is reached in lower field intensity compared to 2 ms (1500 V/cm). In general, longer duration times yield to higher transfection rate. This happens because cells are exposed to external electric field for longer period of time. The delivery rate drops when electric field intensity exceeds1200 V/cm until it becomes equal to 2.4% at 1800 V/cm. The transfection percentage is also very low at lower field intensities. For example, it is only 0.5% at 600 V/cm.

The transfection efficiency at 7 ms duration time has a peak at the lowest electric field intensity compared to both 2 ms and 5 ms. It reaches its highest value at 800 V/cm while the maximum value for delivery rate is reached at 1200 V/cm for 5 ms and at 1500 V/cm for 2 ms. This is expected since longer cell residency time under the same field intensity results in better transfection rate. The efficiency decreases when we apply electric field intensities higher than 800 V/cm. The value for delivery rate decreases until it becomes equal to 1.07% at 1600 V/cm. The transfection percentage for 7 ms is also low at weak field intensities. For example, it is only 2.63% at 400 V/cm. In general, transfection efficiency is not very high for all three different duration times when high flow rate (600 μl/min) is applied in the control channel. The highest delivery rate happens at 2 ms and 1500 V/cm which is only 8.26%. Also, the transfection efficiency results for all duration times are very similar except the peak is reached at lower field intensity for longer duration time.

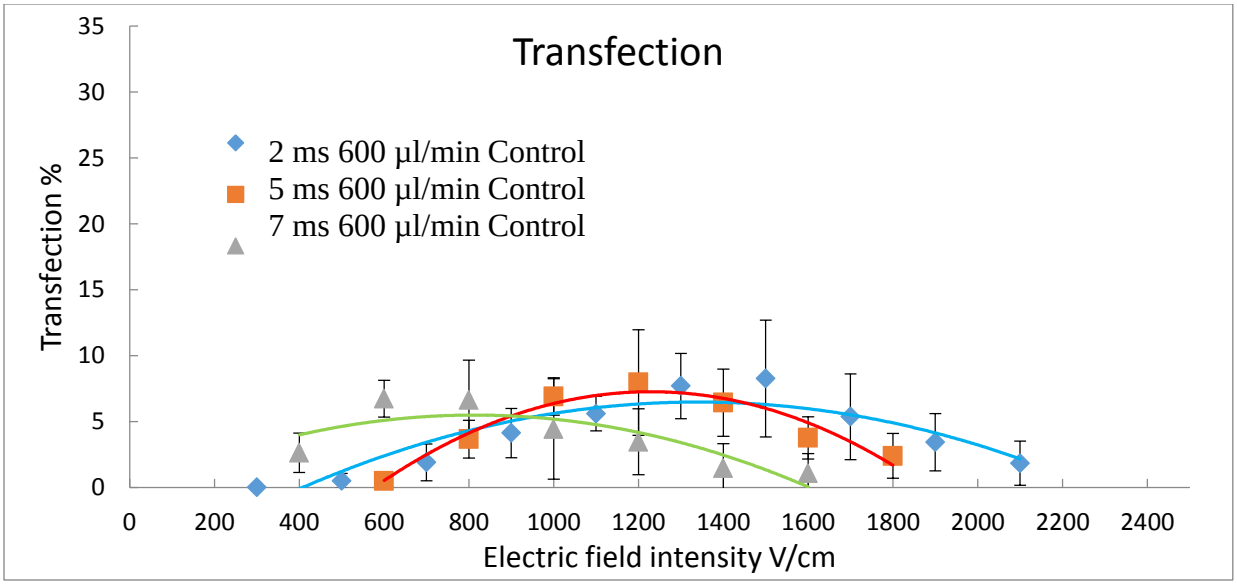

Figure 6.18. Transfection efficiency result for flow rate of 600 µl/min in symmetric curving channel (control channel)

6.7.1. Comparison between 150 µl/min and 600 µl/min flow rate results (control channel)

Figure 6.19 presents data for cell viability at 2 ms in control channel for both 150 µl/min and 600 µl/min. In order to maintain 2 ms electroporation duration time, more narrow sections are needed at higher flow rate. Therefore the number of pulses is higher and duration time for each individual narrow section is shorter (shorter pulses). In fact, when flow rate is 150 µl/min only one narrow section is enough to reach 2 ms duration time while for 600 µl/min 6 narrow sections are needed for the same duration time. Blue dots represent cell viability rates for lower flow rate at various field intensities. And, red squares show the result for higher flow rate. The drop is more intense in the case of channel with more pulses. The viability rates are close at lower electric fields, i. e. up to 800 V/cm. The difference becomes more noticeable at larger field intensities. For example, viability percentage is 77.6% at 1500 V/cm with higher flow rate while it is 94.5% at the same field intensity for the channel with lower flow rate, i. e. 150 µl/min.

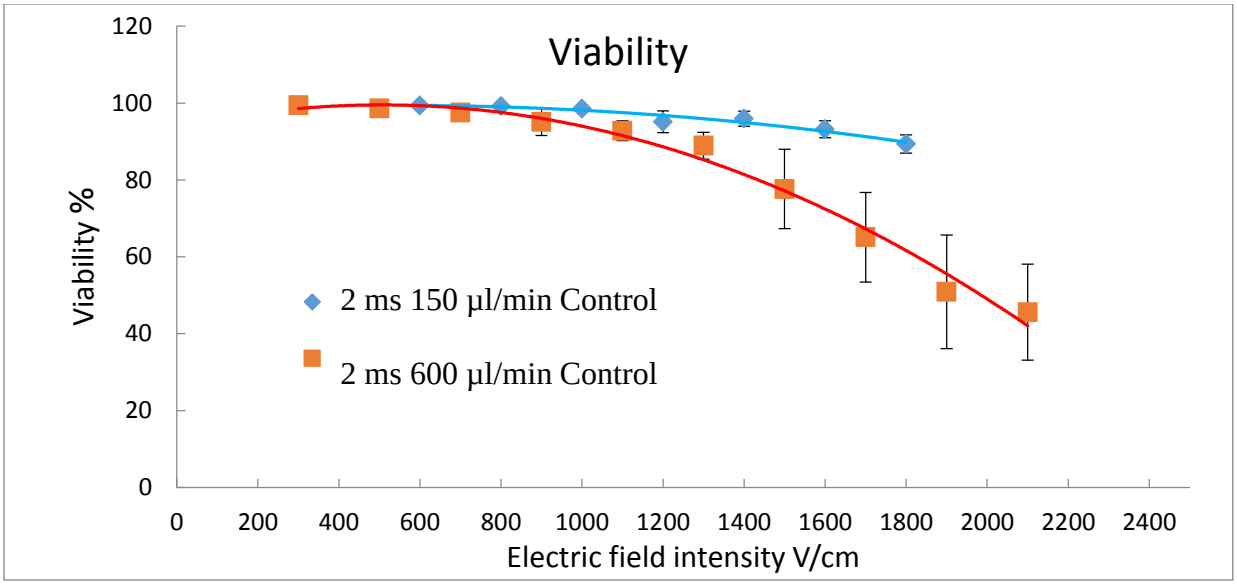

Figure 6.19. Viability result for 2 ms electroporation duration time, comparison between 150 and 600 µl/min flow rates (control channel)

Transfection efficiency data for 2 ms duration time with two different flow rates (150 µl/min and 600 µl/min) in control channel is shown in figure 6.20. The delivery rate has a peak at 1500 V/cm for higher flow rate while it reaches its maximum value at larger field intensity for lower flow condition, i. e. at 1800 V/cm. From very low field intensity (400 V/cm) to 1600 V/cm, the transfection rate is higher for the case of higher flow rate (red squares). However, after 1600 V/cm, the transfection rate at higher flow rate drops while it increases for lower flow rate condition. The maximum delivery rate in both cases is relatively low, i. e. 8.26% for higher flow rate and 8.83% for lower flow rate.

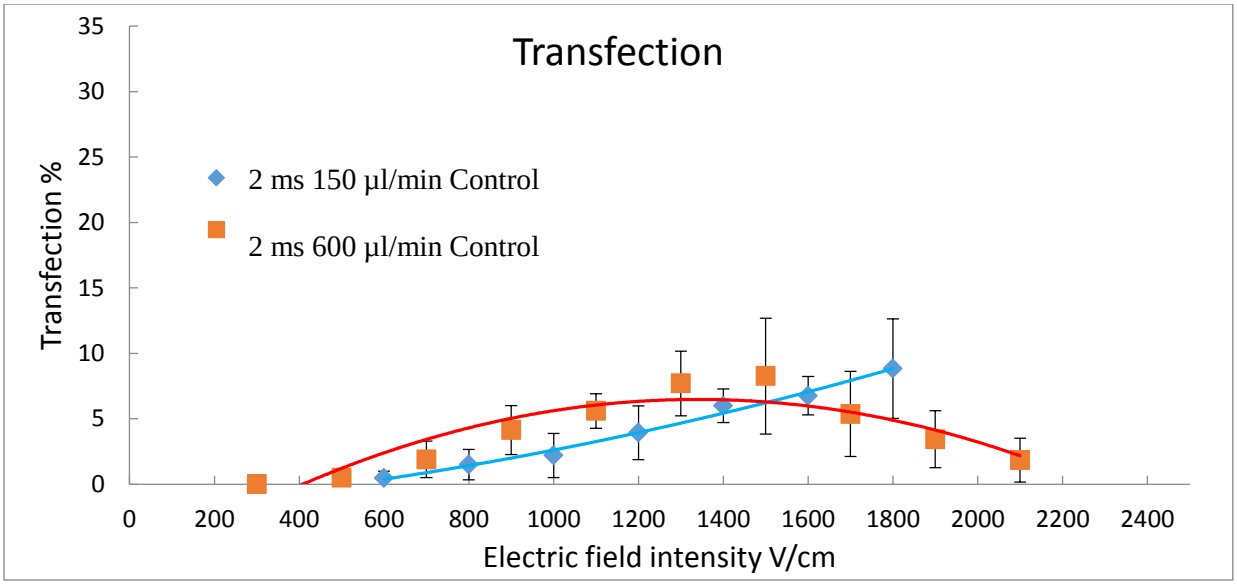

Figure 6.20. Transfection efficiency result for 2 ms electroporation duration time, comparison between 150 and 600 µl/min flow rates (control channel)

For 5 ms electroporation duration time, cell viability data is shown in figure 6.21. It includes the data for both 150 µl/min and 600 µl/min flow rates in control channel. In order to have 5 ms duration time in lower flow rate, only 2 narrow sections are enough while with the higher flow rate, we need 14 narrow sections. This means, cells experience shorter individual pulses with a larger number when we use higher flow rate at control channel. Drop in viability is more noticeable for the higher flow rate (red squares). The maximum difference between two cases happens in the highest field intensity we used which is 1800 V/cm. The viability percentage for the lower flow rate at this field intensity is 82.6% while it is just 23.0% at the higher flow rate.

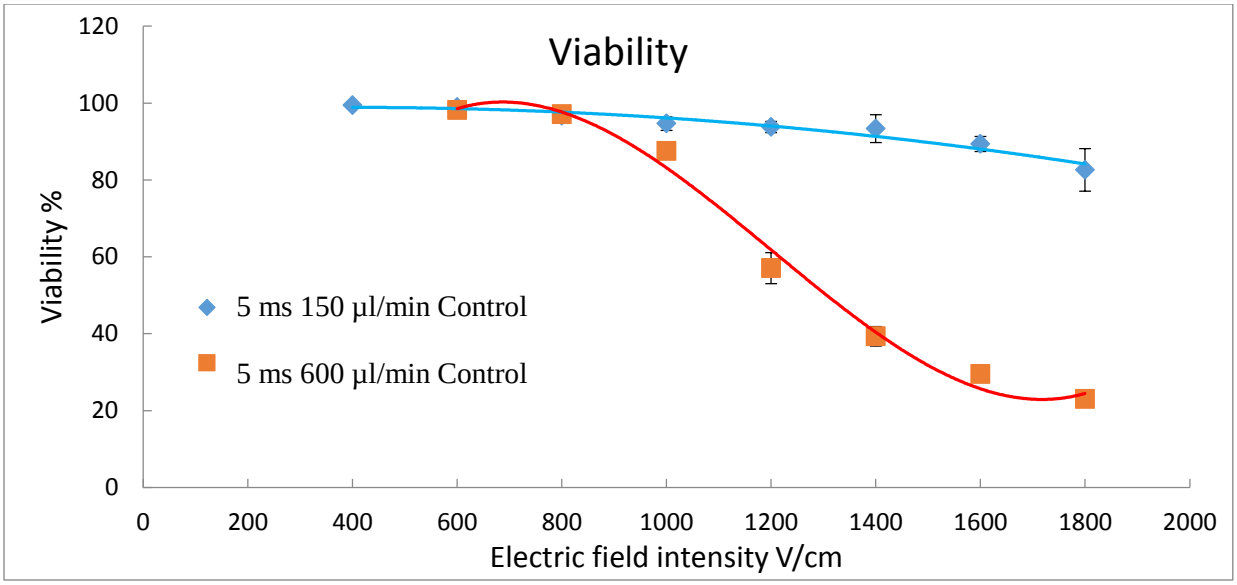

Figure 6.21. Viability result for 5 ms electroporation duration time, comparison between 150 and 600 µl/min flow rates (control channel)

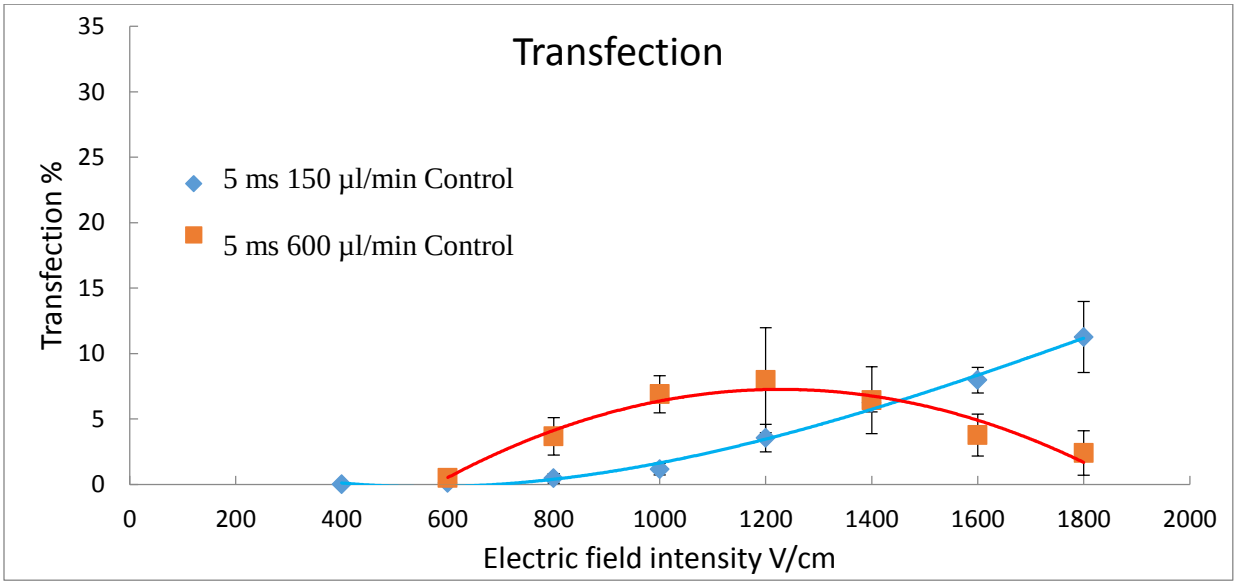

Figure 6.22. Transfection efficiency result for 5 ms electroporation duration time, comparison between 150 and 600 µl/min flow rates (control channel)

The transfection efficiency data at 5 ms electroporation is provided in figure 6.22. This set of data is from control channel and for both 150 µl/min and 600 µl/min flow rates. Transfection efficiency for the higher flow rate (red squares) has a peak at 1200 V/cm (7.96%)

while it reaches its highest value for the lower flow rate (blue dots) at 1800 V/cm (11.2%). The delivery rate for 600 µl/min drops at field intensities beyond 1200 V/cm. Two curves meet each other at field intensity around 1400 V/cm.

Figure 6.23 presents data for cell viability at 7 ms electroporation duration time. This result is for control channel with two different flow rates, i. e. 150 µl/min and 600 µl/min. In order to maintain 7 ms under the higher flow rate condition, 20 narrow sections are needed while for the case of the lower flow rate only 3 turns are enough. Therefore, cells in control channel with larger number of pulses experience shorter individual electric pulses. The drop in viability for the higher flow rate condition is more drastic when electric field intensity is increased under the same duration time (7 ms). The highest difference between two curves is at 1600 V/cm where the viability rate for the lower flow rate is 41.63% while it is much lower for 600 µl/min case, i. e. 0.77%.

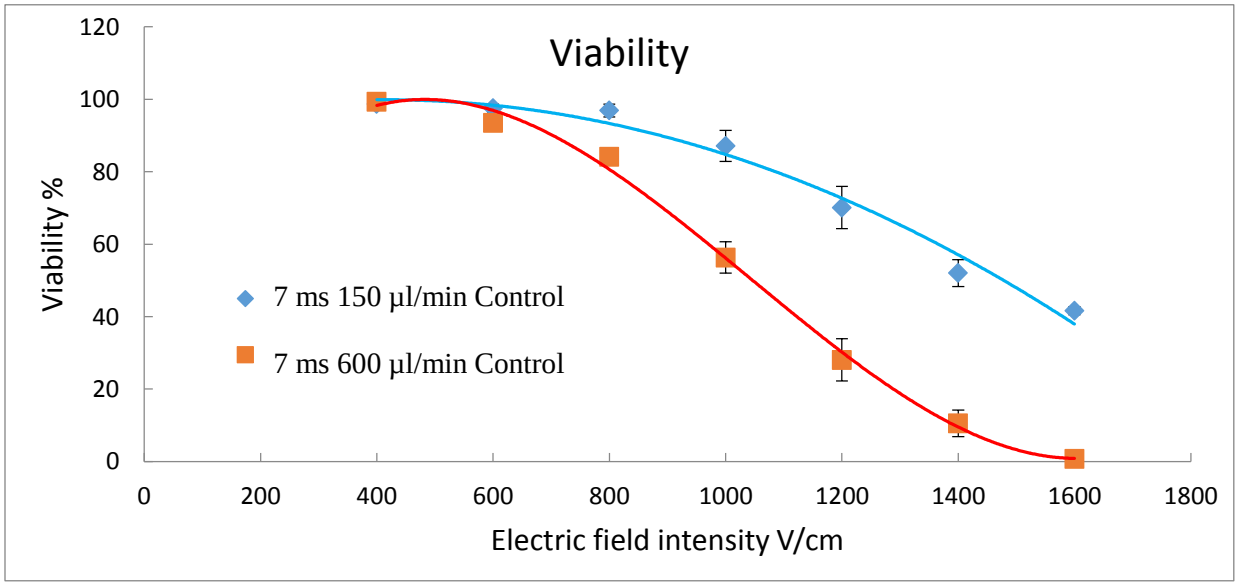

Figure 6.23. Viability result for 7 ms electroporation duration time, comparison between 150 and 600 µl/min flow rates (control channel)

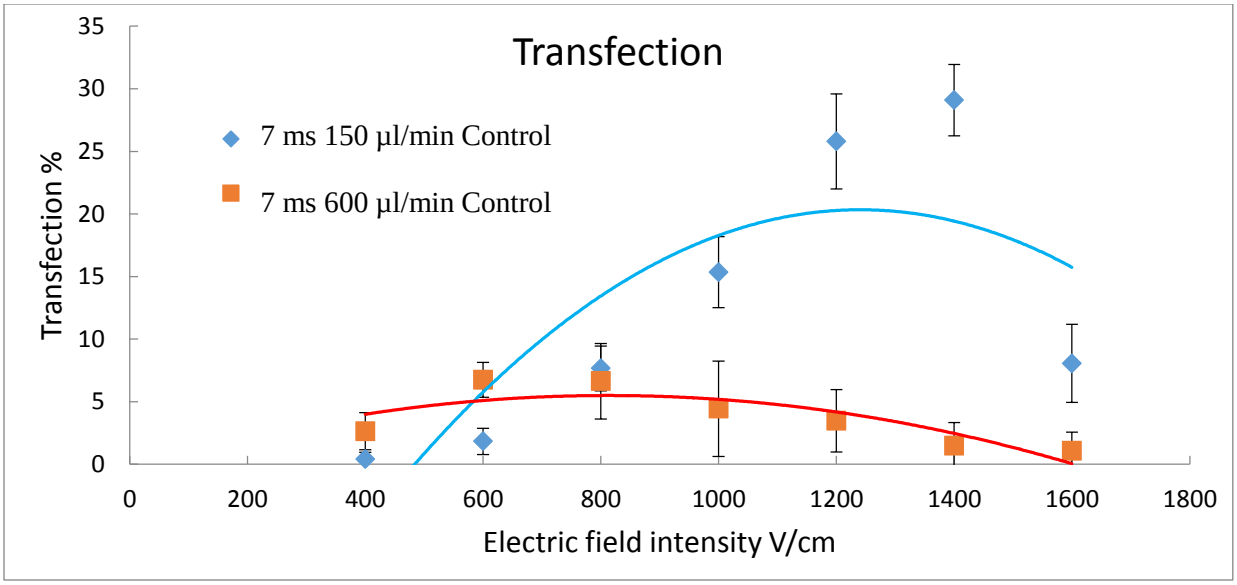

Figure 6.24. Transfection efficiency result for 7 ms electroporation duration time, comparison between 150 and 600 µl/min flow rates (control channel)

Transfection efficiency result at 7 ms electroporation duration time in control channel is presented at figure 6.24. This includes both 150 µl/min and 600 µl/min flow rates. The delivery rate in the case of lower flow rate is generally higher. Transfection for lower flow rate reaches its maximum value at 1400 V/cm which is 29.1%. At the same field intensity, delivery rate is only 1.47% for the case with higher flow rate. The transfection efficiency at lower flow rate decreases when electric field intensity exceeds 1400 V/cm. It drops until it becomes equal to 8.06% at 1600 V/cm while at the same field intensity delivery rate is only 1.07% for the case of 600 µl/min flow rate. On the other hand, at low field intensities (400 and 600 V/cm) transfection rate is higher for 600 µl/min compared to 150 µl/min flow rate. For example, at field intensity of 600 V/cm delivery percentage is 6.74% for higher flow rate while it is only 1.82% for 150 µl/min flow rate. The values for transfection efficiency at higher flow rate (red squares) has a peak at lower field intensity (600 V/cm) compared to peak for the case of 150 µl/min flow rate (1400 V/cm). Transfection rate reaches its minimum value for lower flow rate and 7 ms duration time at 1600 V/cm (1.07%) which is even lower than transfection rate at 400 V/cm (2.63%).

6.8. Comparison between main and control channel when flow rate is 150 µl/min

Figure 6.25 presents the data for cell viability when the flow rate is 150 µl/min, and electroporation duration tome is 2 ms. This includes both main (curved turns) and control (straight narrow sections) channels. The number of pulses is the same in both channels with the same duration time for each pulse. Cell viability for both cases is almost the same. Part of the reason could be related to short duration time. In fact, when duration time is as low as 2 ms cells are not affected with field intensity. Also, it could be related to number of pulses. The data confirms that the change in hydrodynamic forces and flow pattern is not as important as the number of electric pulses for this condition of electroporation.

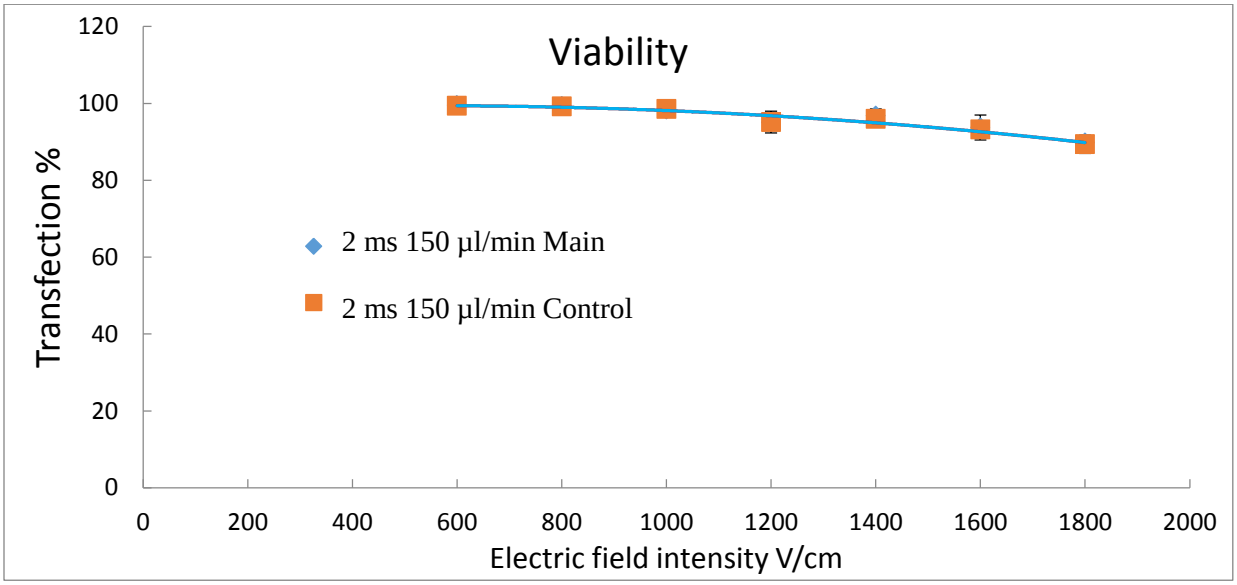

Figure 6.25. Viability result for 2 ms electroporation duration time, comparison between control and main channel in 150 µl/min flow rate

Transfection efficiency data in main and control channel is collected for 2 ms as well. The data is shown in figure 6.26 when flow rate is equal to 150 µl/min. The trend is similar in both conditions however transfection efficiency rises faster in main channel by increasing field intensity. The difference between delivery rates in two channels reaches its maximum value when field intensity is 1800 V/cm. At this field intensity, efficiency rate is 12.9 % at main channel while it is 8.83% at control. The results suggest that the number of pulses could be more important than the fluid dynamic of the system for transfection efficiency.

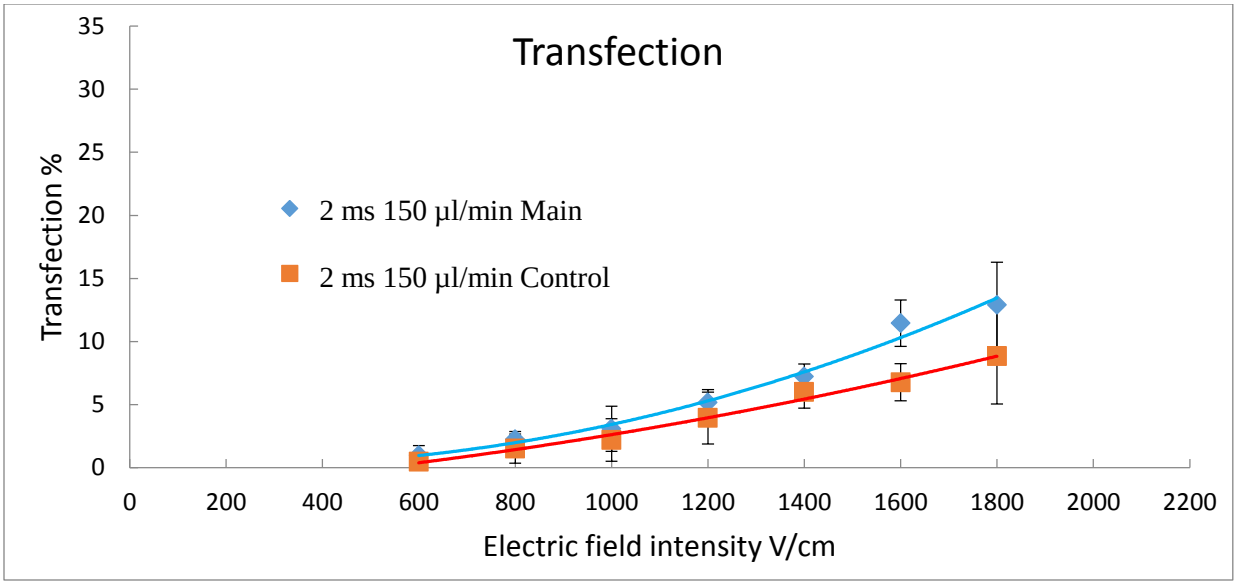

Figure 6.26. Transfection efficiency result for 2 ms electroporation duration time, comparison between control and main channel in 150 µl/min flow rate

Cell viability data for 5 ms at both control and main channel is shown in figure 6.27. This data is gathered when the flow rate is 150 µl/min. The number of electric pulses is the same in both channels. However, the shape of pulses is different which cause different hydrodynamic forces in the channel (Dean flow is not present in straight channel) . The drop in cell viability by increasing electric field intensity is more drastic in main channel. The lowest value for viability in main channel (blue dots) is 24.5% at field intensity equal to 1800 V/cm. At the same field intensity, viability rate in control channel is equal to 82.6%.

Transfection efficiency result for 5 ms electroporation duration time is shown in figure 6.28. This set of data includes both control and main channel when flow rate is 150 µl/min. In main channel, transfection rate rises faster by increasing field intensity from 400 to 1200 V/cm compared to control channel. At 1200 V/cm transfection efficiency has a peak in main channel which is 18.6%. However, in control channel, transfection rate is only 3.54%. At field intensities higher than 1600 V/cm transfection rate is higher in control channel. For example, delivery percentage is 11.2% at 1800 V/cm in control while it is only 0.76% in main channel.

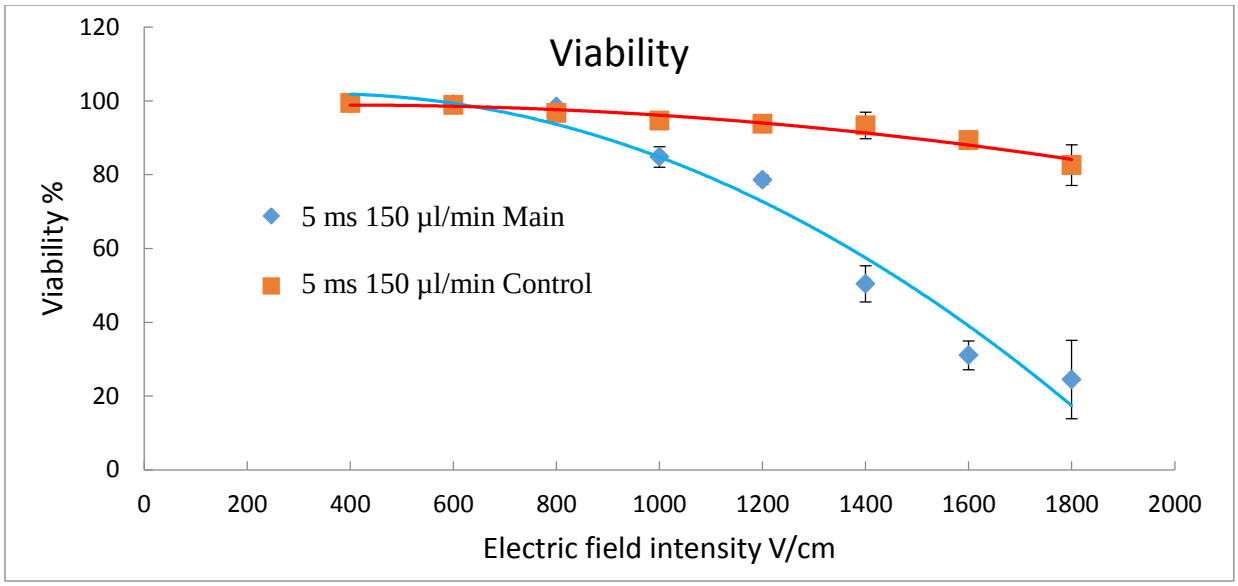

Figure 6.27. Viability result for 5 ms electroporation duration time, comparison between control and main channel in 150 µl/min flow rate

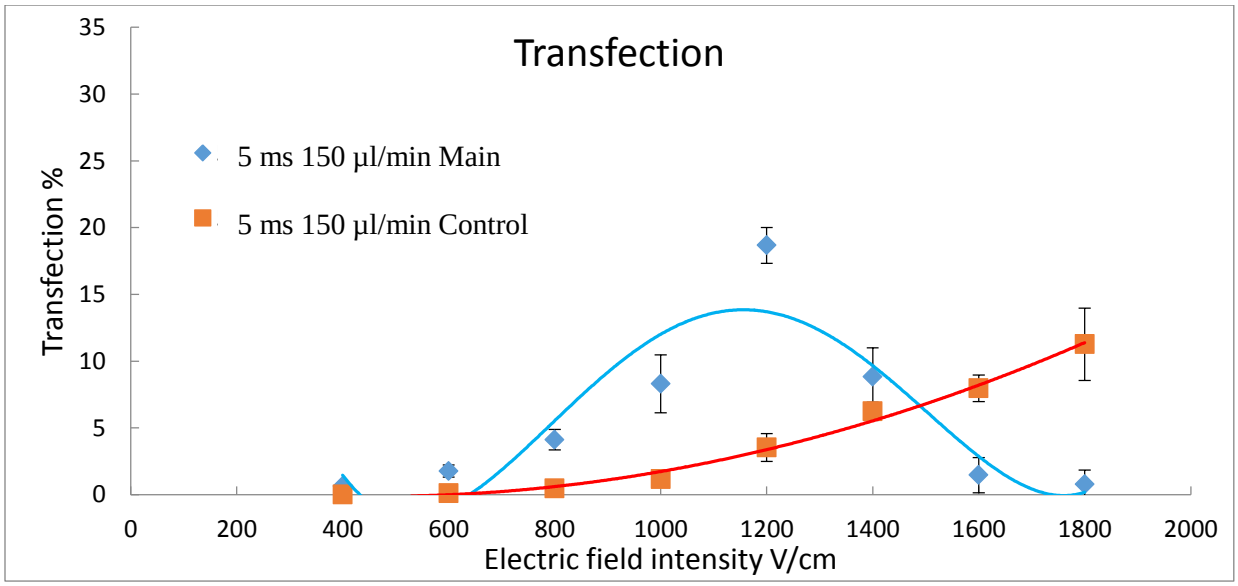

Figure 6.28. Transfection efficiency result for 5 ms electroporation duration time, comparison between control and main channel in 150 µl/min flow rate

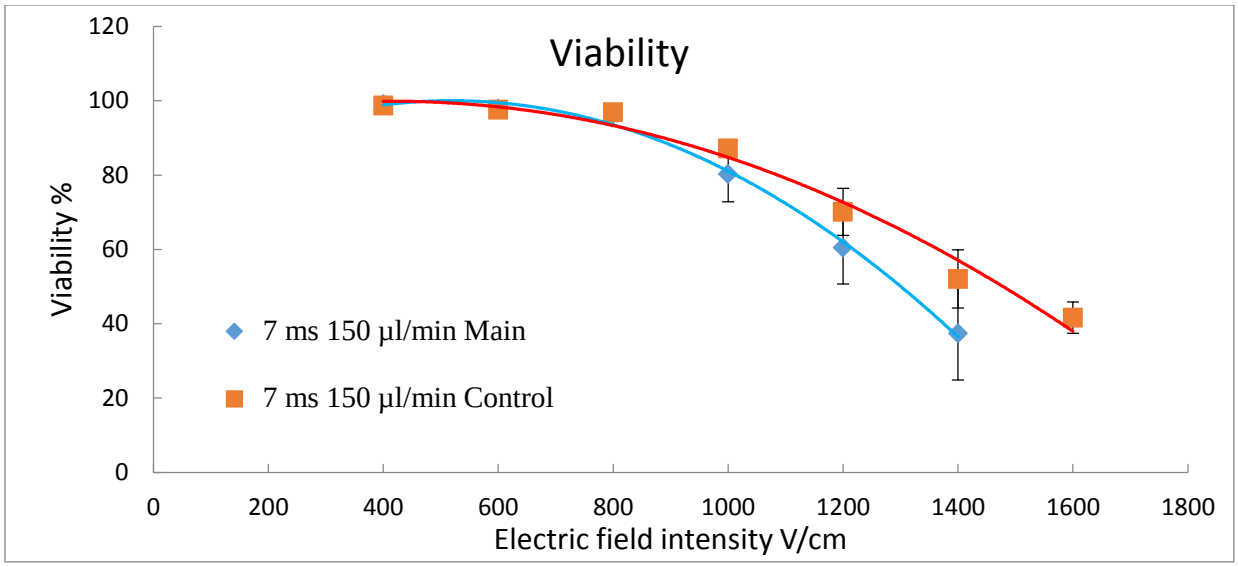

Figure 6.29. Viability result for 7 ms electroporation duration time, comparison between control and main channel in 150 µl/min flow rate

Cell viability result at 7 ms duration time in both control and main channel is examined at a flow rate of 150 µl/min. The number of electric pulses is the same in both conditions however control channel has straight narrow section while narrow sections in main channel are curved.

Cell viability rate (presented in figure 6.29) is very similar in both cases, specifically in filed intensities lower than 1000 V/cm. Small difference between viability rates in both designs suggests that number of pulses at fixed duration time (7 ms) is more influential than the change in hydrodynamic forces.

Transfection efficiency data is presented in figure 6.30 for 7 ms electroporation duration time. This data includes both control and main channel when flow rate is 150 µl/min. The result is almost similar in both channels until electric field intensity exceeds 1000 V/cm. At 1200 and 1400 V/cm, transfection rate is higher in control channel. For example, at 1400 V/cm transfection rate in control (red squares) is 29.09% while it is only 14.46% in main channel. The result suggests that number of pulses is more important at low and mean field intensities however the effect of hydrodynamic forces become more considerable when field intensity exceeds 1200 V/cm.

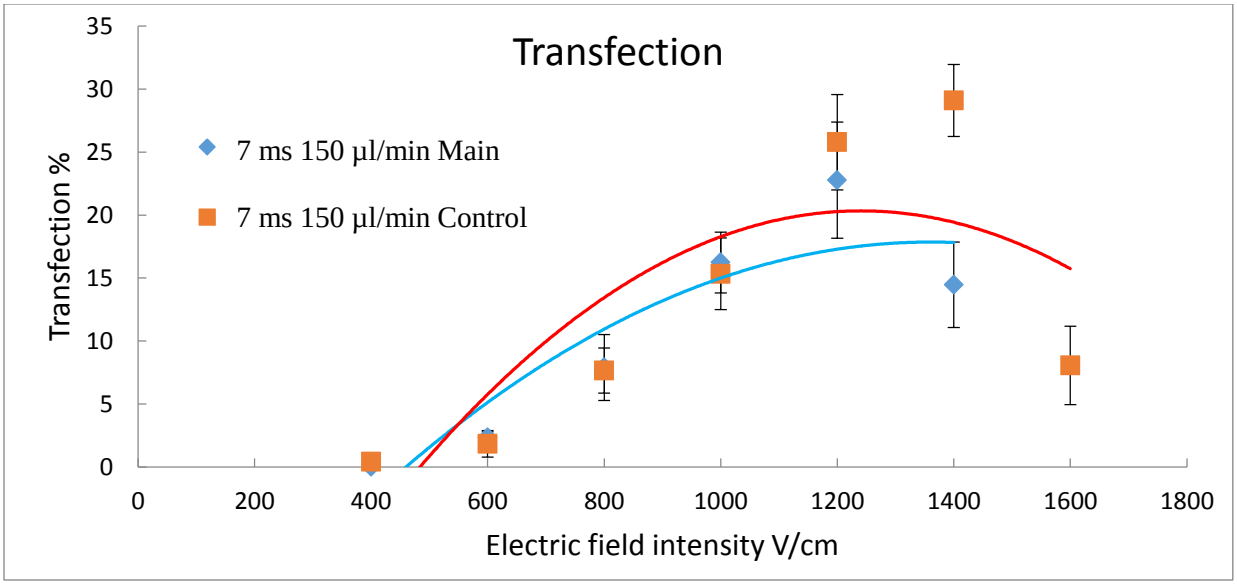

Figure 6.30. Transfection efficiency result for 7 ms electroporation duration time, comparison between control and main channel in 150 µl/min flow rate

6.9. Comparison between main and control channel when flow rate is 600 µl/min

The data for cell viability is shown in figure 6.31 for both control and main channel at 2 ms electroporation duration time. This is for the condition when flow rate is equal to 600 µl/min. The number of electric pulses is the same in both control and main channel. In main channel 6 turns are enough to reach 2 ms of duration time in narrow sections. The same number of narrow sections is enough in control channel however narrow sections are straight channels. When applied field intensity is relatively low (400 and 600 V/cm) viability rate is almost the same in both channels. At higher field intensities, cell viability drops faster in control channel (red squares).

In figure 6.32 transfection efficiency result is shown for 2 ms duration time in both control and main channels. Delivery rate has a peak in complex channel when the applied field intensity is equal to 1500 V/cm which is 8.26%. When electric field intensity exceeds 1500 V/cm, transfection efficiency drops in control channel. In general transfection efficiency is very close in both channels which could be due to the effect of pulse number. In fact it shows the change in hydrodynamic forces is not affecting the result. The delivery rate also experience a

peak in main channel at 1300 V/cm equal to 10.8. After 1300 V/cm the increase in field intensity cause decrease in transfection rate in main channel.

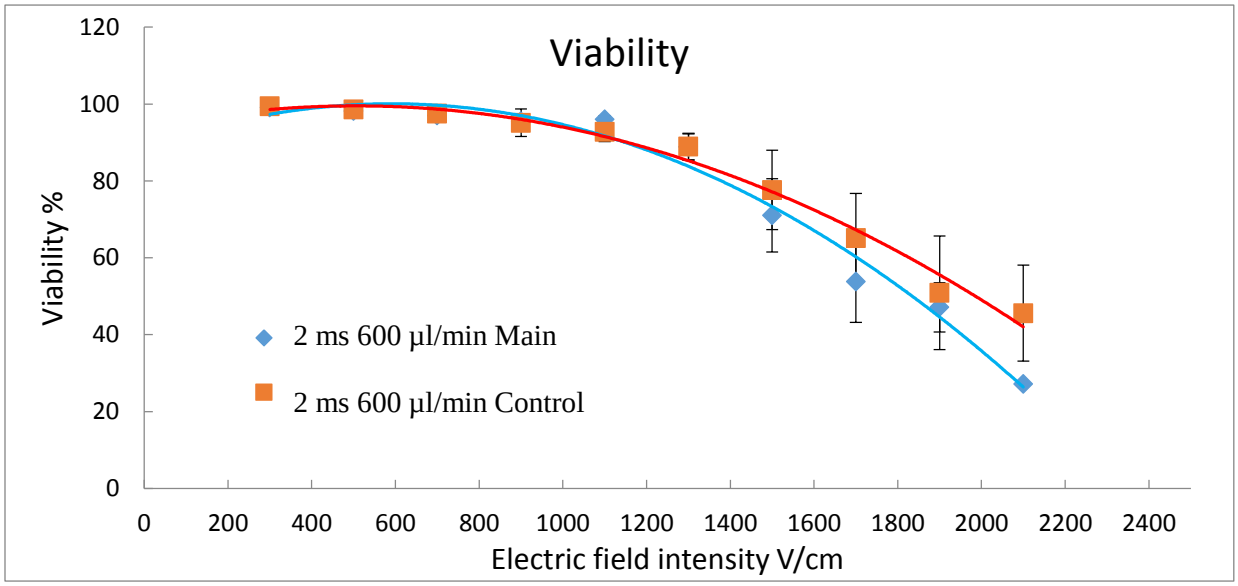

Figure 6.31. Viability result for 2 ms electroporation duration time, comparison between control and main channel in 600 µl/min flow rate

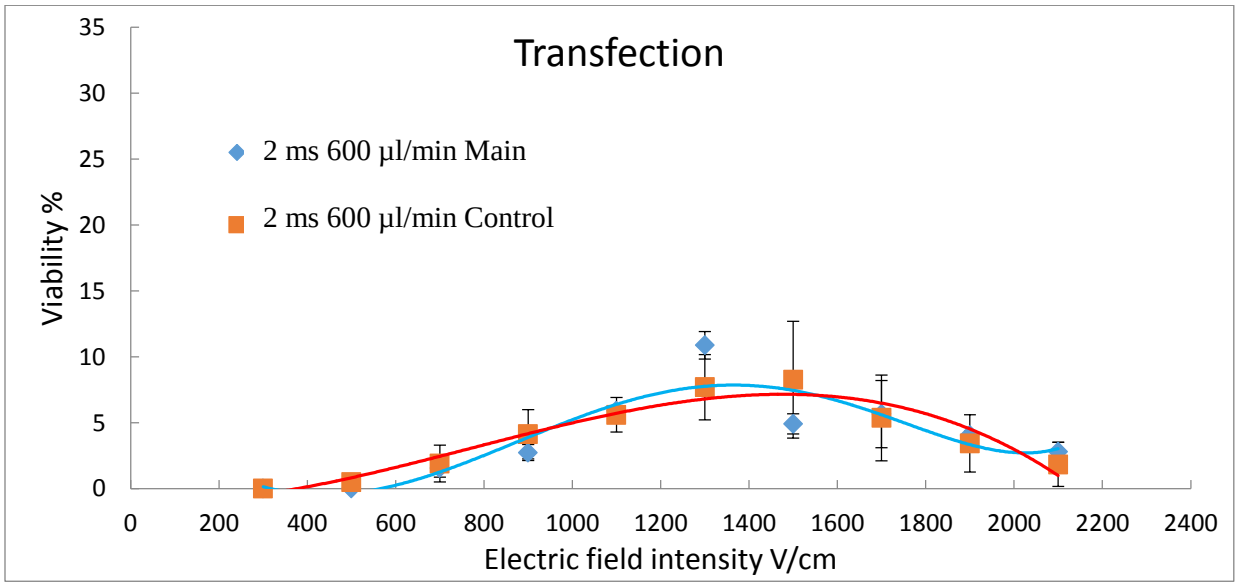

Figure 6.32. Transfection efficiency result for 2 ms electroporation duration time, comparison between control and main channel in 600 µl/min flow rate

Cell viability date for both control and main channel is shown in figure 6.33. This is for 5 ms electroporation duration time. To obtain 5 ms duration time, when flow rate is 600 µl/min, 14 pulses (turns) are enough in main channel. The same number of straight narrow sections are enough in control channel. In both conditions cell viability drops when field intensity exceeds 900 V/cm. The drop is more intense in control channel. For example, at 1600 V/cm cell viability in control channel (red squares) is only 29.04% while it is 56.2% in main channel (blue dots). At 400, and 600 V/cm viability rate is the same in both channels.

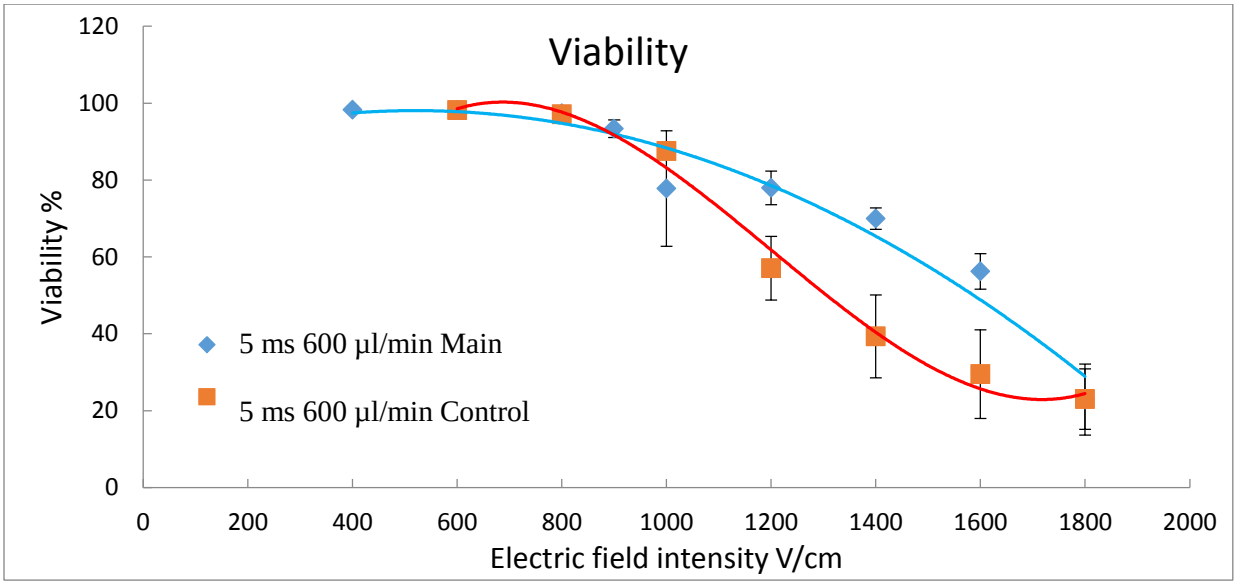

Figure 6.33. Viability result for 5 ms electroporation duration time, comparison between control and main channel in 600 µl/min flow rate

Transfection efficiency in both channels (control and main) is very close at 5 ms electroporation duration time. Figure 6.34 shows the result for transfection when the flow rate is 600 µl/min. Delivery rate has a peak at 1200 V/cm in control channel (red squares) and at 1000 V/cm in main channel (blue dots). Maximum value for transfection in main channel is equal to 7.44% and in control channel it is 7.56%. This similarity of transfection results suggest that individual pulse duration and pulse number is more influential compared to changes in hydrodynamic forces.

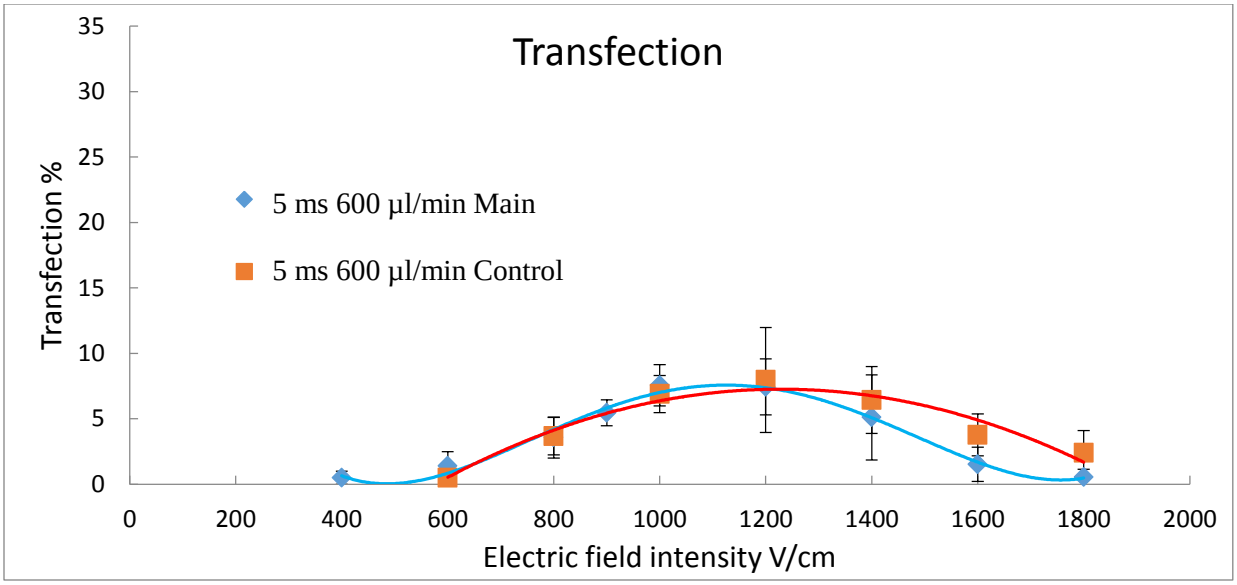

Figure 6.34. Transfection efficiency result for 5 ms electroporation duration time, comparison between control and main channel in 600 µl/min flow rate

Cell viability for 7 ms electroporation duration time is presented in figure 6.35. This data is for both control (red squares) and main channel (blue dots) when flow rate is 600 µl/min. 20 turns are needed for main channel to reach 7 ms duration time. In control channel, the same number of straight narrow sections is needed for the same duration time. The value for call viability is very similar in both channels which suggest that number of electric pulses and individual pulse length are more influential on electroporation performance compared to fluid mechanics of the system.

Transfection efficiency is relatively low in both control and main channel when flow rate is equal to 600 µl/min and electroporation duration time is 7 ms. The data is presented in figure 6.36 where blue dots present the result from main channel and red squares are for control channel. Low difference between transfection efficiency could be an indication of individual pulse length and pulse number influence on delivery rate. In fact, it suggests that hydrodynamic forces are not as important as pulse number and individual pulse length for these electroporation conditions.

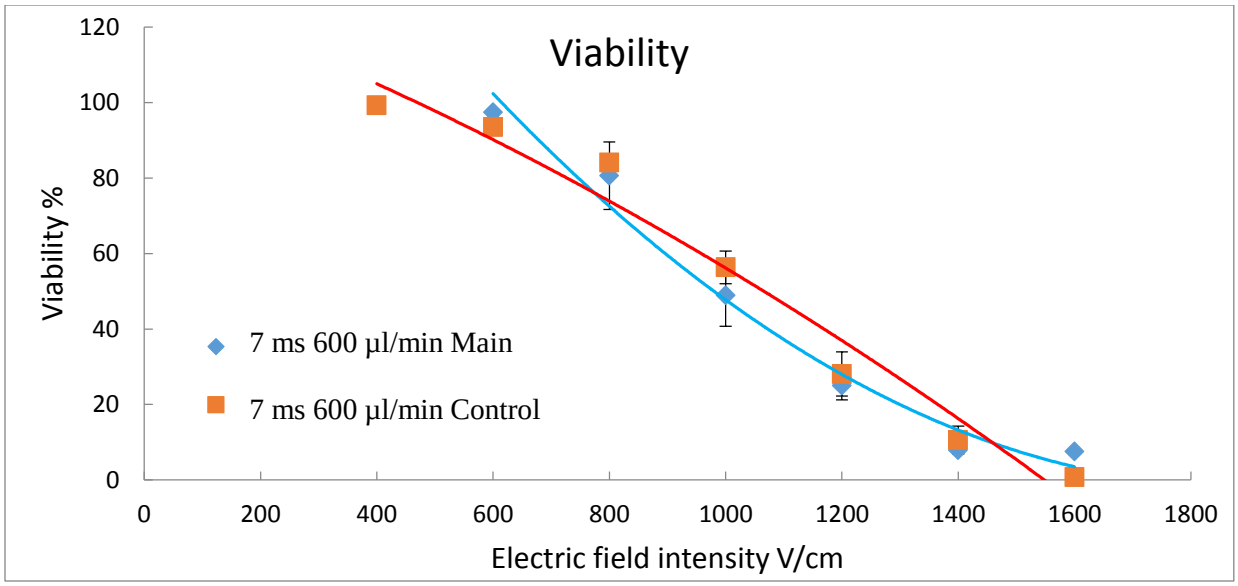

Figure 6.35. Viability result for 7 ms electroporation duration time, comparison between control and main channel in 600 µl/min flow rate

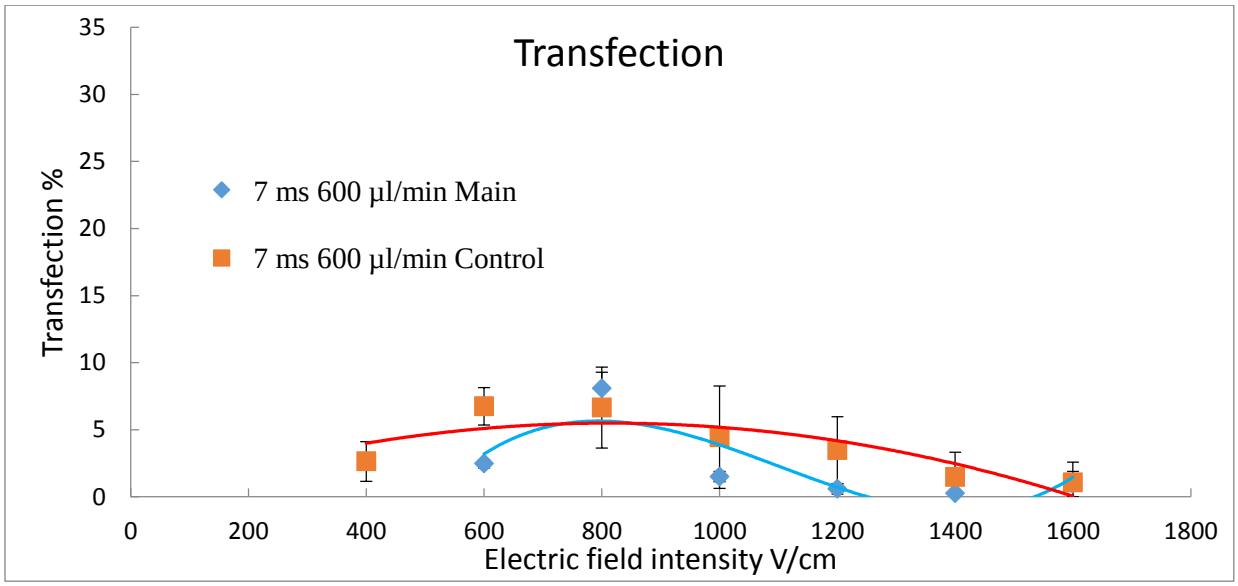

Figure 6.36. Transfection efficiency result for 7 ms electroporation duration time, comparison between control and main channel in 600 µl/min flow rate

Chapter 7. Conclusion

We show that electroporation can be conducted in our asymmetric curving channel. We successfully delivered EGFP (enhanced green fluorescent protein) plasmid DNA into CHO-K1 cells (Chinese hamster ovary). In our electroporation system, we produce electric pulses simply by employing a conventional dc power supply and size variation in our channels width. Various electroporation duration times (2 ms, 5 ms, and 7 ms) are explored in our study. We demonstrate that transfection efficiency increases at higher electric field intensity. Also, we demonstrate that longer duration times yield to higher delivery rate as well. COMSOL Multiphysics is used to simulate field distribution in the microfluidic channels. We used wide ranges of electric field intensity from 300 V/cm to 2200 V/cm. Furthermore, we performed flow-through electroporation at different flow rates in the asymmetric curving channels.

We successfully designed and fabricated asymmetric curving microchannels that can be used to focus cells into one single stream. This happens due to the effect of hydrodynamic forces (Dean flow) present in curving channels. Cell focusing is reached at certain range of flow rates. We demonstrate that at low flow rates (i. e. from 0 to ~75 µl/min) cells are not focused and randomly follow stream lines. However, at higher flow rates, cells laterally migrate in the microfluidic channel towards specific equilibrium positions and become focused in one single line (from ~75 to ~500 µl/min). We find out when flow rate exceeds ~500 µl/min, the focusing disappears and cells follow different paths which are more complex.

In addition, we designed control experiments to separately study the possible impact of hydrodynamic effects on flow-through electroporation in the asymmetric curving channels. Electroporation-based gene delivery was successfully done in control channels too. Based on the result, we postulate that hydrodynamic forces in our channels do not have a considerable impact on transfection efficiency. In fact, our findings suggest that in our channels the individual electric pulse duration has more dominant impact on gene delivery compared to hydrodynamic effects.

Further experiments can be conducted to shed more light on flow-through electroporation in asymmetric curving channels. For example, it is helpful to perform electroporation with longer

duration times (higher than 7 ms). In fact, there is a possibility for reaching higher transfection rates at longer duration times. Also, different cell lines can be examined. Normally cells with larger diameters are easier to be transfected. Finally, systematic channel size optimization can be done in both narrow and wide sections. The change in dimension of turns can modify hydrodynamic forces in curving channels and increase transfection efficiency.

References

1. Thomas, D. P., William, C. E. (2008). Cell biology. Saunders/Elsevier.
2. Bruce, A. (2004). Essential biology -3rd edition. Garland Science.
3. Geoffrey, M. C., Robert, E. H. (2007).The Cell: A Molecular Approach. ASM Press, Sunderland, Mass.
4. Takata, K., Matsuzaki, T., Tajika, Y. (2004). Aquaporins: water channel proteins of the cell membrane. Prog Histochem Cytochem, 1-83.
5. Hapala, I. (1997). Crit. Rev. Biotechnol., 17, 105–122.
6. Neumann, E., Sowers, A. E., Jordan, C. A. (1989). Electroporation and Electrofusion in Cell Biology. Plenum Press, New York.
7. Tsong, T. Y., (1991). Biophys. J., 60, 297–306.
8. Chang, D. C., Chassy, B. M., Saunders, J. A., Potter, A. H. (1988). Anal. Biochem.174, 361–373.
9. Stephen, T. K., Julie, G., Edward, W. L. (2011). Clinical Aspects of Electroporation. Springer.
10. Miller, L., Leor, J., Rubinsky, B. (2005). Cancer cells ablation with irreversible electroporation. Technol Cancer Res Treat. 699-705.
11. Canatella, P. J., Karr, J. F., Petros, J. A., Prausnitz, M. R. (2001). Quantitative study of electroporation-mediated molecular uptake and cell viability. Biophys. J. 80, 755–764.
12. Neumann, E., Schaefer-Ridder, M., Wang, Y., Hofschneider, P. H. (1982). EMBO J. 1, 841–845.
13. Rols, M. P., Delteil, C., Golzio, M., Dumond, P., Cros, S., Teissie, J. (1998). In vivo electrically mediated protein and gene transfer in murine melanoma. Nat. Biotechnol. 16, 168–171.
14. Gothelf, A., Mir, L. M., Gehl, J. (2003). Electrochemotherapy: results of cancer treatment using enhanced delivery of bleomycin by electroporation. Cancer Treat. Rev. 29, 371–387.
15. Andre, F., Mir, L. M. (2004). DNA electrotransfer: its principles and an updated review of its therapeutic applications. Gene Ther. Suppl 11, S33–42.

16. Geng, T., Zhan, Y., Wang, H-Y., Lu C. (2011). Transfection of cells using flow-through electroporation based on constant voltage. Nature Protocols. 6, 1192–1208.
17. Coster, H. (1965). A Quantitative Analysis of the Voltage-Current Relationships of Fixed Charge Membranes and the Associated Property of Punch-Through. Biophys. J. 5, 669-686.
18. Crowley, J., (1973). Electrical Breakdown of Bimolecular Lipid Membranes as an Electromechanical Instability. Biophys. J. 13, 711-724.
19. Sale, A. J. H., Hamilton, W. A. (1967). Effects of high electric fields on microorganisms: I. Killing of bacteria and yeasts. Biochim. Biophys Acta. 148, 781-788.
20. Sale, A. J. H., Hamilton, W. A. (1968). Effects of high electric fields on micro-organisms: III. Lysis of erythrocytes and protoplasts. Biochim. Biophys Acta. 163, 37-43.
21. Zimmermann, U., Pilwat, G., Riemann, F. (1974). Dielectric Breakdown of Cell Membranes. Biophys. J. 14, 881-899.
22. Neumann, E., Schaefer-Ridder, M., Wang, Y., Hofschneider, P. H. (1982). Gene transfer into mouse lyoma cells by electroporation in high electric fields. EMBO J. 1, 841-845.
23. Potter, H., Weir, L., Leder, P. (1984). Enhancer-dependent expression of human kappa immunoglobulin genes introduced into mouse pre-B lymphocytes by electroporation. Proc. Natl. Acad. Sci. U. S. A. 81, 7161-7165.
24. Fromm, M., Taylor, L., Walbot, V. (1985). Expression of genes transferred into monocot and dicot plant cells by electroporation. Proc. Natl. Acad. Sci. U. S. A. 82, 5824-5828.
25. Toneguzzo, F., Keating, A., (1986). Stable expression of selectable genes introduced into human hematopoietic stem cells by electric field-mediated DNA transfer. Proc. Natl. Acad. Sci. U. S. A. 83, 3496- 3499.
26. Prausnitz, M., Bose, V., Langer, R., Weaver, J. (1993). Electroporation of mammalian skin: a mechanism to enhance transdermal drug delivery. Proc. Natl. Acad. Sci. U.S. A. 90, 10504-10508.
27. Mir L. M., Orlowski S., Belehradek J. J., Paoletti C. (1991). Electrochemotherapy potentiation of antitumour effect of bleomycin by local electric pulses. Eur. J. Cancer 27,68-72.

28. Belehradek, M., Domenge, C., Luboinski, B., Orlowski, S., Belehradek, J., Mir, L. (1993). Electrochemotherapy, a new antitumor treatment. First clinical phase I-II trial. Cancer. 72, 3694-3700.
29. Ramirez, L. H., Orlowski, S., An, D., Bindoula, G., Dzodic R., Ardouin, P., Bognel, C., Belehradek, J., Munck, J. N., Mir. L. M. (1998). Electrochemotherapy on liver tumours in rabbits. Br. J. Cancer. 77, 2104- 2111.
30. Hacein-Bey-Abina, S. et al. (2003). LMO2-associated clonal T cell proliferation in two patients after gene therapy for SCID-X1. Science. 302, 415–419.
31. Hacein-Bey-Abina, S. et al. (2008). Insertional oncogenesis in 4 patients after retrovirus-mediated gene therapy of SCID-X1. J. Clin. Invest. 118, 3132–3142.
32. Yang, Y. et al. (1994). Cellular immunity to viral antigens limits E1-deleted adenoviruses for gene therapy. Proc. Natl. Acad. Sci. U. S. A. 91, 4407–4411.
33. Raper, S.E. et al. (2003). Fatal systemic inflammatory response syndrome in a ornithine transcarbamylase deficient patient following adenoviral gene transfer. Mol. Genet. Metab. 80, 148–158.
34. Luo, D., Saltzman, W.M. (2000). Synthetic DNA delivery systems. Nat. Biotechnol. 18, 33–37.
35. Fedorov, Y. et al. (2005). Different delivery methods—different expression profiles. Nat. Methods. 2, 241.
36. Teissie, J., Rols, M. P. (1993). An experimental evaluation of the critical potential difference inducing cell membrane electropermeabilization. Biophys. J. 65, 409-413.
37. Fedorov, Y. et al. (2005). Different delivery methods—different expression profiles. Nat. Methods. 2, 241.
38. Jun Wang, et al. (2010).Vortex-assisted DNA delivery. Lab Chip. 10, 2057-2061.
39. Weaver J. C., Chizmadzhev Y. A. (1996). Theory of electroporation: A review. Bioelectrochem. Bioenerg. 41, 135–160.
40. Ho S. Y., Mittal G. S. (1996). Effects of high field electric pulses on the activity of selected enzymes. Crit. Rev. Biotechnol. 16, 349–362.
41. Chen, C., Smye, S. W., Robinson M. P., Evans, J. A. (2006). Membrane electroporation theories: a review. Med. Biol. Eng. Comput. 44, 5–14.

42. Teissie J., Golzio M., Rols, M. P. (2005). Mechanisms of cell membrane electropermeabilization: A minireview of our present (lack of ?) knowledge. Biochim. Biophys. Acta, Gen. Subj. 1724, 270–280.
43. Escoffre, J. M., Portet, T., Wasungu, L., Teissie, J., Dean D., Rols, M. P. (2009). What is (Still not) Known of the Mechanism by Which Electroporation Mediates Gene Transfer and Expression in Cells and Tissues. Mol. Biotechnol. 41, 286–295.
44. Chen, C., Smye, S.W., Robinson, M.P., Evans, J.A. (2006). Membrane electroporation theories: a review. Med Biol Eng Comput. 44: 5–14.
45. Fox, M. B., Esveld, D. C., Valero, A., Luttge, R., Mastwijk, H. C., Bartels, P. V., Van den Berg, A., Boom, R. M. (2006). Electroporation of cells in microfluidic devices: a review. Anal. Bioanal. Chem. 385, 474–485.
46. Lee, W. G., Demirci, U., Khademhosseini, A. (2009). Microscale electroporation: challenges and perspectives for clinical applications. Integr. Biol. 1, 242–251
47. Movahed, S., Li, D., (2011). Microfluidics cell electroporation. Microfluid. Nanofluid. 10, 703–734.
48. Wang, S., Lee, L. J. (2013). Micro-/nanofluidics based cell electroporation. Biomicrofluidics. 7, 11301.
49. Titomirov, V. A., Sukharev, S., Kistanova, E. (1991). In vivo electroporation and stable transformation of skin cells of newborn mice by plasmid DNA. Biochimica Biophysica Acta. 1, 131–134.
50. Olofsson, J., Nolkrantz, K., Ryttsen, F., Lambie, B. A., Weber, S. G., Orwar, O. (2003). Single-cell electroporation. Curr. Opin. Biotechnol. 14, 29–34.
51. Wang, M., Orwar, O., Olofsson, J., Weber, S. G. (2010). Single-cell electroporation. Anal. Bioanal. Chem. 397, 3235–3248.
52. Whitesides, G. M. (2006). The origins and the future of microfluidics. Nature. vol 442, 368-373.
53. Beebe, D. J., Mensing, G. A., Walker, G. M. (2002). Physics and applications of microfluidics in biology. Annu. Rev. Biomed. Eng. 4, 261–86.
54. Colin, S. (2010). Microfluidics. Wiley.
55. Dino Di Carlo. (2009). Inertial microfluidics. Lab on Chip. 9, 3038-3046.

56. Dino Di Carlo et al. (2009). Particle Segregation and Dynamics in Confined Flows. Physical Rev. Letters. 102. 094503.
57. Daniel R. Gossett et al. (2009). Particle Focusing Mechanisms in Curving Confined Flows. Anal. Chem. 81, 8459-8465.
58. Dino Di Carlo et al. (2007). Continuous inertial focusing, ordering, and separation of particles in microchannels. PNAS. vol 104, 18892-18897.
59. Dino Di Carlo et al. (2008). Equilibrium separation and filtration of particles using differential inertial Focusing. Anal. Chem. 80, 2204-2211.
60. E. S. Asmolov, (1999). J. Fluid Mech. 381, 63–87
61. Cheng, J. Sheldon, E. L. Wu, L. Uribe, A. Gerrue, L. O. Carrino, J. Heller, M. J. O'Connell, (1998). J. P. Nat. Biotechnol. 16, 541-546
62. Lee, S. W., Tai, Y. C. (1999). A micro cell lysis device. Sens. Actuators. A 73, 74-79.
63. McClain, M. A., Culbertson, C. T., Jacobson, S. C., Allbritton, N. L., Sims, C. E. Ramsey, J. M. (2003). Microfluidic Devices for the High-Throughput Chemical Analysis of Cells. Anal. Chem. 75, 5646-5655.
64. Gao, J., Yin, X. F., Fang, Z. L. (2004). Integration of single cell injection, cell lysis, separation and detection of intracellular constituents on a microfluidic chip. Lab Chip. 4, 47-52.
65. Lu, H., Schmidt, M. A., Jensen, K. F. (2005). A microfluidic electroporation device for cell lysis. Lab Chip. 5, 23-29.
66. Munce, N. R., Li, J., Herman, P. R., Lilge, L. (2004). Microfabricated system for parallel single-cell capillary electrophoresis. Anal. Chem. 76, 4983- 4989.
67. Khine, M., Lau, A., Ionescu-Zanetti, C., Seo, J., Lee, L. P. (2005). A single cell electroporation chip. Lab Chip. 5, 38-43.
68. Huang, Y., Rubinsky, B., (2001). Microfabricated electroporation chip for single cell membrane permeabilization. Sens. Actuators. A, 89, 242-249.
69. Huang, Y., Rubinsky, B. (2003). Microfabricated electroporation chip for single cell membrane permeabilization. Sens. Actuators. A, 104, 205-212.
70. Shin, Y. S. et al. (2004). Electrotransfection of mammalian cells using microchannel-type electroporation chip. Anal. Chem. 76, 7045-7052.

71. Movahed, S., Li, D. (2011). Microfluidics cell electroporation. Microfluidics and Nanofluidics. 10, Issue 4, 703-734.
72. Jacobson, S. C. et al. (1998). Microchip Structures for Submillisecond Electrophoresis. Anal. Chem. 70, 3476-3480.
73. Plenert, M. L., Shear, J. B. (2003). Microsecond electrophoresis. Proc. Natl. Acad. Sci. U. S. A. 100, 3853- 3857.
74. Hansen, C. L. et al. (2004). Systematic investigation of protein phase behavior with a microfluidic formulator. Proc. Natl. Acad. Sci. U. S. A. 101, 14431-14436.
75. Zhu, T., Luo, C., Huang, J., Xiong, C., Ouyang, Q., Fang, J. (2010). Electroporation based on hydrodynamic focusing of microfluidics with low dc voltage. Biomed. Microdevices.12, 35–40.
76. Wei, Z., Zhao, D., Li, X., Wu, M., Wang, W., Huang, H., Wang, X., Du, Q., Liang, Z., Li, Z. (2011). Microfluidic approaches for gene delivery and gene therapy. Anal. Chem. 83, 5881–5887.
77. Selmeczi, D., Hansen, T. S., Met, O., Svane, I. M., Larsen, N. B. (2011). Efficient large volume electroporation of dendritic cells through micrometer scale manipulation of flow in a disposable polymer chip. Biomed. Microdevices.13, 383–392.
78. Geng, T., Lu, C. (2013). Microfluidic electroporation for cellular analysis and delivery. Lab on a Chip. 13. 3803-3821.
79. Thorsen, T. et al. (2002). Microfluidic large-scale integration. Science. 298, 580-584
80. Wang, H-Y., Lu, C. (2006). High-Throughput and Real-Time Study of Single Cell Electroporation Using Microfluidics: Effects of Medium Osmolarity. Biotechnology and Bioengineering. vol 95, 1116–1125.
81. Bao, N., Le, T. T., Cheng, J-X., Lu, C. (2010). Microfluidic electroporation of tumor and blood cells: observation of nucleus expansion and implications on selective analysis and purging of circulating tumor cells. Integr. Biol. 2, 113–120.
82. QIAfilter Plasmid Giga Kit Handbook. (2003).
83. Kimber Hardy. (1986). Bacterial plasmids. American Society for Microbiology.
84. Invitrogen, FilmTracer, Calcein Biofilm Stains Manual. (2009).
85. Tao Geng et al. (2010). Flow-through electroporation based on constant voltage for large-volume transfection of cells. Journal of Controlled Release. 144, 91–100.